FINITE ELEMENT MODELING OF SCATTERING FROM OBJECTS IN RECTANGULAR WAVEGUIDES

A THESIS SUBMITTED TO
THE GRADUATE SCHOOL OF NATURAL AND APPLIED SCIENCES
OF
MIDDLE EAST TECHNICAL UNIVERSITY

BY

HÜSEYİN GÜLBAŞ

IN PARTIAL FULLFILLMENT OF THE REQUIREMENTS
FOR
THE DEGREE OF MASTER OF SCIENCE
IN
ELECTRICAL AND ELECTRONICS ENGINEERING

JANUARY 2017

Approval of the thesis:

FINITE ELEMENT MODELING OF SCATTERING FROM OBJECTS IN RECTANGULAR WAVEGUIDES

submitted by **HÜSEYİN GÜLBAŞ** in partial fulfillment of the requirements for the degree of **Master of Science in Electrical and Electronics Engineering Department, Middle East Technical University** by,

Prof. Dr. Gülbin Dural Ünver
Dean, Graduate School of **Natural and Applied Sciences** _____

Prof. Dr. Tolga Çiloğlu
Head of Department, **Electrical and Electronics Engineering** _____

Prof. Dr. Mustafa Kuzuoğlu
Supervisor, **Electrical and Electronics Engineering Dept., METU** _____

Assoc. Prof. Dr. Özlem Özgün
Co-Supervisor, **Electrical and Electronics Engineering Dept., Hacettepe University** _____

Examining Committee Members:

Prof. Dr. Gönül Turhan Sayan
Electrical and Electronics Engineering Dept., METU _____

Prof. Dr. Mustafa Kuzuoğlu
Electrical and Electronics Engineering Dept., METU _____

Prof. Dr. Gülbin Dural Ünver
Electrical and Electronics Engineering Dept., METU _____

Prof. Dr. Adnan Köksal
Electrical and Electronics Engineering Dept., Hacettepe University _____

Assoc. Prof. Dr. Egemen Yılmaz
Electrical and Electronics Engineering Dept., Ankara University _____

Date: 30.01.2017

I hereby declare that all information in this document has been obtained and presented in accordance with academic rules and ethical conduct. I also declare that, as required by these rules and conduct, I have fully cited and referenced all material and results that are not original to this work.

Name, Last Name: Hüseyin GÜLBAŞ

Signature :

ABSTRACT

FINITE ELEMENT MODELING OF SCATTERING FROM OBJECTS IN RECTANGULAR WAVEGUIDES

Gülbaş, Hüseyin
M.S. Department of Electrical and Electronics Engineering
Supervisor : Prof. Dr. Mustafa Kuzuoğlu
Co-Supervisor : Assoc. Prof. Dr. Özlem Özgün

January 2017, 112 pages

Numerical analysis of scattering parameters of split ring resonators which are one of the microwave circuit elements is performed by the Finite Element Method in this thesis. The fundamentals of the model and analysis method will be discussed firstly. Afterwards, the basics of Finite Element Method including weak variational form of the wave equation, 3D formulations and application to scattering parameters will be presented. The concepts of Perfectly Matched Layer and resonators will be examined in detail. The accuracy of the method will be tested and the effects of different design parameters on the scattering parameters of split ring resonators will be investigated. These design parameters will be slit width, side width, and operation frequency. Moreover, reflection and transmission from the dielectric surfaces will be discussed. Additionally, each result will be compared with the ones achieved by using CST (Computer Simulation Technology) simulation software.

Keywords: Scattering Parameters, Finite Element Method, Waveguide, Split Ring Resonators,

ÖZ

DİKDÖRTGEN DALGA KILAVUZLARI İÇİNDEKİ CİSİMLERDEN SAÇILMANIN SONLU ELEMANLARLA MODELLENMESİ

Gülbaş, Hüseyin
Yüksek Lisans, Elektrik ve Elektronik Mühendisliği Bölümü
Tez Yöneticisi : Prof. Dr. Mustafa Kuzuoğlu
Ortak Tez Yöeticisi : Doç. Dr. Özlem Özgün

Ocak 2017, 112 sayfa

Bu tezde açık halka rezonatörlerin saçılma parametreleri sayısal olarak analiz edilmiştir ve yöntem olarak da Sonlu Elemanlar Yöntemi kullanılmıştır. Öncelikle, analiz yönteminin temelleri incelenecektir. Sonrasında, Sonlu Elemanlar Yöntemi dalga denkleminin zayıflatılmış formu, üç boyutlu modelleme ve bunların saçılma parametlerine uygulanması sunulacaktır. Daha sonra, Tamamen Eşlenmiş Katman ve rezonatörlerin prensipleri detaylıca anlatılacaktır. Yöntemin doğruluğunu içeren test sonuçları ve çeşitli tasarım parametrelerinin saçılma parametrelerine olan etkileri sunulacaktır. Bu tasarım parametreleri, yarık genişliği, kenar genişliği ve çalışma frekansıdır. Ayrıca, yalıtkan yüzeylerden yansımalar ve iletimler de incelenecektir. Her bir test sonucu CST (Computer Simulation Technology) yazılımıyla elde edilenlerle karşılaştırılacaktır.

Anahtar Kelimeler: Saçılma Parametreleri, Sonlu Elemanlar Yöntemi, Dalga Kılavuzu, Açık Halka Rezonatörler,

Dedicated to My Daughter…

ACKNOWLEDGMENTS

I would like to specially express my sincere thanks to my supervisor Prof. Dr. Mustafa Kuzuoğlu and co-supervisor Assoc. Prof. Dr. Özlem Özgün for their great support, patience, guidance, and valuable evaluation throughout the development of this thesis.

I am grateful to my wife Betül Gülbaş for her understanding and patience. Also, I am grateful to my parents for their moral support.

Finally, I thank to Mustafa Gökgöz for considerations during my studies.

TABLE OF CONTENTS

LIST OF TABLES

TABLES

LIST OF FIGURES

FIGURES

CHAPTER 1

INTRODUCTION

Maxwell's equations describe the behavior of electromagnetic waves. They become in their simplest form when the waves propagate in unbounded medium with no scatterers. But, this case can be described as ideal and in practice it may not be possible to have such a medium. Scatterers always exist and people make use of the scattered fields reflected from them in their applications, like radar cross section calculations, medical imaging, and optics. In addition to these, scattering parameters calculations are one of the main applications found from scattered fields. Scattering parameters measure the signals that are reflected or transmitted by objects and networks. Under steady state conditions, they give an idea about the productivity and how the design meets the needs. For microwave circuits and components, they are one of the most important methods to identify the characteristics. For complex geometries, it is difficult to calculate scattering parameters of microwave components analytically, and hence, they have to be found by network analyzers after production or with the help of some simulation programs. This thesis provides a numerical solution approach for the problem of calculation of scattering parameters of structures with different shapes and also metamaterial resonators.

Finite element method is one of the most powerful numerical methods for 3D structures. It allows us to investigate structures with complicated shapes and geometries by reducing the solutions to subdomains without doing any simplifications in the geometries. Moreover, it can be easily applied when they composed of different materials with complicated features. In addition to these, applications of boundary conditions are easy to handle and by generalizing mathematically, the same model can

be used to solve different problems. Also, it requires less memory usage and CPU thanks to having sparse matrices.

Metamaterials are artifical structures that have unnatural properties. The main purpose in their designs is to reach some features not found in nature like negative permittivity, permeability, and refractive index. In the applications, they consist of periodic structures whose shapes, sizes and other physical properties provide the main function of metamaterials [1]. This groundbreaking invention has been the subject of many studies over the past decades. Antennas, absorbers, superlenses, cloaks, sensors, and phase compensators are some application areas of metamaterials. Furthermore, they commonly used in design of a kind of resonators named as split ring resonator. Due to their properties mentioned above, they designate fundamental principles of the resonators. In detail, when the resonators are manufactured to manage the metamaterials' specifications, they have the characteristics of magnetic dipoles where the rings and the gaps between them act as inductors and capacitors respectively [2].

In general, resonators are mechanical or electrical devices that transmit and/or strengthen the signals at a certain frequency by vibrations. As they can be manufactured by ordinary components, it is possible to produce them to generate metamaterial properties by reconsidering the details in their designs. It was mentioned that metamaterials have negative permittivity and negative permeability values. Negative permittivity was achieved thanks to thin wire strings. Besides this, split ring resonators were used to get negative permeability and Shelby combined them ([3]-[4]). After this novel approach was brought forward, academic and industrial studies were come to light to use them in more effective manner. Due to having periodic structure, the resulting styles of split ring resonators or the others can be very large. Also, reaching the optimum and desired design features may be difficult and repeated experiments might be needed. On such an occasion, costs increase and waste of time is unavoidable. In these circumstances, instead of doing the tests on the whole design, taking a piece from the periodic structure and performing the measurements on this small part can be possible.

In this thesis, by making use of the advantages of finite element method, the main aim is to calculate the scattering parameters of structures having complex geometries and split ring resonator is chosen for this kind of a structure. The method that takes a single cell from the periodic structure and collecting results just by analyzing the single cell is developed. In order to achieve this, the single cell is put in a rectangular waveguide whose dimensions are arranged to fit it inside and have only fundamental mode of electrical field. This problem is analyzed by finite element method by paying attention to different parts of the geometry, like waveguide walls, resonator structure, vacuum region, and absorbing layers at the open ends of waveguide. The simulations are performed by starting with a simple rectangular prism. The final geometry is design step by step by changing this simple geometry. Also, the tests are performed with commercial simulation software, CST, and compared with the results of the finite element method.

Waveguides are microwave circuit components with conductor boundaries that carry electromagnetic waves from one end to other. According to their shapes and sizes the carried signal may vary and they can be used for different microwave applications. Analytic solutions of waveguide can be found easily if there are no obstacles inside, and in Chapter 2 these solutions are provided in detail. However, for arbitrary obstacles, numerical methods are needed. Many researchers were interested in discontinuity problems and their solutions by finite difference method and finite element method. They solved some problems involving dielectric structures inside waveguides that are loaded with different types of material. Also, for the solution of eigenvalue problems via finite element method, there are several publications in the literature ([5]-[8]). In this study, the waveguide problem containing a PEC resonator structure inside was solved using finite element method by considering the TE_{10} mode. Also in Chapter 2, the design parameters and properties of split ring resonators are discussed by referring to the studies performed in the past. Earlier research was mainly about resonance frequency and the factors that affect it, such as the dimensions of the split ring resonator. This thesis examines how scattering parameters are affected by design parameters. The open ends of the waveguide are terminated by Perfectly

Matched Layer (PML) absorbers. The details of numerical method and the use of absorbing layer are presented in Chapter 3 and Chapter 4, respectively.

The test results are presented in Chapter 5. Moreover, information about the accuracy of MATLAB code and effects of sizes of structure, element and design parameters on scattering parameters can be found. Also, the comparison of results of PEC and dielectric obstacles are presented. The problem is also analyzed by changing the frequency. Furthermore, the results are commented and compared with those of the past studies and CST.

CHAPTER 2

BACKGROUND INFORMATION

2.1. MAXWELL'S EQUATIONS

James Clerk Maxwell, who was a physicist and a mathematician, studied on and reviewed the equations that describe the relations between electric and magnetic fields and also their relations between charges and currents. He came up with four famous equations called Maxwell's equations. These underpin not only electromagnetic theory and communication theory but also important principles of electrical systems. These can be expressed into two forms namely integral form and differential form and all are given below.

$$\nabla \times \boldsymbol{E} = -\frac{\partial \boldsymbol{B}}{\partial t} \tag{2.1}$$

$$\nabla \times \boldsymbol{H} = \boldsymbol{J} + \frac{\partial \boldsymbol{D}}{\partial t} \tag{2.2}$$

$$\nabla \cdot \boldsymbol{D} = \rho \tag{2.3}$$

$$\nabla \cdot \boldsymbol{B} = 0 \tag{2.4}$$

The equations above are Maxwell's equations in differential form and below are the ones in integral from.

$$\oint \boldsymbol{E} \cdot d\boldsymbol{l} = -\frac{d}{dt} \iint \boldsymbol{B} \cdot d\boldsymbol{S} \tag{2.5}$$

$$\oint \boldsymbol{B} \cdot d\boldsymbol{l} = \iint \boldsymbol{J} \cdot d\boldsymbol{S} + \frac{d}{dt} \iint \boldsymbol{D} \cdot d\boldsymbol{S} \tag{2.6}$$

$$\oiint \boldsymbol{D} \cdot d\boldsymbol{S} = \iiint \rho d\boldsymbol{V} \tag{2.7}$$

$$\oiint \boldsymbol{B} \cdot d\boldsymbol{S} = 0 \tag{2.8}$$

where

$\boldsymbol{E}$ is electric field intensity, *V/m*

$\boldsymbol{H}$ is magnetic field intensity, *A/m*

$\boldsymbol{D}$ is electric flux density, C/m^2

$\boldsymbol{B}$ is magnetic flux density, Wb/m^2

$\boldsymbol{J}$ is electric current density, A/m^2

ρ is charge density, C/m^3

The first, second, third and fourth equations are also known as Faradays law of induction, Ampere's circuital law, Gauss's law, and Gauss's law for magnetism, respectively.

Another equation, called continuity equation, can be derived by using Ampere's circuital law and Gauss's law. The continuity equation, derived below, allows us to know the relation between current that enters and leaves a specific volume.

$$\nabla \cdot \nabla \times \boldsymbol{H} = \nabla \cdot (\boldsymbol{J} + \frac{\partial \boldsymbol{D}}{\partial t}) = 0$$

$$\frac{\partial \nabla \cdot \boldsymbol{D}}{\partial t} = -\nabla \cdot \boldsymbol{J}$$

$$\nabla \cdot \boldsymbol{D} = \rho \Rightarrow$$

$$\nabla \cdot \boldsymbol{J} = -\frac{\partial \rho}{\partial t} \tag{2.9}$$

2.2. CONSTITUTIVE RELATIONS

Electric field intensity, ***E***, and magnetic field intensity, ***H***, have relations with electric flux density, ***D***, and magnetic flux density, ***B***. By the constitutive relations, these relationships are established. They depend on the properties of the medium or the material that electric field or magnetic field exists.

The simplest forms of the constitutive relations are expressed in vacuum.

$$\boldsymbol{D} = \varepsilon_0 \boldsymbol{E} \tag{2.10}$$

$$\boldsymbol{B} = \mu_0 \boldsymbol{H} \tag{2.11}$$

ε_0 and μ_0 are called permittivity of vacuum and permeability of vacuum respectively. In addition, speed of light in vacuum, c_0, and intrinsic impedance of vacuum, η_0, are associated with ε_0 and μ_0 by some mathematical operations.

$$c_0 = \frac{1}{\sqrt{\varepsilon_0 \mu_0}} \tag{2.12}$$

$$\eta_0 = \sqrt{\frac{\varepsilon_0}{\mu_0}} \tag{2.13}$$

Numerical values of c_0 and η_0 are 3×10^8 *m/s* and $377\ \Omega$ respectively where

$$\varepsilon_0 = 8.854 \times 10^{-12}\ F/m$$

$$\mu_0 = 4\pi \times 10^{-7}\, H/m$$

Here, *F* stands for Farad, *C/V*, and *H* stands for Henry, *Wb/A*.

When the material has magnetic or dielectric properties, the constitutive relations turn into more involved forms.

$$\boldsymbol{D} = \varepsilon \boldsymbol{E} \tag{2.14}$$

$$\boldsymbol{B} = \mu \boldsymbol{H} \tag{2.15}$$

where

$$\varepsilon = \varepsilon_0(1 + \chi_e)$$

$$\mu = \mu_0(1 + \chi_m)$$

As the formulas above are stated, permittivity and permeability of materials depend on susceptibilities, χ_e and χ_m. They change according to the material properties, electric polarization and magnetic polarization.

At this stage, the wavenumber, *k*, can be expressed in terms of *c* and angular frequency $\omega = 2\pi f$. Physically, wavenumber shows electromagnetic field's number of full wave period in per unit distance.

$$k = \frac{\omega}{c} \quad and \quad c = \frac{1}{\sqrt{\varepsilon\mu}} \Rightarrow$$

$$k = \omega\sqrt{\varepsilon\mu} \tag{2.16}$$

Ohm's law is another constitutive relation, used to derive waveguide equations, and expressed in terms of current density, $\boldsymbol{J}$, electric field intensity, $\boldsymbol{E}$, conductivity, σ.

$$\boldsymbol{J} = \sigma \boldsymbol{E} \tag{2.17}$$

2.3. HELMHOLTZ EQUATION

Helmholtz equation is a linear partial differential equation and named after Hermann von Helmholtz, a German physicist. It is derived by using Maxwell's equations, the constitutive relations mentioned in previous sections, and vector identities.

The first step to derive the equation is taking the curl of first Maxwell's equation.

$$\nabla \times \nabla \times \boldsymbol{E} = -\nabla \times \left(\frac{\partial \boldsymbol{B}}{\partial t}\right) \quad \text{where} \quad \boldsymbol{B} = \mu \boldsymbol{H}$$

$$\nabla \times \nabla \times \boldsymbol{E} = -\mu \nabla \times \left(\frac{\partial \boldsymbol{H}}{\partial t}\right) \tag{2.18}$$

Next, using the vector identity given below in (2.19) and the second Maxwell's equation (2.2) the above equation is rewritten as:

$$\nabla \times \nabla \times \boldsymbol{A} = \nabla(\nabla \cdot \boldsymbol{A}) - \nabla^2 \boldsymbol{A} \tag{2.19}$$

$$\Rightarrow \nabla \times \nabla \times \boldsymbol{E} = \nabla(\nabla \cdot \boldsymbol{E}) - \nabla^2 \boldsymbol{E} \tag{2.20}$$

and in a source free region $\rho = 0 \Rightarrow \nabla \cdot \boldsymbol{E} = 0$

$$\Rightarrow \nabla \times \nabla \times \boldsymbol{E} = -\nabla^2 \boldsymbol{E} = -\mu \nabla \times \left(\frac{\partial \boldsymbol{H}}{\partial t}\right) \tag{2.21}$$

$$-\mu\nabla\times\left(\frac{\partial \boldsymbol{H}}{\partial t}\right)=-\mu\left(\frac{\partial\nabla\times \boldsymbol{H}}{\partial t}\right) \tag{2.22}$$

$$\nabla\times \boldsymbol{H}=\boldsymbol{J}+\frac{\partial \boldsymbol{D}}{\partial t}\Rightarrow -\mu\nabla\times\left(\frac{\partial \boldsymbol{H}}{\partial t}\right)=-\mu\left(\frac{\partial}{\partial t}\left(\boldsymbol{J}+\frac{\partial \boldsymbol{D}}{\partial t}\right)\right) \tag{2.23}$$

$$\Rightarrow -\mu\nabla\times\left(\frac{\partial \boldsymbol{H}}{\partial t}\right)=-\mu\left(\frac{\partial \boldsymbol{J}}{\partial t}+\frac{\partial^2 \boldsymbol{D}}{\partial t^2}\right) \tag{2.24}$$

$$\Rightarrow -\nabla^2\boldsymbol{E}=-\mu\left(\frac{\partial \boldsymbol{J}}{\partial t}+\frac{\partial^2 \boldsymbol{D}}{\partial t^2}\right) \tag{2.25}$$

After that, taking account of the fact that $\boldsymbol{D}=\varepsilon\boldsymbol{E}$ and the region is source free, $\boldsymbol{J}=0$, the above equation (2.26) below is obtained

$$\nabla^2\boldsymbol{E}=\mu\varepsilon\frac{\partial^2\boldsymbol{E}}{\partial t^2} \tag{2.26}$$

Lastly, the derivation can be taken a step further by writing its time-harmonic case while the time dependence is $e^{j\omega t}$.

$$\nabla^2\boldsymbol{E}=-\omega^2\mu\varepsilon\boldsymbol{E} \tag{2.27}$$

and defining the wave number, k, as $\omega\sqrt{\epsilon\mu}$, Helmholtz equation for $\boldsymbol{E}$ takes its final form as follows

$$\nabla^2\boldsymbol{E}+k^2\boldsymbol{E}=0 \tag{2.28}$$

Similarly, Helmholtz equation for $\boldsymbol{H}$ is derived:

$$\nabla \times \nabla \times \boldsymbol{H} = \nabla \times \left(\boldsymbol{J} + \frac{\partial \boldsymbol{D}}{\partial t}\right) \quad \text{where} \quad \boldsymbol{D} = \varepsilon \boldsymbol{E} \quad \text{and in a source free region}$$

$$\nabla \times \nabla \times \boldsymbol{H} = \frac{\partial \nabla \times \boldsymbol{E}}{\partial t} \tag{2.29}$$

$$\nabla \times \boldsymbol{E} = -\frac{\partial \boldsymbol{B}}{\partial t} \Rightarrow$$

$$\nabla \times \nabla \times \boldsymbol{H} = -\frac{\partial^2 \boldsymbol{B}}{\partial t^2} \quad \text{and} \quad \nabla \times \nabla \times \boldsymbol{H} = -\nabla^2 \boldsymbol{H} \Rightarrow$$

$$\nabla^2 \boldsymbol{H} = \frac{\partial^2 \boldsymbol{B}}{\partial t^2} \tag{2.30}$$

Taking the time dependence as $e^{j\omega t}$ and k as $\omega\sqrt{\epsilon\mu}$, we obtain:

$$\nabla^2 \boldsymbol{H} + k^2 \boldsymbol{H} = 0. \tag{2.31}$$

2.4. BOUNDARY CONDITIONS

Boundary conditions are important to have a unique solution to partial differential equations. They are used to solve Maxwell's equations for fields applied between two media with different permittivity and permeability values.

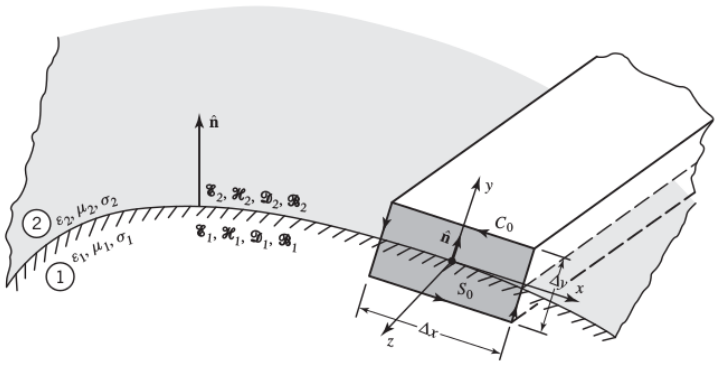

Figure 2.1: Boundary between two different media [9]

Figure 2.1 pictures two different media where $\boldsymbol{E_1}$, $\boldsymbol{H_1}$, $\boldsymbol{D_1}$, $\boldsymbol{B_1}$, ε_1, μ_1, σ_1 are field intensities, flux densities and constitutive parameters of medium-1 and $\boldsymbol{E_2}, \boldsymbol{H_2}, \boldsymbol{D_2}, \boldsymbol{B_2}$, ε_2, μ_2, σ_2 are field intensities, flux densities and constitutive parameters of medium-2.

Without existence a perfect conductor medium, if charge and current densities are present, the boundary conditions for field intensities and field densities are defined in the following formats.

$$-\boldsymbol{n} \times (\boldsymbol{E}_2 - \boldsymbol{E}_1) = \boldsymbol{M_s} \tag{2.32}$$

$$\boldsymbol{n} \times (\boldsymbol{H}_2 - \boldsymbol{H}_1) = \boldsymbol{J_s} \tag{2.33}$$

$$\boldsymbol{n} \cdot (\boldsymbol{D}_2 - \boldsymbol{D}_1) = \rho_{es} \tag{2.34}$$

$$\boldsymbol{n} \cdot (\boldsymbol{B}_2 - \boldsymbol{B}_1) = \rho_{ms} \tag{2.35}$$

where $\boldsymbol{M_s}$ is magnetic current density, $\boldsymbol{J_s}$ is surface electric current density, ρ_{es} is electric surface charge density, and ρ_{ms} is magnetic surface charge density.

2.5. DERIVATION OF WAVEGUIDE EQUATIONS

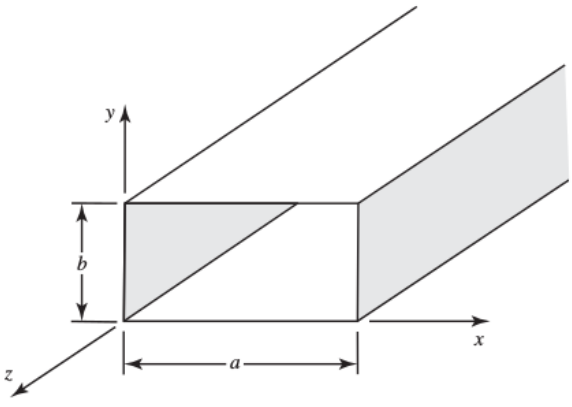

Figure 2.2: Rectangular waveguide [9]

Rectangular waveguides are microwave circuit components that guide electromagnetic waves as much as possible without losing energy. Only transverse electric (TE) and transverse magnetic (TM) wave can propagate inside hollow rectangular waveguides. The reason why transverse electromagnetic waves cannot propagate is that the structure includes only one conductor and therefore the boundary conditions cannot be satisfied.

2.5.1. TE Mode

According to Figure 2.2, the waveguide lies on a rectangular coordinate system and the dimension along x-axis is *a* and dimension along y-axis is *b*, z being the longitudinal component.

In order to find the expression for TE mode waves with $E_z=0$, the starting point is to solve Helmholtz equation for magnetic field intensity.

$$\nabla^2 \boldsymbol{H} + k^2 \boldsymbol{H} = 0 \tag{2.36}$$

with boundary conditions

$$\frac{\partial H_z(0,y,z)}{\partial x} = 0 \tag{2.37.a}$$

$$\frac{\partial H_z(a,y,z)}{\partial x} = 0 \tag{2.37.b}$$

$$\frac{\partial H_z(x,0,z)}{\partial y} = 0 \tag{2.37.c}$$

$$\frac{\partial H_z(x,b,z)}{\partial y} = 0 \tag{2.37.d}$$

and the general solution with $e^{-j\beta z}$ z-dependence is

$$H_z(x,y,z) = A_{mn} cos\left(\frac{m\pi x}{a}\right) cos\left(\frac{n\pi y}{b}\right) e^{-j\beta z} \tag{2.38}$$

where

$$\text{propagation constant, } \beta = \sqrt{k^2 - {k_c}^2}$$

$$\text{cutoff wavenumber, } k_c = \sqrt{\left(\frac{m\pi}{a}\right)^2 + \left(\frac{n\pi}{b}\right)^2}$$

$$H_z(x,y,z) = h_z(x,y)e^{-j\beta z} \quad \text{and} \quad h_z(x,y) = X(x)Y(y)$$

which is an assumption to solve Helmholtz equation with method of separation of variables.

A_{mn} is the mode amplitude. In the equation above *m* and *n* can take natural numbers but the point to take into consideration is that *m* and *n* cannot be zero at the same time.

Assuming that the waveguide has a source free region, Maxwell's equations can be written in frequency domain as follows;

$$\nabla \times \boldsymbol{E} = -j\omega\mu\boldsymbol{H} \quad \text{where} \quad \boldsymbol{B} = \mu\boldsymbol{H} \tag{2.39}$$

$$\nabla \times \boldsymbol{H} = j\omega\varepsilon\boldsymbol{E} \quad \text{where} \quad \boldsymbol{D} = \varepsilon\boldsymbol{E} \tag{2.40}$$

x, y and z components are stated as

$$\frac{\partial E_z}{\partial y} + j\beta E_y = -j\omega\mu H_x \tag{2.41.a}$$

$$\frac{\partial E_z}{\partial x} + j\beta E_x = j\omega\mu H_y \tag{2.41.b}$$

$$\frac{\partial E_y}{\partial y} - \frac{\partial E_x}{\partial y} = -j\omega\mu H_z \tag{2.41.c}$$

$$\frac{\partial H_z}{\partial y} + j\beta H_y = j\omega\varepsilon E_x \tag{2.41.d}$$

$$\frac{\partial H_z}{\partial x} + j\beta H_x = -j\omega\varepsilon E_y \tag{2.41.e}$$

$$\frac{\partial H_y}{\partial x} - \frac{\partial H_x}{\partial y} = j\omega\varepsilon E_z \tag{2.41.f}$$

Then, *x, and y* components of $\boldsymbol{E}$ and $\boldsymbol{H}$ are expressed in terms of H_z where E_z=0 as

$$E_x = -j\frac{\omega\mu}{{k_c}^2}\frac{\partial H_z}{\partial y} \tag{2.42.a}$$

$$E_y = j\frac{\omega\mu}{{k_c}^2}\frac{\partial H_z}{\partial x} \tag{2.42.b}$$

$$H_x = -j\frac{\beta}{{k_c}^2}\frac{\partial H_z}{\partial x} \tag{2.42.c}$$

$$H_y = -j\frac{\beta}{{k_c}^2}\frac{\partial H_z}{\partial y} \tag{2.42.d}$$

Finally, by inserting the general solution into the above equations, field equations for TE mode can be found.

$$E_x = j\frac{\omega\mu n\pi}{{k_c}^2 b}A_{mn}cos\left(\frac{m\pi x}{a}\right)sin\left(\frac{n\pi y}{b}\right)e^{-j\beta z} \tag{2.43.a}$$

$$E_y = -j\frac{\omega\mu m\pi}{{k_c}^2 a}A_{mn}sin\left(\frac{m\pi x}{a}\right)cos\left(\frac{n\pi y}{b}\right)e^{-j\beta z} \tag{2.43.b}$$

(2.43.c)

$$H_x = j\frac{\beta m\pi}{{k_c}^2 a} A_{mn} sin\left(\frac{m\pi x}{a}\right) cos\left(\frac{n\pi y}{b}\right) e^{-j\beta z}$$

$$H_y = j\frac{\beta n\pi}{{k_c}^2 b} A_{mn} cos\left(\frac{m\pi x}{a}\right) sin\left(\frac{n\pi y}{b}\right) e^{-j\beta z} \quad (2.43.d)$$

2.5.2. TM Mode

Helmholtz equation for *E* in TM modes will be solved using:

$$\nabla^2 \boldsymbol{E} + k^2 \boldsymbol{E} = 0 \quad (2.44)$$

with the boundary conditions given as:

$$E_z(0, y, z) = 0, E_z(\mathrm{a}, y, z) = 0, E_z(\mathrm{x}, 0, z) = 0, \text{and } E_z(\mathrm{x}, b, z) = 0 \quad (2.45.\mathrm{a,b,c,d})$$

where E_z can be stated with $e^{-j\beta z}$ z-dependence as

$$E_z(x, y, z) = e_z(x, y) e^{-j\beta z}$$

$e_z(x,y)$ has to be solved by the method of separation of variables with a general assumption $e_z(x,y)=X(x)Y(y)$

Then, the general solution is obtained as

$$E_z(x, y, z) = A_{mn} sin\left(\frac{m\pi x}{a}\right) cos\left(\frac{n\pi y}{b}\right) e^{-j\beta z} \quad (2.46)$$

where *m* and *n* can take positive integers.

The equations for E_x, E_y, H_x, and H_y in terms of E_z where H_z=0 are

$$E_x = -j\frac{\beta}{{k_c}^2}\frac{\partial E_z}{\partial x} \tag{2.47.a}$$

$$E_y = -j\frac{\beta}{{k_c}^2}\frac{\partial E_z}{\partial y} \tag{2.47.b}$$

$$H_x = j\frac{\omega\varepsilon}{{k_c}^2}\frac{\partial E_z}{\partial y} \tag{2.47.c}$$

$$H_y = -j\frac{\omega\varepsilon}{{k_c}^2}\frac{\partial E_z}{\partial x} \tag{2.47.d}$$

By using the general expression of E_z in the above equations (2.47), TM mode equations are derived as

$$E_x = -j\frac{\beta m\pi}{{k_c}^2 a}A_{mn}cos\left(\frac{m\pi x}{a}\right)sin\left(\frac{n\pi y}{b}\right)e^{-j\beta z} \tag{2.48.a}$$

$$E_y = -j\frac{\beta n\pi}{{k_c}^2 b}A_{mn}sin\left(\frac{m\pi x}{a}\right)cos\left(\frac{n\pi y}{b}\right)e^{-j\beta z} \tag{2.48.b}$$

$$H_x = j\frac{\omega\varepsilon n\pi}{{k_c}^2 b}A_{mn}sin\left(\frac{m\pi x}{a}\right)cos\left(\frac{n\pi y}{b}\right)e^{-j\beta z} \tag{2.48.c}$$

$$H_y = -j\frac{\omega\varepsilon m\pi}{{k_c}^2 a}A_{mn}cos\left(\frac{m\pi x}{a}\right)sin\left(\frac{n\pi y}{b}\right)e^{-j\beta z} \tag{2.48.d}$$

2.5.3. Cutoff Frequency

For a rectangular waveguide, the propagation constant, β, is represented in terms of wavenumber, k, and cutoff wavenumber, k_c, as

$$\beta = \sqrt{k^2 - \left(\frac{m\pi}{a}\right)^2 - \left(\frac{n\pi}{b}\right)^2} \tag{2.49}$$

The equation above holds for both TE and TM mode waves. Assuming that the waveguide is loaded with a lossless material, the propagation constant vanishes at the wavenumber, which is called as cutoff wavenumber of the *mn* mode and this is given as:

$$k = (k_c)_{mn} = \sqrt{\left(\frac{m\pi}{a}\right)^2 + \left(\frac{n\pi}{b}\right)^2} \tag{2.50}$$

The modes are considered as propagation mode, cutoff mode and evanescent mode in terms of their frequencies or wavenumbers. In order for the wave to be a propagation mode, the condition is $k>(k_c)_{mn}$. If this condition is not valid, the wave is either in cutoff mode, $k=(k_c)_{mn}$, or in evanescent mode, $k<(k_c)_{mn}$.

$$\beta = \sqrt{k^2 - (k_c)_{mn}^2} \quad where \quad k = 2\pi f\sqrt{\varepsilon\mu}, k_c$$
$$= 2\pi f_c\sqrt{\varepsilon\mu} \quad and \quad f_c \; is \; cutoff \; frequency$$

$$j\beta = \begin{cases} j\sqrt{k^2 - (k_c)_{mn}^2} & ; k > (k_c)_{mn} \\ 0 & ; k = (k_c)_{mn} \\ \sqrt{(k_c)_{mn}^2 - k^2} & ; k > (k_c)_{mn} \end{cases} \tag{2.51}$$

and

$$j\beta = \begin{cases} jk\sqrt{1-\left({}^{f_c}/_{f}\right)^2} & ;f > f_c \\ 0 & ;f = f_c \\ k_c\sqrt{1-\left({}^{f}/_{f_c}\right)^2} & ;f > f_c \end{cases} \tag{2.52}$$

where

$$(f_c)_{mn} = \frac{(k_c)_{mn}}{2\pi\sqrt{\varepsilon\mu}} \Rightarrow$$

$$(f_c)_{mn} = \frac{1}{2\pi\sqrt{\varepsilon\mu}}\sqrt{({}^{m}/_{a})^2 + \left({}^{n}/_{b}\right)^2} \tag{2.53}$$

The cutoff wavelength, λ_c, can also be written in terms of cutoff frequency and it is represented as

$$(\lambda_c)_{mn} = {}^{c}/_{(f_c)_{mn}} \Rightarrow$$

$$(\lambda_c)_{mn} = \frac{1}{\sqrt{\varepsilon\mu}(f_c)_{mn}} \tag{2.54}$$

where

$$c = {}^{1}/_{\sqrt{\varepsilon\mu}}$$

2.5.4. Fundamental and Degenerate Modes

The mode having the lowest cutoff frequency is called as the fundamental mode. It also depends on the geometry of a rectangular waveguide such that for TE modes, if $a \geq b$, then the fundamental mode is TE_{10}, if vice versa, then TE_{01} is accepted as the fundamental mode.

The modes with the same propagation constants or cutoff frequency but having different field patterns are named as degenerate modes. For example, except that TE_{0n} and TM_{mn} modes, since m or n cannot be zero for TM modes, TE_{mn} and TM_{mn} are degenerate modes because of the fact that the definitions of cutoff frequency for those are same.

2.6. RESONATORS

Metamaterials are one of the most famous research areas for scientists interested in electromagnetics in recent years. One reason why metamaterials are very attractive to them is that they have properties cannot be found in the nature and in ordinary materials. The materials found in nature have positive permittivity and positive permeability values. However, with appropriate design of the microwave circuits, which are composed of dielectric materials and conductors, and under suitable frequencies negative values of permittivity and permeability can be reached [10]. This allows us to design waveguides, antennas, and various microwave circuits elements like filters with smaller sizes. In addition to these, at certain frequencies, left-handed propagation was observed with the materials that have negative permittivity and permeability [11]. Also the materials showing these artificial properties can be called as left-handed materials and their properties produce a left-handed coordinate system. Additionally, another property that is negative for such material is index of refraction. The important results of this are having direction of propagation opposite to direction

of energy flow which means direction of the two velocities, group and phase velocity, are reversed [12].

Split ring resonators (SRRs) are the designs showing magnetic resonance, which is the situation when magnitude of the capacitive reactance equals to magnitude of the inductive reactance, properties at specific frequency values [13]. They are composed of two interwoven rings with splits or slits positioned on opposite directions of the rings. These splits and the space between the rings provide high capacitive effects and thanks to this, the conduction can be achieved. Also, thanks to these, magnetic resonance is observed and the resonant wavelengths, which are much larger than the size of SRRs, can be obtained. The rings are made from metals that have nonmagnetic properties on top of dielectric materials like FR-4 where the FR stands for flame retardant. Moreover, researchers and scientist use SRRs under gigahertz frequencies but for some experiments and applications they can be designed to operate at terahertz frequency bands.

2.6.1. Equivalent Circuit Model and Types of SRRs

In the literature there are several models for the SRRs and the simplest equivalent model of SRRs is an LC circuit. It can be a parallel LC circuit, whose property is that capacitance increases when the inductance decreases, or a series LC circuit, whose working principle is opposite to the parallel LC circuits.

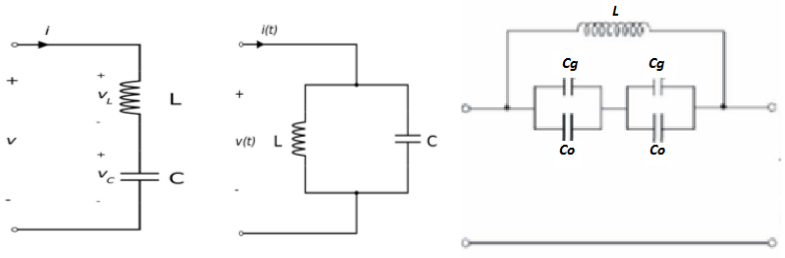

(a) (b)

Figure 2.3: Series and parallel LC circuit [13]

The resonant frequency for these circuits can be found by the following formula.

$$f = \frac{1}{2\pi\sqrt{LC}} \tag{2.55}$$

In addition to these, the models in Figure 2.3.a can be the equivalent circuit model of the SRRs, whose shapes can be circular or square, in Figure 2.3.a. When the SRRs have two rings the equivalent model can be the one in Figure 2.3.b. In Figure 2.3.b, there are two different capacitances one is C_o, distributed capacitance due to rings, and the other is C_g, the capacitances due to the splits.

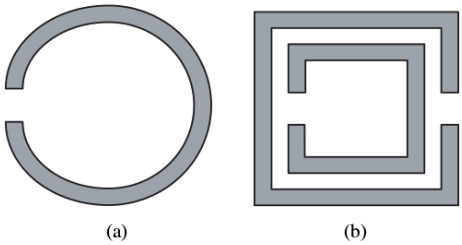

Figure 2.4: (a) Circular SRR with single ring, (b) square SRR with two rings

The most general type of SRRs is circular one with a single ring shown in Figure 2.4.a or the two concentric one. The difficulty for those is controlling the coupling between the circles. Thanks to the rectangular SRRs, people overcome this problem and besides, appropriate inner couplings are achieved [14].

2.6.2. Effects of Design Parameters of SRRs

2.6.2.1. Effects on Electric and Magnetic Fields

Pendry *et al* presented the SRR design and this design as mentioned before, consists of two concentric metallic rings. Also they have splits and separated by a gap. The reason why split and separation gap exist in the design is that the magnetic resonance is generated by them [15]. In Figure 2.5, the metal width, w, the split width, s, and the separation distance, t, can be seen.

Figure 2.5: General model of a square SRR

There are capacitance effects that occur due to the existence of splits and the gap. The current flows through the metallic structure by the mutual capacitance of the gap while the capacitances by the splits are trying to block the current flow [15].

When the SRRs are used to form an array, then at the resonance frequency or at the frequencies close to it, the negative permeability is observed. Moreover, at resonance frequencies, current loops are induced around the metallic part of the SRRs by applied uniform and time-varying magnetic field. Also the behavior of oscillation of *LC* circuit exists by the rings and due to current loop's being closed through the capacitance by the gaps, the *LC* circuit resonator effect is seen. Like the magnetic field, current loops are also generated by electric field. This electric field is perpendicular to the surface that the slits are on and it lies in the particle's plane [16].

2.6.2.2. Effects on Resonance Frequency

In this section, it will be presented how the resonance frequency is affected by changes in the design parameters. Many researchers probed this topic and their publications shed light on the design principles of SRRs in order to achieve perfection and design the SRRs truthfully and according to the needs.

Castro *et al* set up and experiment and studied the effect of slit widths on resonance frequency. For this study, SRRs with different slit widths are manufactured. After that, a rectangular waveguide was loaded with the manufactured SRRs. Then, the

experimental setups were connected to a network analyzer and for the dominant mode, TE_{10}, changes in resonance frequencies were monitored. Also these experiment results were compared with a simulation program's output and verified. As a conclusion it was stated that increase in slit width increases the resonance frequency since the capacitance and mutual inductance decrease [17].

In addition to these, in Pradeep's *et al* work, manufactured SRRs was placed on a 50 Ω transmission line and by using significates of the S_{21}, the behavior of resonance frequency was determined. Again, the setup was connected to a network analyzer and the system was excited with signal at fundamental mode. They showed that due to the effects of inductive and capacitive variations, increase in metal widths makes the resonance frequency also increase [16]. Additionally, another important result obtained was similar to the Castro's *et al* that the resonance frequency was slightly affected by the change of the slit width in the same manner.

Furthermore, Aydin *et al* published a more detailed article than the ones mentioned above. Their study was again based on the effects of design parameters on the magnetic resonance frequency. Differently, the SRRs were placed between two monopole antennas and the electromagnetic waves are tried to be measured. On top of changing the slit and metal widths, how the resonance frequency influenced by the change in the gap between the metallic wires was examined. The experiments and the simulations at the same frequency presented that the larger the gap distance, the larger the resonance frequency. This effect was results of decrease in the mutual inductance and capacitance between the metallic wires. Moreover, in this article, not only the geometrical structure of SRRs was changed but also additional capacitances effects were studied. By integrating capacitors with different capacitances, the transmission was measured. The outcome of measurements showed that the resonance frequency decreases with increasing additional capacitance [12].

In addition to the studies mentioned above, the concern of this thesis was to investigate s-parameters of SRRs with the change of their design parameters. In MATLAB, in order to achieve to code PEC structure, the boundary condition on its surface was chosen as incident field equaled to scattered field. Also, the elements inside SRR were

excluded from the matrix. Therefore, hollow, 3D, and PEC structure were designed and elements on its surface became 2D triangular elements. The details of the experiments conducted concerning SRR were shared in chapter 5.

Since metamaterials and their applications are popular research areas nowadays, many more papers and dissertations are being published concerning the SRRs. Different types, designs and implementations of them are being dealt. The answers of questions about SRRs are being brought to light day by day.

CHAPTER 3

3D FINITE ELEMENT IMPLEMENTATION

3.1. BASICS OF FINITE ELEMENT METHOD

Finite Element Method (FEM) is a numerical technique to get approximate solutions of partial differential equations (PDE). FEM is a powerful variational method used in various engineering disciplines and science fields. Thanks to FEM, any structure or domain having any geometry can be modeled without requiring high CPU load and memory since the matrices that will be solved are sparse.

In this method, the entire domain is divided into smaller subdomains which are called elements. After that, these elements are connected in a systematical way at the nodes which are the connection points of the elements in order to model the domain. Then it can be imagined that all the structures are combinations of the elements. In other words, by these procedures, the domains are discretized and meshes are achieved. This subdivision helps us to represent the solution in an easy way, to find an accurate solution while having complex structures, and to take into account different materials with different properties if there is any. The types of finite elements are selected by considering the number of dimensions of the entire domain, the shape of the structure, and the tolerance of accuracy of result. Also choice of the size of elements is very important because while the size decreases the memory usage and the cost increase although elements with smaller sizes provide more accurate results. Some examples of finite elements are shown in Figure 3.1 and they are classified according to the dimension of the structure.

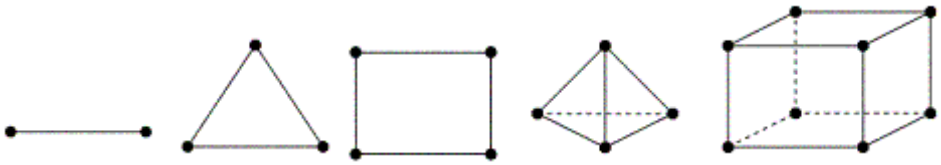

3.1.a 3.1.b 3.1.c 3.1.d 3.1.e

Figure 3.1: 1D, 2D, and 3D finite elements types

Here, 3.1.a is 1D linear element, 3.1.b and 3.1.c are 2D triangular and quadrilateral elements respectively, and 3.1.d and 3.1.e are 3D tetrahedral and hexahedral elements, respectively..

Mesh quality is an important criterion that must be taken into account during mesh generation. The aspect ratio which is ratio of longest edge to shortest edge, skew angle, and the amount of how elements diverge from ideal elements are important subjects for element quality. The length of an edge must be small enough as mentioned before and this distance can be chosen as λ/10.

After the choice of the type of finite element and the discretization of the domain by using the elements, one can proceed to the next step that is specifying the shape functions. They are also named as basis functions that interpolate the solution within the finite elements. The equations 3.1, 3.2 and 3.3 state the mathematical formulations of examples of 1D, 2D and 3D shape functions respectively. In equations 3.2 and 3.3, a_i, b_i, c_i and d_i are the coefficients to be calculated.

$$N_1(x) = \frac{x_2 - x}{x_2 - x_1}, N_2(x) = \frac{x - x_1}{x_2 - x_1} \tag{3.1}$$

$$N_i = a_i + b_i x + c_i y, \quad i = 1, 2 \; or \; 3 \tag{3.2}$$

$$N_i = a_i + b_i x + c_i y + d_i z, \quad i = 1, 2, 3 \; or \; 4 \tag{3.3}$$

Variational calculus is an analysis used to maximize and minimize the functionals which are mostly defined as themselves and their derivatives in definite integrals. While applying finite element analysis, the PDEs are transformed into their functionals and the variational calculus is the way to get their functional forms. A common variational method is the Method of Weighted Residuals, where the PDE is multipled with weight functions and integrated over the domain. Here, if the weight functions are chosen to be equal to the shape functions, this method is known as Galerkin method. Then, by use of integration by parts and the boundary conditions related to the PDEs, the weak variational form of the PDE is found. Rayleigh-Ritz method is another variational method to solve the PDEs. The scope of Rayleigh-Ritz method is to reach solution by finding the extreme values of the known functional. It is better to make use of this method if the functionals related to the PDEs are known.

Finally, the solutions for each element in region of interest are assembled in matrices and solved with appropriate matrix solvers.

Up to now, the main idea and steps of FEM are discussed, and the mathematical formulations related to those are presented in the rest of this section.

Let u be an unknown function and f be a known function. Then, a boundary value problem (BVP) can be described as

$$\mathcal{L}u = f$$

where $\mathcal{L}$ is a linear operator which is positive-definite and self adjoint. And the vector space of shape function for elements can be expressed as

$$\boldsymbol{N}^e = \begin{bmatrix} N_1^e \\ N_2^e \\ \vdots \\ N_N^e \end{bmatrix}$$

and the solution for each element can be assumed as

$$\boldsymbol{u}^e = \sum_i^n N_i^e \, u_i^e$$

where u_i^e and N_i^e are value of the unknown function and shape function respectively and the vector space of $\boldsymbol{u^e}$ can be

$$\boldsymbol{u}^e = \begin{bmatrix} u_1^e \\ u_2^e \\ \vdots \\ u_N^e \end{bmatrix}$$

The main aim is to solve matrix equation, $[A]\boldsymbol{u}=\boldsymbol{b}$ in which $[A]$ is a result of assembling of local element matrices, $[A^e]$ and $\boldsymbol{b}$, includes $\boldsymbol{b^e}$s, is an unknown vector to be found. In general, the expression of functionals for elements which depends on unknown functions, local element matrices and unknown vectors can be written as

$$\boldsymbol{F^e} = [A^e]\boldsymbol{u^e} - \boldsymbol{b^e}$$

And for an element, the functional can expressed in terms of BVP and element shape functions in an integral form.

$$F_i^e = \int (\mathcal{L}\boldsymbol{u^e} - f) N_i^e \, d\Omega$$

By substituting the expression of solution for each element into the above equation, a detailed one can be stated as

$$F_i^e = \boldsymbol{u^e} \int N_i^e \mathcal{L}(\boldsymbol{N^e})^T d\Omega - \int f N_i^e \, d\Omega$$

$$\text{where} \quad \sum_i^n N_i^e \, u_i^e = (\boldsymbol{N^e})^T \boldsymbol{u^e}$$

This statement gives us the expressions for local element matrices and unknown element vectors as follows

$$A_{ij}^e = \int N_i^e \mathcal{L}(\boldsymbol{N^e})^T d\Omega \quad and \quad b_i = \int f N_i^e \, d\Omega$$

Lastly, after assembling the local element matrices and vectors, the boundary conditions are imposed and the system of matrix equation given below is solved.

$$\boldsymbol{F} = \sum_1^E [A^e]\boldsymbol{u^e} - \boldsymbol{b^e} = 0 \quad \Rightarrow$$

$$[A]\boldsymbol{u} = \boldsymbol{b}$$

where the range of e is 1 to E which is the number of total elements in the computational domain.

3.2. WAVE EQUATION AND ITS WEAK VARIATIONAL FORM

The wave equation can be derived simply by taking curl of the first Maxwell equation in frequency domain and substituting the second Maxwell equation in frequency domain in right hand side of the resulted equation. When a scatterer exists in a medium, the wave equation, $\boldsymbol{E}$, is written as the sum of the incident field and the scattered field. Also a BVP can be derived for the scattered field with boundary condition including the incident field. And the derivation of the BVP is given as

$$\nabla \times \nabla \times \boldsymbol{E} = -j\omega\mu\nabla \times \boldsymbol{H} \Rightarrow$$

$$\nabla \times \nabla \times \boldsymbol{E} = \omega^2\varepsilon\mu\boldsymbol{E} \Rightarrow$$

$$\nabla \times \nabla \times \boldsymbol{E} - k^2\boldsymbol{E} = 0 \tag{3.4}$$

where $\boldsymbol{E}=\boldsymbol{E}^i+\boldsymbol{E}^s$ and $\boldsymbol{E}^i$ is the incident field and $\boldsymbol{E}^s$ is scattered field

$$\nabla \times \nabla \times \boldsymbol{E}^s = k^2\boldsymbol{E}^s$$

where $\boldsymbol{n} \times \boldsymbol{E}^s + \boldsymbol{n} \times \boldsymbol{E}^i = 0$

In free space, $\Omega_{fs,}$ the inner product of the wave equation and weight function is taken as mentioned in section 3.1 and let this function be $\boldsymbol{W}$.

$$\int (\nabla \times \nabla \times \boldsymbol{E}^s) \cdot \boldsymbol{W} d\Omega = k^2 \int \boldsymbol{E}^s \cdot \boldsymbol{W} d\Omega \tag{3.5}$$

Using the divergence theorem formulated in Equation 3.7 and the vector identity in equation 3.8, the weak variational form of the wave equation can be written as

$$\int (\nabla \times \boldsymbol{E^s}) \cdot (\nabla \times \boldsymbol{W}) d\Omega - k^2 \int \boldsymbol{E^s} \cdot \boldsymbol{W} d\Omega = 0 \tag{3.6}$$

where

$$\oiint \boldsymbol{F} \cdot d\boldsymbol{S} = \iiint \nabla \cdot \boldsymbol{F} dV\,; \quad \boldsymbol{F} = \boldsymbol{E^s} \times \boldsymbol{W} \text{ and } \iiint dV = \int d\Omega \tag{3.7}$$

$$(\nabla \times \boldsymbol{E^s}) \cdot \boldsymbol{W} = \boldsymbol{E^s} \cdot (\nabla \times \boldsymbol{W}) + \nabla \cdot (\boldsymbol{E^s} \times \boldsymbol{W}) \tag{3.8}$$

3.3. 3D FEM FORMULATION

After finding the weak variational form of the wave equation, it can be solved using FEM and as the element type tetrahedral elements, in Figure 3.1.d, are going to be used.

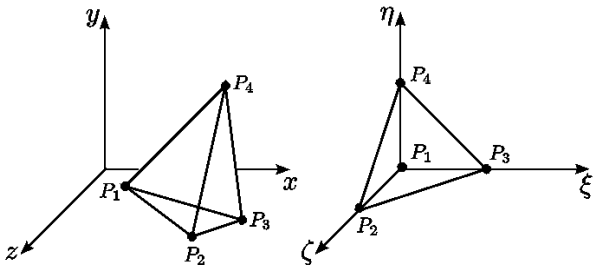

3.2.a 3.2.b

Figure 3.2: Tetrahedral finite element in original and transformed coordinate systems

In order to simplify the calculations, the original rectangular coordinate system is transformed to a new coordinate system whose axes are ξ, η, and ζ as shown in figure 3.2 [18].

Then, recalling equation 3.3, the new shape functions can be expressed considering the transformed coordinate system as follows.

$$N_1(\xi,\eta,\zeta) = 1 - \xi - \eta - \zeta \tag{3.9.a}$$

$$N_2(\xi,\eta,\zeta) = \xi \tag{3.9.b}$$

$$N_3(\xi,\eta,\zeta) = \eta \tag{3.9.c}$$

$$N_4(\xi,\eta,\zeta) = \zeta \tag{3.9.d}$$

Also, the general form of the shape functions at the edges of elements for transformed coordinate system, equation 3.10, and the shape functions for each six edges, equations 3.11.a-3.11.f, from equation 3.10 can be stated as

$$\boldsymbol{N_i}(\xi,\eta,\zeta) = (N_{i1}\nabla N_{i2} - N_{i2}\nabla N_{i1})l_i \tag{3.10}$$

where l_i is the length of the edge, i_1 and i_2 are the nodes of the edge and N_{i1} and N_{i2} are shape functions for the nodes of the edge

$$\boldsymbol{N_1}(\xi,\eta,\zeta) = (\nabla\xi(1-\eta-\zeta) + \xi\nabla\eta + \xi\nabla\zeta)l_1 \tag{3.11.a}$$

$$\boldsymbol{N_2}(\xi,\eta,\zeta) = (\nabla\eta(1-\xi-\zeta) + \eta\nabla\xi + \eta\nabla\zeta)l_2 \tag{3.11.b}$$

$$\boldsymbol{N_3}(\xi,\eta,\zeta) = (\nabla\zeta(1-\eta-\xi) + \zeta\nabla\eta + \zeta\nabla\xi)l_3 \tag{3.11.c}$$

$$\boldsymbol{N_4}(\xi,\eta,\zeta) = (\xi\nabla\eta + \eta\nabla\xi)l_4 \tag{3.11.d}$$

$$\boldsymbol{N_5}(\xi,\eta,\zeta) = (\zeta\nabla\xi + \xi\nabla\zeta)l_5 \tag{3.11.e}$$

$$\boldsymbol{N_6}(\xi,\eta,\zeta) = (\eta\nabla\zeta + \zeta\nabla\eta)l_6 \tag{3.11.f}$$

In addition to these, gradients of ξ, η, and ζ are calculated by taking the inverse of the matrix whose expression is given in equation 3.15. The first column of the inverse

matrix gives the gradient of ξ, the second column gives the gradient of η, and from the entries of last column the gradient of ζ is obtained.

The Jacobian matrix, which involves first order partial derivatives of *x*, *y* and *z* in equations 3.13, according to ξ, η, and ζ, can be written by rewriting the points of the original coordinate system in terms of points of the transformed coordinate system.

$$J = \begin{bmatrix} \frac{\partial x}{\partial \xi} & \cdots & \frac{\partial z}{\partial \xi} \\ \vdots & \ddots & \vdots \\ \frac{\partial x}{\partial \zeta} & \cdots & \frac{\partial z}{\partial \zeta} \end{bmatrix} \tag{3.12}$$

In general *x*, *y* and *z* can be expressed as

$$x = \sum_{i=1}^{4} x_i \, N_i(\xi, \eta, \zeta) \tag{3.13.a}$$

$$y = \sum_{i=1}^{4} y_i \, N_i(\xi, \eta, \zeta) \tag{3.13.b}$$

$$z = \sum_{i=1}^{4} z_i \, N_i(\xi, \eta, \zeta) \tag{3.13.c}$$

By taking the equation a step further and doing some algebraic manipulations, *x*, *y* and *z* in equation 3.13 can be restated as

$$x = x_1 + (x_2 - x_1)\xi + (x_3 - x_1)\eta + (x_4 - x_1)\zeta \quad (3.14.a)$$

$$y = y_1 + (y_2 - y_1)\xi + (y_3 - y_1)\eta + (y_4 - y_1)\zeta \quad (3.14.b)$$

$$z = z_1 + (z_2 - z_1)\xi + (z_3 - z_1)\eta + (z_4 - z_1)\zeta \quad (3.14.c)$$

Using equations 3.12 and 3.14.a-3.14.c, the Jacobian matrix is expressed as

$$J = \begin{bmatrix} x_2 - x_1 & y_2 - y_1 & z_2 - z_1 \\ x_3 - x_1 & y_3 - y_1 & y_4 - y_1 \\ x_4 - x_1 & y_4 - y_1 & z_4 - z_1 \end{bmatrix} \quad (3.15)$$

Now, using the weak variational form of the wave equation in 2.6 and the expression of scattered field for edges of each element in equation 3.16, the local matrices, a_{ij}^e and b_j^e, can be calculated. Here, the weight function, $\boldsymbol{W}$, is chosen to be equal to the shape functions that is the Galerkin approach is preferred.

$$\boldsymbol{E^{s,e}} = \sum_{i=1}^{6} \boldsymbol{N_i} E_i^e \quad (3.16)$$

where $\boldsymbol{N_i}$ is the shape function and E_i^e is the tangential field, is an unknown to be found, along the ith edge

The LHS of the obtained equation after substituting equation 3.16 into equation 3.6 gives a_{ij}^e, which is a 6x6 matrix and while getting b_j^e, a 6x1 matrix and whole entries are equal to zero, from the RHS of the equation.

In free space;

$$a_{ij}^{e} = \int (\nabla \times \boldsymbol{N_i}).\left(\nabla \times \boldsymbol{N_j}\right) d\Omega - k^2 \int \boldsymbol{N_i N_j} d\Omega \tag{3.17.a}$$

$$b_j^e = \begin{bmatrix} 0 \\ 0 \\ 0 \\ 0 \\ 0 \\ 0 \end{bmatrix} \tag{3.17.b}$$

where

$$\nabla \times \boldsymbol{N_1}(\xi, \eta, \zeta) = 2(\nabla\xi \times \nabla\eta + \nabla\xi \times \nabla\zeta) l_1 \tag{3.18.a}$$

$$\nabla \times \boldsymbol{N_2}(\xi, \eta, \zeta) = 2(\nabla\eta \times \nabla\xi + \nabla\eta \times \nabla\zeta) l_2 \tag{3.18.b}$$

$$\nabla \times \boldsymbol{N_3}(\xi, \eta, \zeta) = 2(\nabla\zeta \times \nabla\eta + \nabla\zeta \times \nabla\xi) l_3 \tag{3.18.c}$$

$$\nabla \times \boldsymbol{N_4}(\xi, \eta, \zeta) = 2(\nabla\xi \times \nabla\eta) l_4 \tag{3.18.d}$$

$$\nabla \times \boldsymbol{N_5}(\xi, \eta, \zeta) = 2(\nabla\xi \times \nabla\zeta) l_5 \tag{3.18.e}$$

$$\nabla \times \boldsymbol{N_6}(\xi, \eta, \zeta) = 2(\nabla\eta \times \nabla\zeta) l_6 \tag{3.18.f}$$

The expressions for $\nabla\xi, \nabla\eta,$ and $\nabla\zeta$ in the equations 3.18.a-3.18.f can be calculated according to the information given before.

3.4. SCATTERING PARAMETERS CALCULATION

Scattering parameters (S-parameters) are the parameters that define the behavior of linear electric circuits under steady state conditions. The properties of networks such as reflection coefficient, transmission coefficient, and gain can be written in terms of S-parameters.

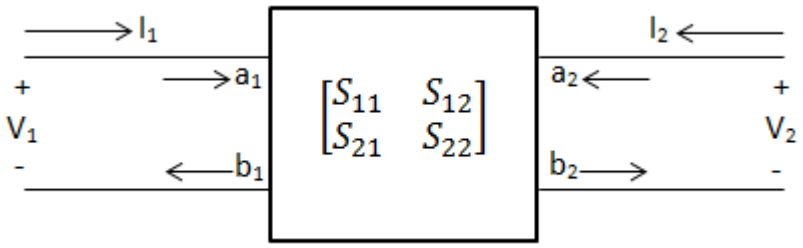

Figure 3.3: 2-port network defined by S-parameters

In order to model an n-port network by S-parameters, incident power waves (a_1, a_2, a_3,…, a_n) and reflected power waves (b_1, b_2, b_3,…, b_n) must be defined. Figure 3.3 shows a 2-port network whose S-parameter definition is given by

$$\begin{bmatrix} b_1 \\ b_2 \end{bmatrix} = \begin{bmatrix} S_{11} & S_{12} \\ S_{21} & S_{22} \end{bmatrix} \begin{bmatrix} a_1 \\ a_2 \end{bmatrix} \tag{3.19}$$

In addition, complex power waves are written in terms of input/output currents and voltages and constant characteristic reference impedances at the input and output (Z_{o1}, Z_{o2}).

$$a_1 = \frac{V_1 + I_1 Z_{o1}}{2\sqrt{Z_{o1}}} \tag{3.20.a}$$

$$a_2 = \frac{V_2 + I_2 Z_{o2}}{2\sqrt{Z_{o2}}} \tag{3.20.b}$$

$$b_1 = \frac{V_1 - I_1 Z_{o1}}{2\sqrt{Z_{o1}}} \tag{3.20.c}$$

$$b_2 = \frac{V_2 - I_2 Z_{o2}}{2\sqrt{Z_{o2}}} \tag{3.20.d}$$

Furthermore, reflection coefficient and transmission coefficient are equal to S_{11} and S_{21} respectively when the output is perfectly matched to characteristic reference impedance Z_{o2}. In general, the equations for these can be stated as

$$R = S_{11} + \frac{S_{12}S_{21}\Gamma_L}{1 - S_{22}\Gamma_L} \tag{3.21.a}$$

$$T = S_{21} + \frac{S_{12}S_{21}\Gamma_L}{1 - S_{22}\Gamma_L} \tag{3.21.b}$$

In equations 3.21.a and 3.21.b, Γ_L is the reflection coefficient at the load and equals to zero when the load is perfectly matched.

For an object in a waveguide, like in figure 3.4, in which the wave propagates in TE_{10} mode, reflection coefficient and transmission coefficient are calculated by applying the following formulas respectively. Scattering parameters are found by considering the surfaces at the both sides of the waveguide. Reflection coefficient (S_{11} or R), is calculated by using the scattered fields, $\boldsymbol{E}^s$, on the surface, S_1, that is designated at the side the incident wave is coming towards the object while for the transmission coefficient (S_{21} or T), the total fields, $\boldsymbol{E}^t$, become a part of the calculation at the surface, S_2, which is specified at the other side of the object [19].

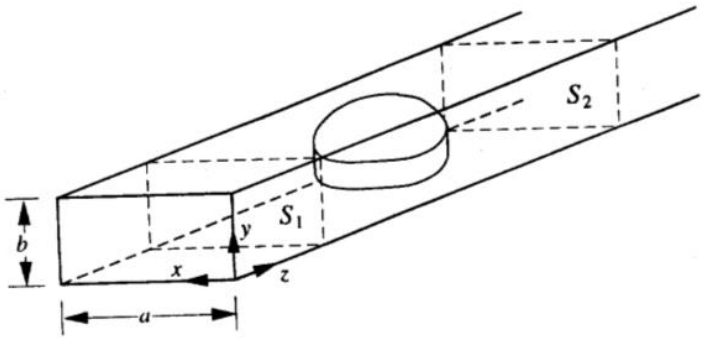

Figure 3.4: An object in a rectangular waveguide [19]

$$S_{11} = \frac{|\boldsymbol{E}^s|_{max}}{|\boldsymbol{E}^i|_{max}} \tag{3.22.a}$$

$$S_{21} = \frac{|\boldsymbol{E}^t|_{max}}{|\boldsymbol{E}^i|_{max}} \tag{3.22.b}$$

CHAPTER 4

PERFECTLY MATCHED LAYER (PML)

In numerical solutions of partial differential equations (PDE), truncation of the computational domain is needed. Except solutions of periodic structures and some structures whose solutions decay with admissible speeds naturally, artificial regions have to be in consideration in order to be able to truncate the domain properly.

The solutions of wave equations decay slowly e.g. the decay rate is $1/(\sqrt{r})^{(d-1)}$ when the distance that the waves decay is r in d dimensions. The decay rate problem is overcome by regarding absorbing boundary conditions (ABC). In this technique, structure is considered to be extended to infinity. Projecting from the given data which is inside points at the edges is the main idea of ABC. However, ABC is useful when the computational domain is one dimensional. For 2D or 3D problems having inhomogeneous medium, applications of ABC become very complex and difficult.

A more efficient method for mesh truncation is to use an artificial absorbing layer known as perfectly matched layer (PML). One of the most important properties of PML is that the waves, coming and hitting the PML, do not reflect but all of them transmitted into the layer. Additionally, the transmitted waves attenuate and decay. At the outer boundary of the PML region, Ω_{PML}, the waves vanish, and hence totally absorbed by the PML region.

In this thesis, the locally-conformal PML method is presented. This method depends on complex coordinate transformations. Thanks to complex coordinate stretching, the transformations of elements from real coordinate system to complex coordinate system are performed [20].

4.1. LOCALLY-CONFORMAL PML METHOD

This method was presented by Ozgun and Kuzuoglu ([21]-[22]). Its underlying concept is complex coordinate transformation. In the design, there are some conditions that have to be satisfied namely transmitting of all waves in the Ω_{PML}, decaying of waves in Ω_{PML} and on the surface of Ω_{PML} the magnitudes of the waves have to be insignificant [20]. Assuming that, like in figure 4.1, the computation region is union of Ω_{PML} and Ω_{PHY}, which is a physical region that can be composed of different types of materials like vacuum, and the time dependence is e^{jwt}, the mapping from real coordinates of $\boldsymbol{r}$ to complex coordinates of $\boldsymbol{r'}$ is done by applying the following formulas [23].

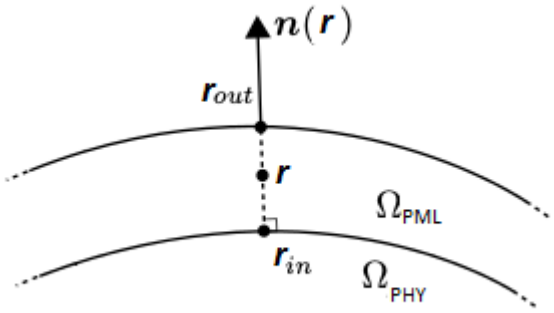

Figure 4.1: Modelling of implementation of the method

$$\boldsymbol{r}^{\iota} = \boldsymbol{r} + \frac{1}{jk} f(\boldsymbol{r})\boldsymbol{n}(\boldsymbol{r}) \tag{4.1}$$

where k is wavenumber while absorption vector is denoted by $\boldsymbol{n(r)}$, $\boldsymbol{f(r)}$ represents the absorption function and they are written as

$$\boldsymbol{n}(\boldsymbol{r}) = \frac{\boldsymbol{r} - \boldsymbol{r}_{in}}{\|\boldsymbol{r} - \boldsymbol{r}_{in}\|} \tag{4.2}$$

$$f(\boldsymbol{r}) = \frac{a\|\boldsymbol{r} - \boldsymbol{r}_{in}\|^m}{m\|\boldsymbol{r}_{out} - \boldsymbol{r}_{in}\|^{m-1}} \tag{4.3}$$

In formula 4.3, *a* is a positive parameter and *m* is a positive integer. Also, the distance between $\boldsymbol{r}_{out}$ and $\boldsymbol{r}_{in}$ ($\|\boldsymbol{r}_{out} - \boldsymbol{r}_{in}\|$) can be denoted by d_{PML}. Moreover, by means of *a*, proper rate of decay of the waves in Ω_{PML} are ensured [20]. Here, $\boldsymbol{r}_{in}$ is found by minimizing the following

$$\min_{\boldsymbol{r}_{in} \in R} \|\boldsymbol{r} - \boldsymbol{r}_{in}\| \tag{4.4}$$

Furthermore, the PML width, which mainly depends on wavelength, must be chosen properly e.g. they cannot be too long or too short since ill-conditioning and absorption troubles may occur [24]. In general, the PML thickness can be chosen in the range λ/4-λ/2. .

4.2. FEM IN 3D COMPLEX SPACE

Given the expression of electric field in PML region like in (4.5), electric field, magnetic field and Jacobian tensor equations are derived as in (4.6.a), (4.6.b) and (4.7) respectively.

$$\boldsymbol{E}^{\boldsymbol{c}} = \boldsymbol{a}_{\boldsymbol{p}} e^{-jk\boldsymbol{a}_{\boldsymbol{k}}.\boldsymbol{r}} \tag{4.5}$$

where $\boldsymbol{a}_{\boldsymbol{p}}$ is a unit vector that denotes the polarization and $\boldsymbol{a}_{\boldsymbol{k}}$ must satisfy $\boldsymbol{a}_{\boldsymbol{k}}.\boldsymbol{n}(\boldsymbol{r}) > 0$.

$$\tilde{\nabla} \times \boldsymbol{E^c} = -j\omega\mu_o \boldsymbol{H^c} \tag{4.6.a}$$

$$\tilde{\nabla} \times \boldsymbol{H^c} = j\omega\varepsilon_o \boldsymbol{E^c} \tag{4.6.b}$$

$$\bar{\bar{J}} = \frac{\partial(\tilde{x}, \tilde{y}, \tilde{z})}{\partial(x, y, z)} = \begin{bmatrix} \frac{\partial \tilde{x}}{\partial x} & \frac{\partial \tilde{x}}{\partial y} & \frac{\partial \tilde{x}}{\partial z} \\ \frac{\partial \tilde{y}}{\partial x} & \frac{\partial \tilde{y}}{\partial y} & \frac{\partial \tilde{y}}{\partial z} \\ \frac{\partial \tilde{z}}{\partial x} & \frac{\partial \tilde{z}}{\partial y} & \frac{\partial \tilde{z}}{\partial z} \end{bmatrix} \tag{4.7}$$

Starting from Maxwell's equation in (4.6.a), weak variational form of the wave equation in complex space is written as in (4.9).

$$\tilde{\nabla} \times \tilde{\nabla} \times \boldsymbol{E^c} - k^2 \boldsymbol{E^c} = 0 \tag{4.8}$$

$$\int (\tilde{\nabla} \times \boldsymbol{E^c}).(\tilde{\nabla} \times \boldsymbol{W^c}) d\Omega_{PML} - k^2 \int \boldsymbol{E^c W^c}.d\,\Omega_{PML} = 0 \tag{4.9}$$

where $\tilde{\nabla}$ is nabla operator and $\boldsymbol{W^c}$ is weighted residual in complex space [20].

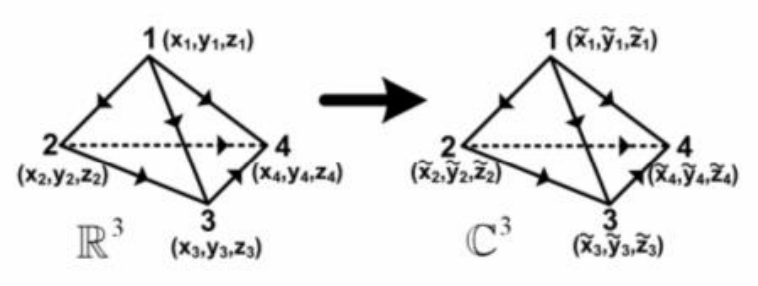

Figure 4.2: Transformation of 3D tetrahedral elements to complex space [20]

Figure 4.2 shows how to map the elements to complex elements. Using the weak variational form of the wave equation in 4.9 and the expression of scattered field for edges of each element in equation 4.10, the local matrix, a_{ij}^e, can be calculated. Here,

the weight function, $\boldsymbol{W^c}$, is chosen to be equal to the shape functions that is the Galerkin approach is preferred.

$$\boldsymbol{E^{c,e}} = \sum_{i=1}^{6} \boldsymbol{N_i} E_i^{c,e} \tag{4.10}$$

where $\boldsymbol{N_i}$ is the shape function and $E_i^{c,e}$ is the tangential field, is an unknown to be found, along the ith edge

The LHS of the obtained equation after substituting equation 4.10 into equation 4.9 gives a_{ij}^{e}, which is a 6x6 matrix, from the RHS of the equation [20].

In the complex space;

$$a_{ij}^{e} = \int \left(\tilde{\nabla} \times \boldsymbol{N_i}\right).\left(\tilde{\nabla} \times \boldsymbol{N_j}\right) d\Omega - k^2 \int \boldsymbol{N_i N_j} d\Omega \tag{4.11}$$

From now, the expression of unknown electric field can be calculated by using the information mentioned in chapter 3. The formulas, (3.9.a-d), (3.10) and (3.13.a-d), also holds for the complex space. However, changing ∇ with $\tilde{\nabla}$, x, y, z with $\tilde{x}, \tilde{y}, \tilde{z}$ respectively in these equations and by using the figure 3.2, unknown electric field in PML region and a_{ij}^{e} in terms of ξ, η, and ζ, can be written as [23]

$$\boldsymbol{E^{c,e}}(\xi, \eta, \zeta) = \sum_{i=1}^{6} \boldsymbol{N_i}(\xi, \eta, \zeta) E_i^{c,e} \tag{4.12}$$

$$\begin{aligned} a_{ij}^{e} = & \int \left(\tilde{\nabla} \times \boldsymbol{N_i}(\xi, \eta, \zeta)\right).\left(\tilde{\nabla} \times \boldsymbol{N_j}(\xi, \eta, \zeta)\right) d\Omega \\ & - k^2 \int \boldsymbol{N_i}(\xi, \eta, \zeta) \boldsymbol{N_j}(\xi, \eta, \zeta) d\Omega \end{aligned} \tag{4.13}$$

where $d\Omega = d\xi d\eta d\zeta$

Also the Jacobian matrix expression become

$$J = \begin{bmatrix} \tilde{x}_2 - \tilde{x}_1 & \tilde{y}_2 - \tilde{y}_1 & \tilde{z}_2 - \tilde{z}_1 \\ \tilde{x}_3 - \tilde{x}_1 & \tilde{y}_3 - \tilde{y}_1 & \tilde{z}_4 - \tilde{z}_1 \\ \tilde{x}_4 - \tilde{x}_1 & \tilde{y}_4 - \tilde{y}_1 & \tilde{z}_4 - \tilde{z}_1 \end{bmatrix} \tag{4.14}$$

CHAPTER 5

APPLICATION OF FEM IN SCATTERING PARAMETERS CALCULATION

The scope of this thesis is to calculate scattering parameters of split ring resonators by FEM. For modelings and simulations MATLAB (Matrix Laboratory) was used and the results are compared with those obtained by CST (Computer Simulation Technology). The studies were begun with design of a rectangular waveguide in MATLAB. The 3D structure was placed on the rectangular coordinate system and the mesh was generated. As 3D elements tetrahedron elements were preferred. Two open ends of the waveguide were considered as PML regions where the resonator was positioned at the middle (like in figure 3.4). After that, x, y, and z coordinates of elements, elements' nodes, and middle points of edges and elements' surface were individually found and saved for PML region, waveguide surface, inside of the waveguide and resonator, and resonator surface. Also, information of which edge and surface belongs to which element was noted down. Then, boundary conditions on waveguide and resonator surfaces were imposed according to TE_{10} mode incident wave and, complex coordinate transformations in PML regions were implemented. Later on, by taking surface integrals numerically, the scattered, reflected and total fields from resonator were summed up on the two surfaces at the both sides of resonator and also between the PML regions and resonator. Lastly, by means of field's summation on the surfaces, scattering parameters were calculated.

The MATLAB code was tested by changing different parameters in the design comparing with CST outcomes and also with the knowledge of TE_{10} mode fields appear as half sinusoidal. Initially, a simple structure, a rectangular prism, was placed in waveguide and by enlarging and reducing the size of the structure, change of

reflected and transmitted electric fields was tried to be observed. The expectations from the trials were to observe an increase in the reflected field and decrease in the transmitted filed, as the size gets larger. When the size of the structure is enlarged, the reflection surface gets larger. Also when it was reduced, the expectations were vice versa. The outputs satisfied not only the expectations but also the CST results. Taking the frequency as 3 GHz, results of two structures with sizes, in terms of wavelength, on x, y and z coordinates 0.1λ, 0.1λ, 0.1λ and 0.5λ, 0.3λ, 0.1λ respectively were considered where the waveguide sizes were 0.6λ, 0.4λ and 2.1λ. The results were in terms of their magnitudes, not in dB.

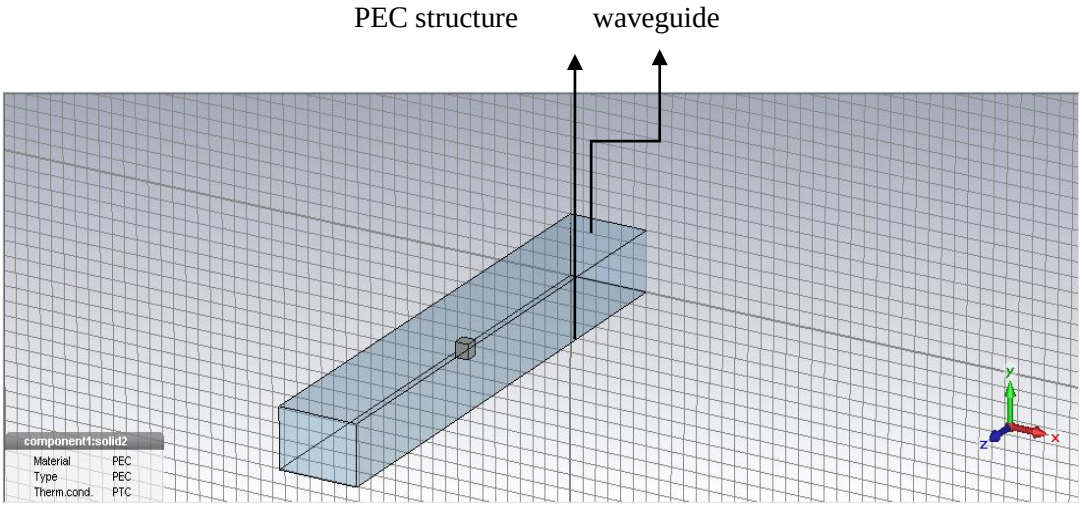

Figure 5.1: CST model of structure with sizes 0.1λx0.1λx0.1λ

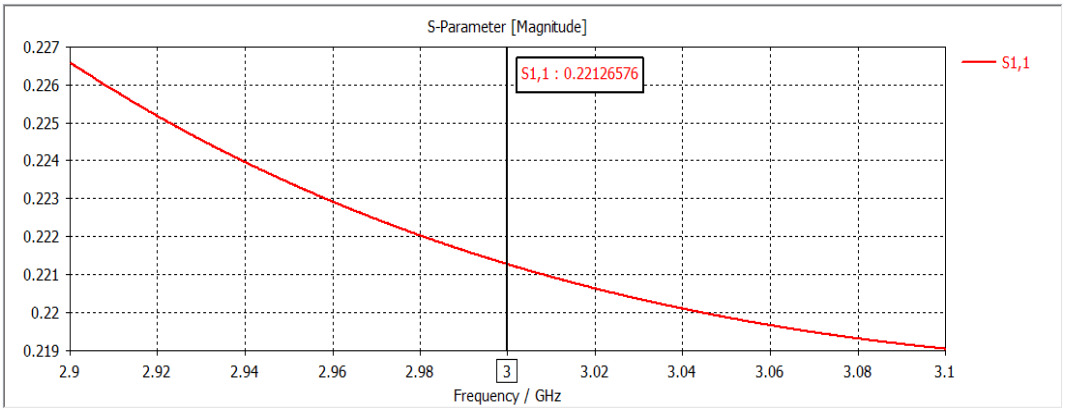

Figure 5.2: S11 of structure with sizes 0.1λx0.1λx0.1λ in CST

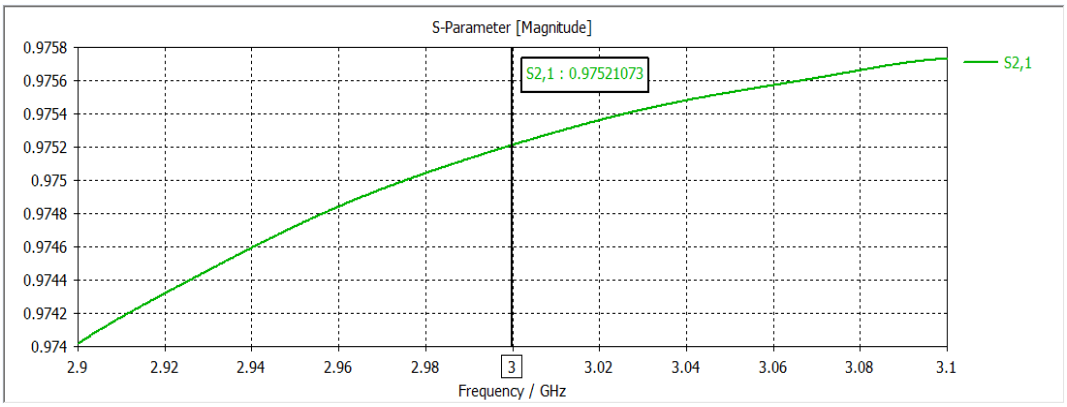

Figure 5.3: S21 of structure with sizes 0.1λx0.1λx0.1λ in CST

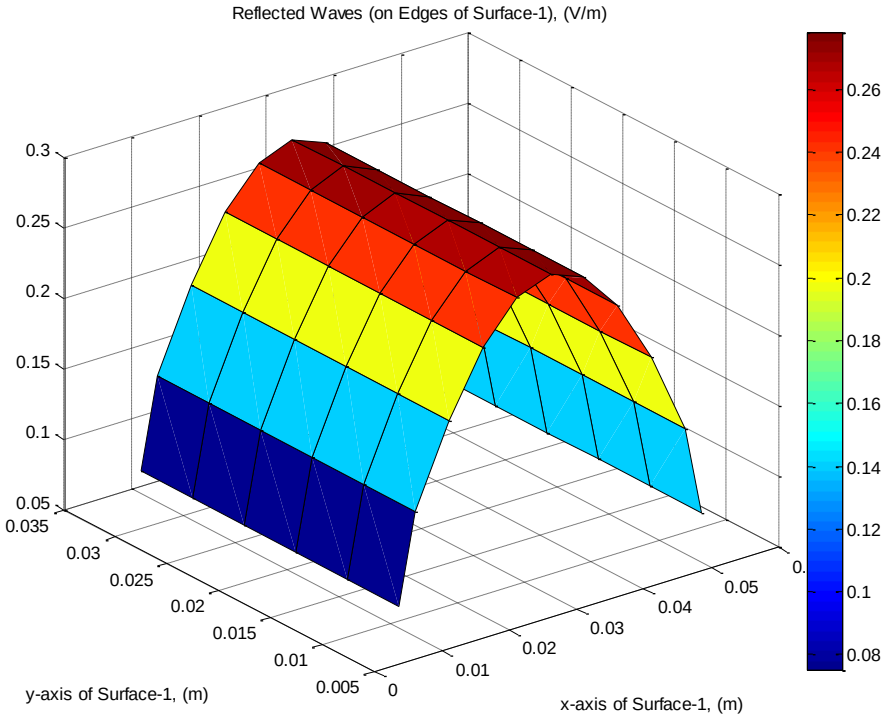

Figure 5.4: Reflected waves from structure with sizes 0.1λx0.1λx0.1λ in MATLAB

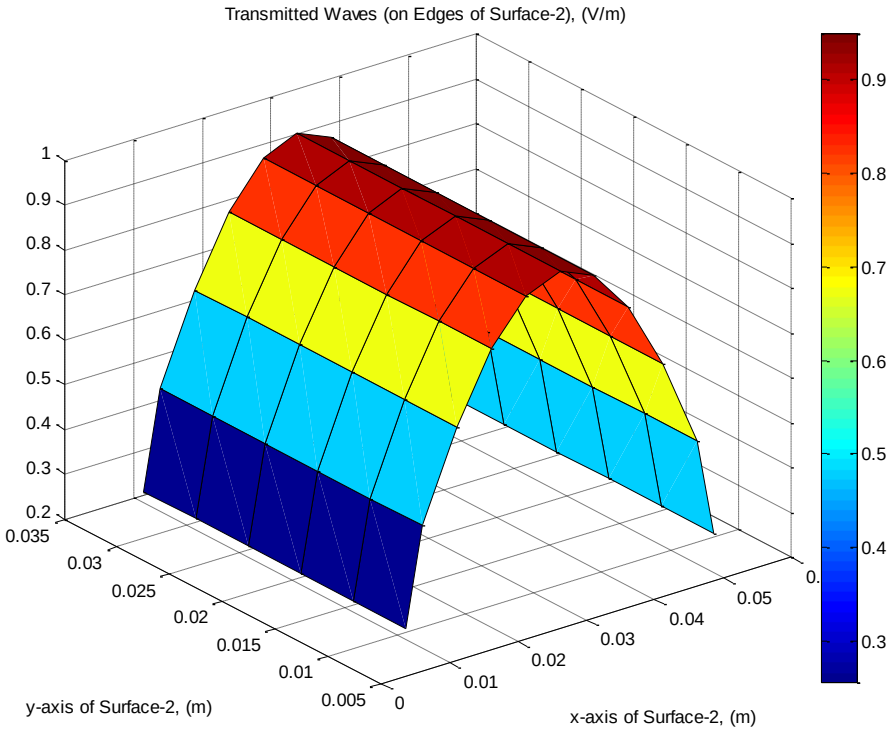

Figure 5.5: Transmitted waves from structure with sizes 0.1λx0.1λx0.1λ in MATLAB

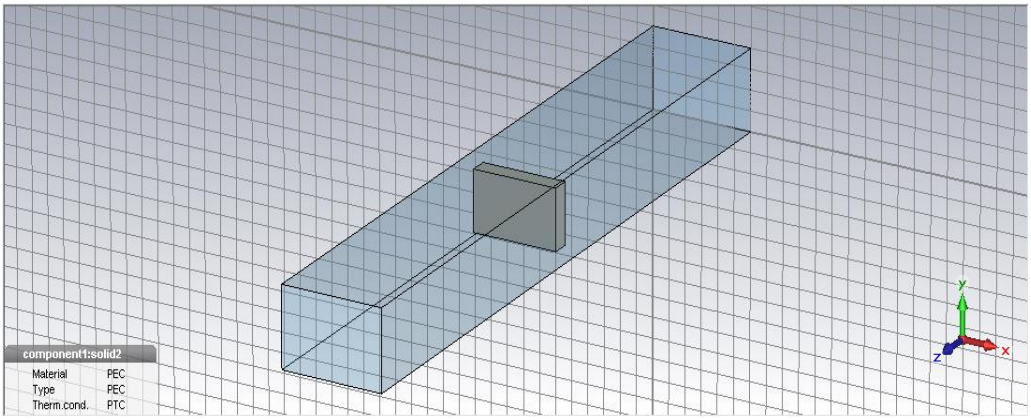

Figure 5.6: CST model of structure with sizes 0.5λx0.3λx0.1λ

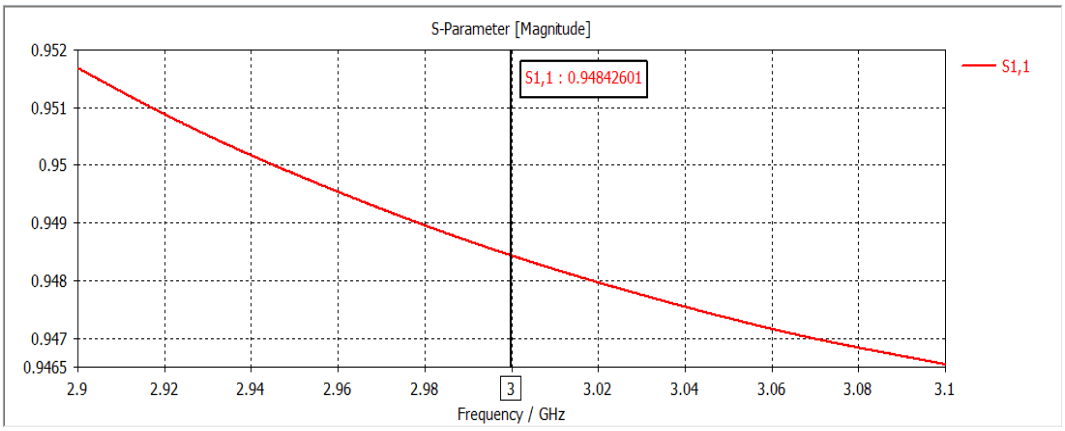

Figure 5.7: S_{11} of structure with sizes 0.5λx0.3λx0.1λ in CST

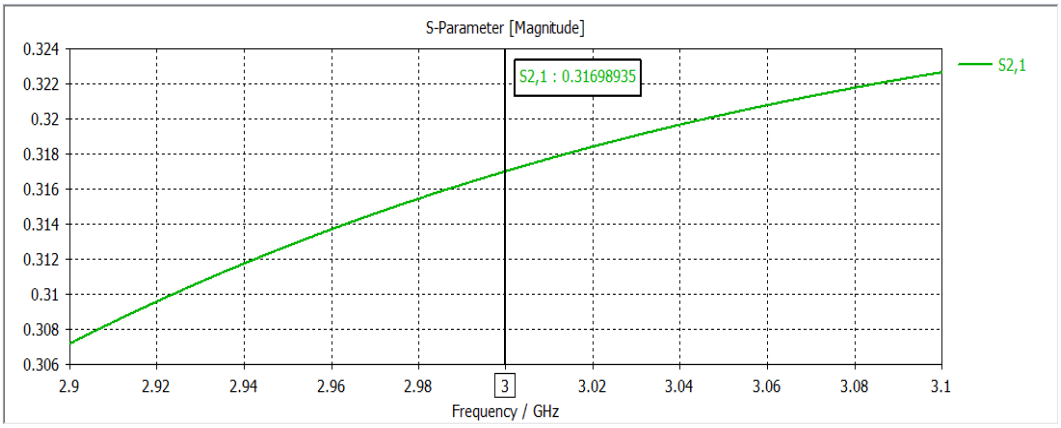

Figure 5.8: S_{21} of structure with sizes 0.5λx0.3λx0.1λ in CST

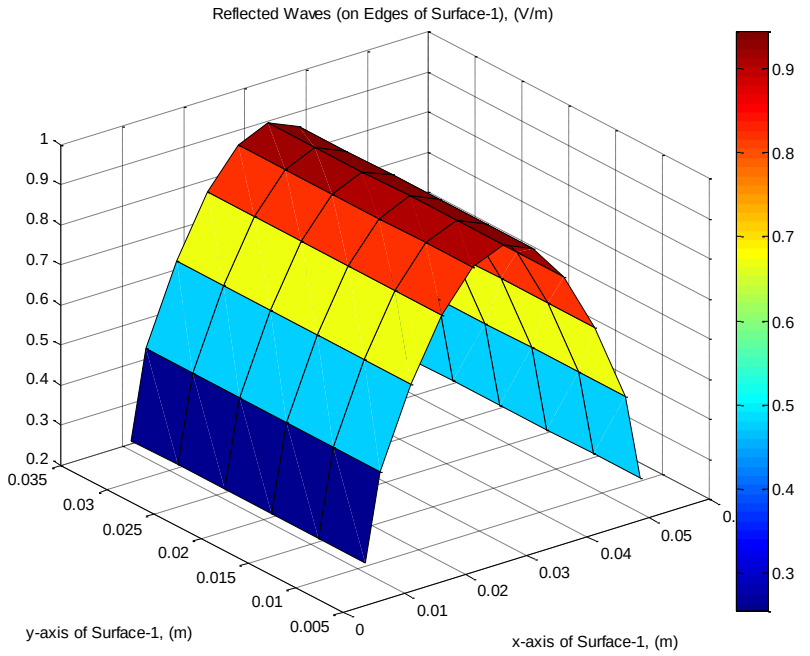

Figure 5.9: Reflected waves from structure with sizes 0.5λx0.3λx0.1λ in MATLAB

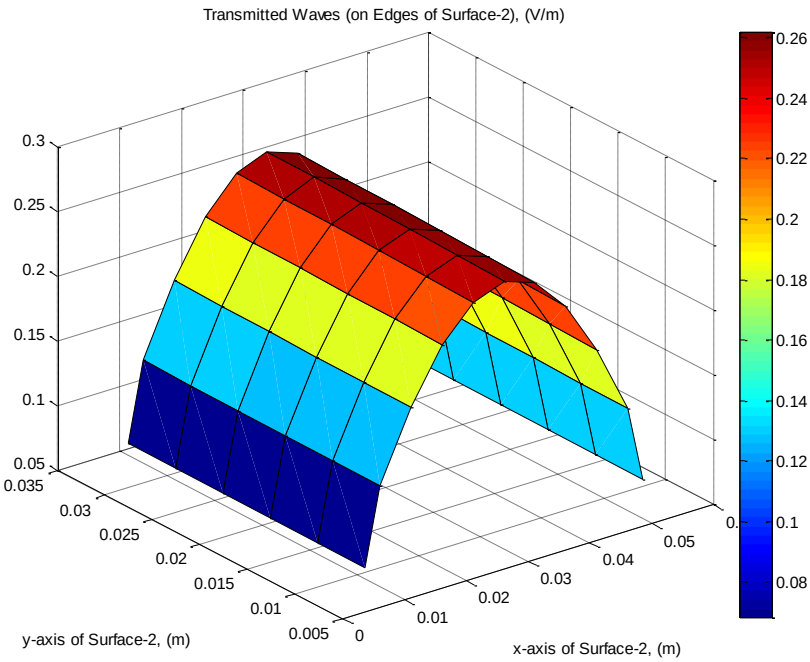

Figure 5.10: Transmitted waves from structure with sizes

0.5λx0.3λx0.1λ in MATLAB

The element size was chosen as λ/20 in MATLAB design. The distance of surfaces to structure and PML surfaces was 0.75λ. Figures 5.1-5.10 show that when the structure size was increased, magnitudes of reflected electric fields were also increased and magnitudes of transmitted electric fields were decreased. These were the expected results mentioned above.

Table 5.1: Comparison of MATLAB code and CST results according to change of structure

	S_{11} (MATLAB)	S_{11} (CST)	S_{21} (MATLAB)	S_{21} (CST)
0.1λx0.1λx0.1λ	0.27	0.22	0.94	0.98
0.5λx0.3λx0.1λ	0.94	0.95	0.25	0.31

The results from MATLAB code and CST were similar but in order to make them better, the element size was decreased to λ/40 from λ/20 and they were presented in oncoming sections.

Another experiment is performed to observe the effect of place of the surfaces on scattered parameters. The answer to the question how close the surfaces could be to the structure was looked for. Since larger waveguide sizes result in more elements and this increases the memory usage, its size had to be minimized. Taking the surfaces so close to structure caused to have higher order mode fields. Therefore, it was a must that searching for an optimum surface distance to structure. The distance was changed from 0.05λ to 1.45λ and seven samples were taken for the structure with size 0.5λx0.3λx0.1λ.

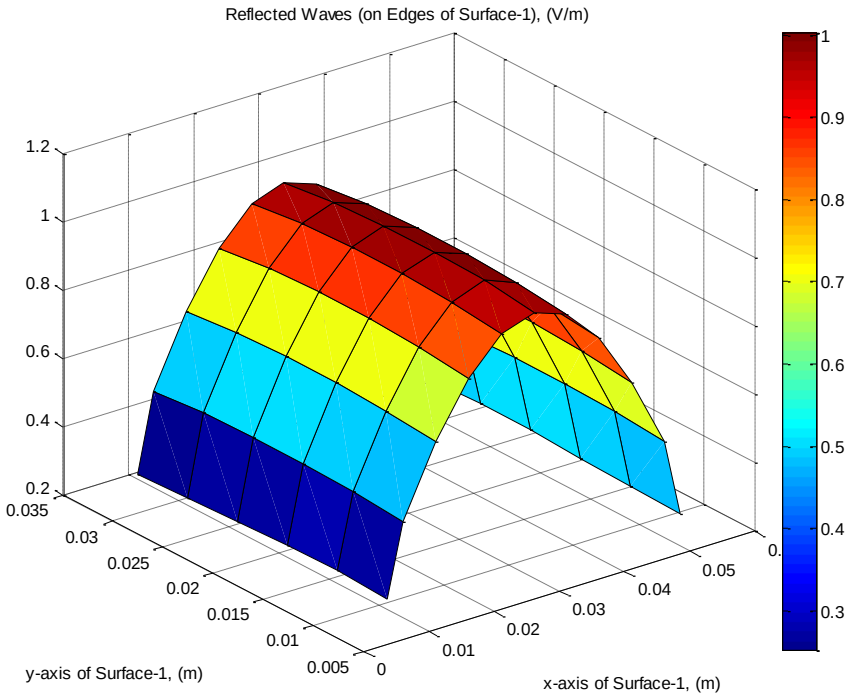

Figure 5.11: Reflected waves from structure when distance is 0.05 λ

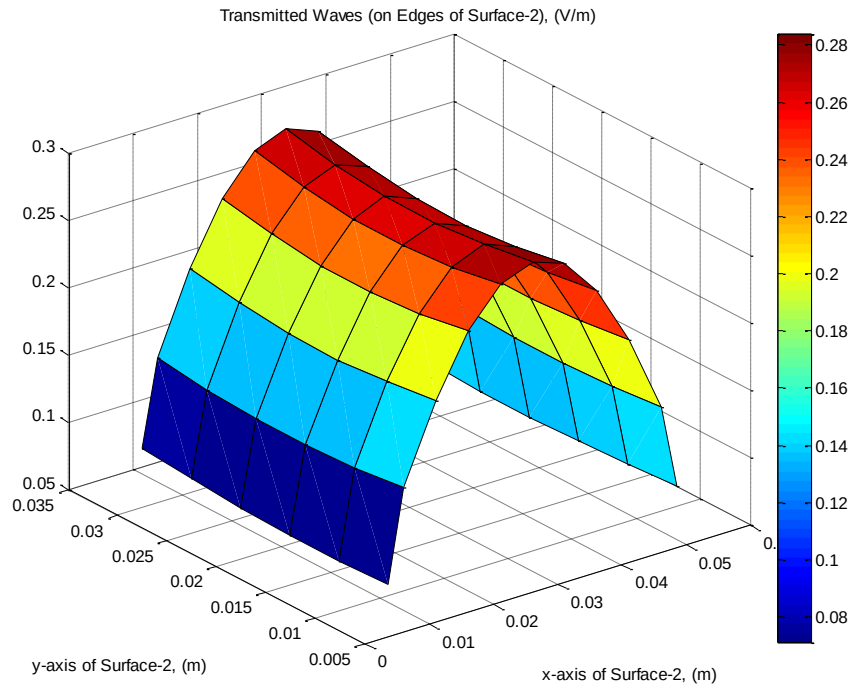

Figure 5.12: Transmitted waves from structure when distance is 0.05 λ

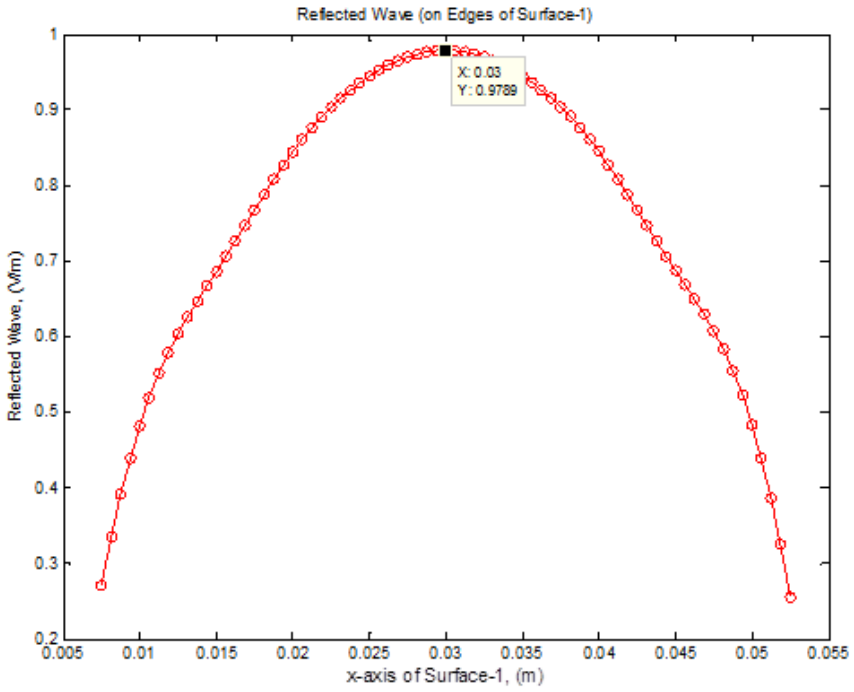

Figure 5.13: Reflected wave from structure when distance is 0.05 λ

(a single half sinusoid)

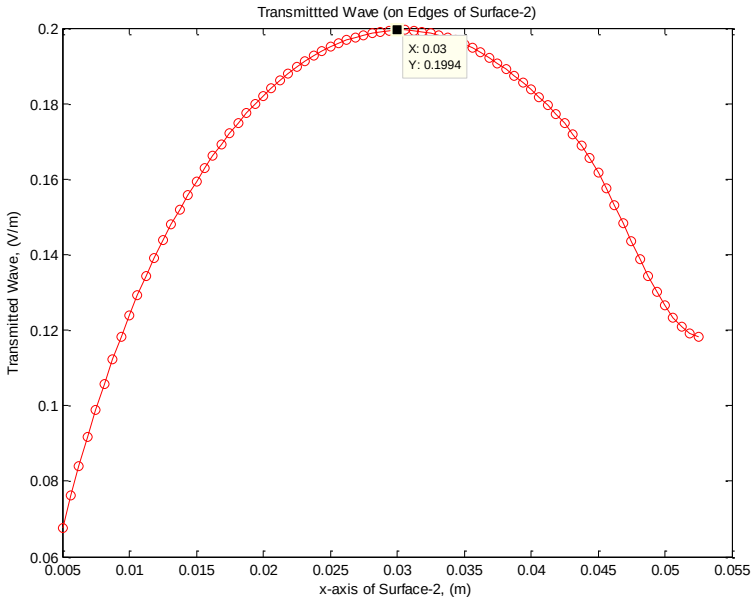

Figure 5.14: Transmitted wave from structure when distance is 0.05 λ

(a single half sinusoid)

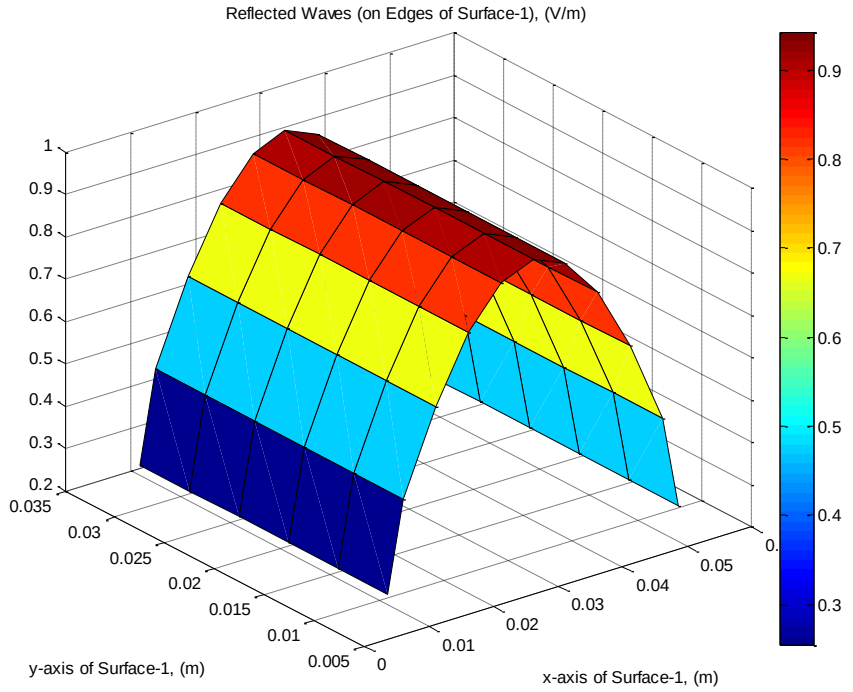

Figure 5.15: Reflected waves from structure when distance is 0.5 λ

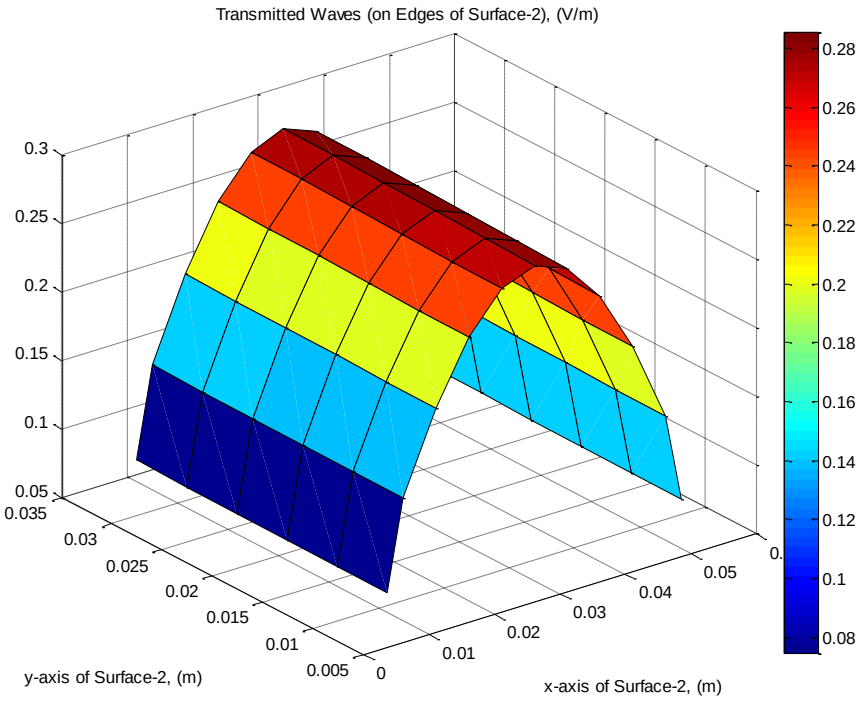

Figure 5.16: Transmitted waves from structure when distance is 0.5 λ

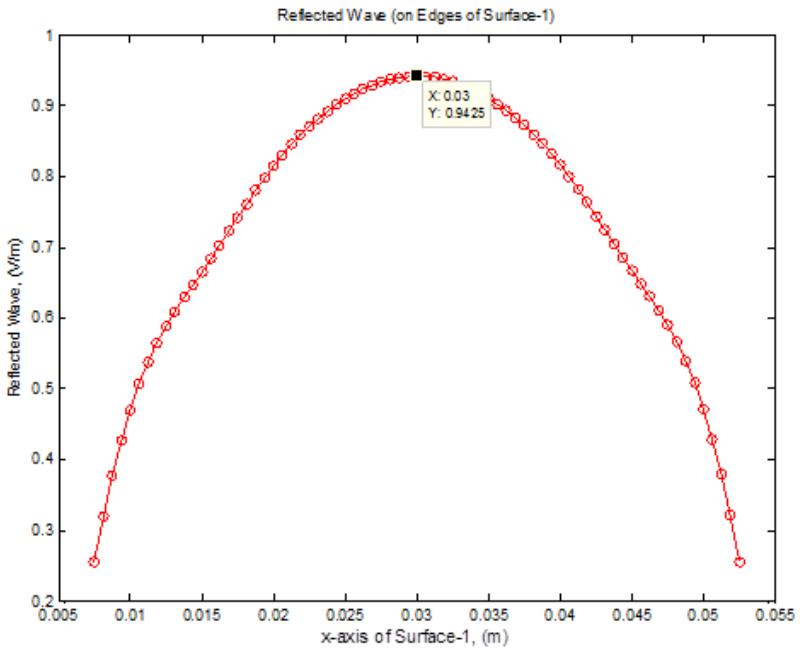

Figure 5.17: Reflected wave from structure when distance is 0.5 λ

(a single half sinusoid)

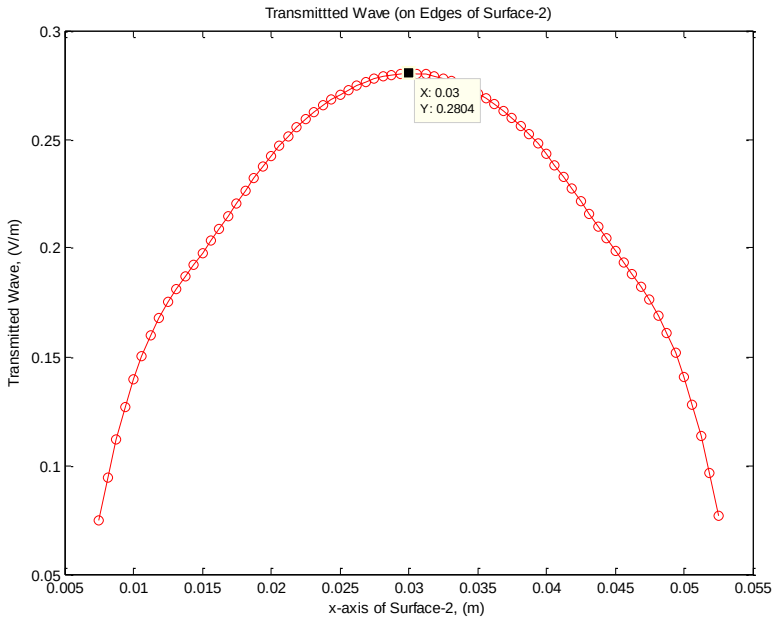

Figure 5.18: Transmitted wave from structure when distance is 0.5 λ

(a single half sinusoid)

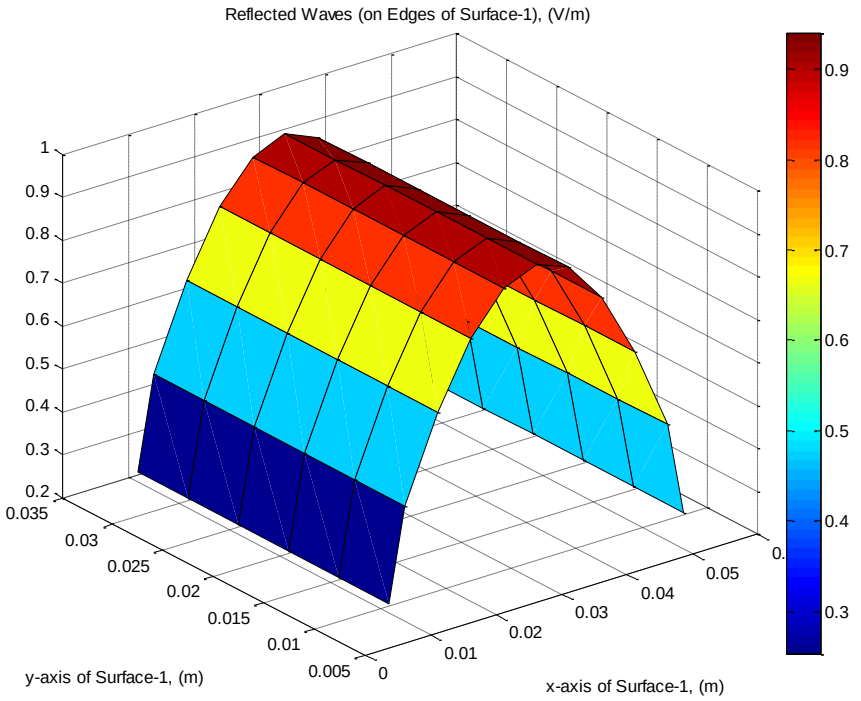

Figure 5.19: Reflected waves from structure when distance is 1.45 λ

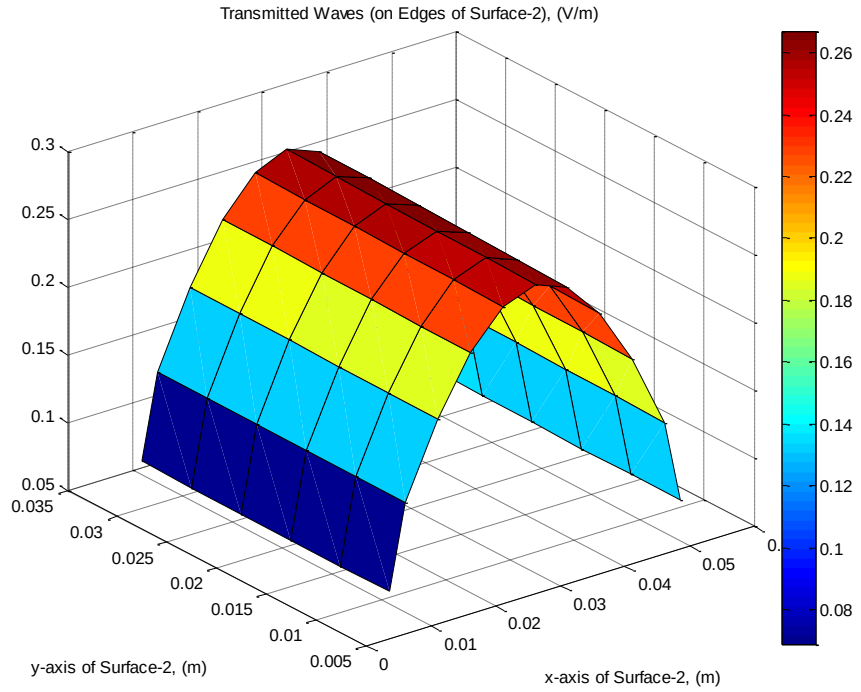

Figure 5.20: Transmitted waves from structure when distance is 1.45 λ

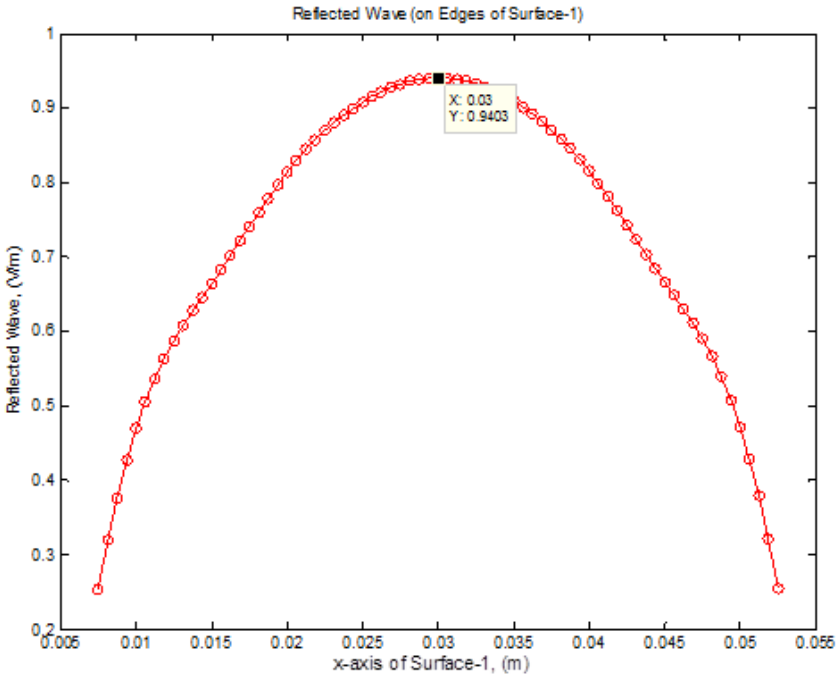

Figure 5.21: Reflected wave from structure when distance is 1.45 λ

(a single half sinusoid)

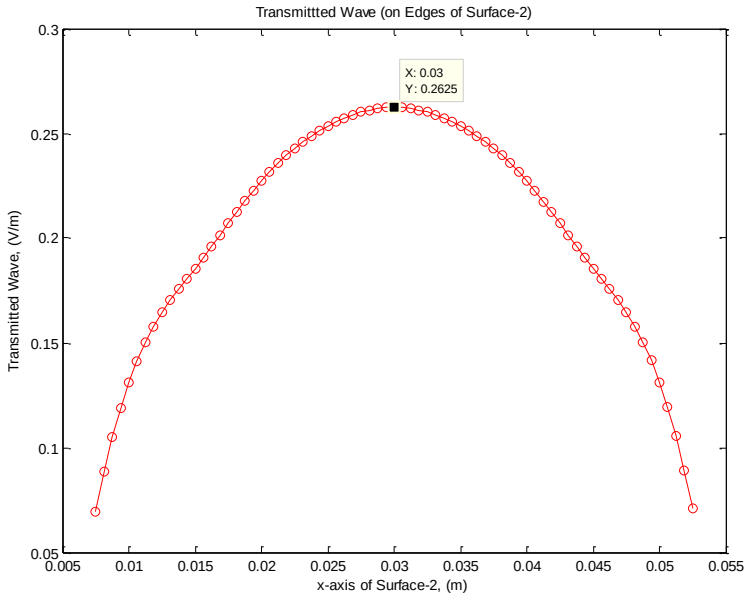

Figure 5.22: Transmitted wave from structure when distance is 1.45 λ

(a single half sinusoid)

How the higher order modes effect the fields can be seen from figures 5.11-5.14. The sinusoidal shapes of the fields were disrupted. Magnitude of reflected field increases and transmitted filed decreases remarkably by those. As moving away from structure, the sinusoids and field values converged their levels as they should be. Figures of three samples were presented and data from other four samples can be found from Table 5.2. It can be inferred that choosing the surface distance as 0.5λ is enough to get correct results. Thanks to this inference the size of waveguide was shorten as 1λ in total. Also, these provided less memory usage.

Table 5.2: Change of scattering parameters with change of surface distance

	0.05λ	**0.25λ**	**0.5λ**	**0.75λ**	**1.0λ**	**1.25λ**	**1.45λ**
S_{11} (MATLAB)	0.98	0.98	0.94	0.94	0.95	0.95	0.94
S_{21} (MATLAB)	0.20	0.28	0.28	0.26	0.25	0.26	0.26

Smaller element sizes give more accurate outputs unless the element quality was disrupted [25]. As mentioned before, reducing element size makes the results from MATLAB code closer to results from CST since the element number was increased. However, with greater number of elements increased the memory usage and the compiling time. Besides, thanks to smaller waveguide size, these negative effects were reduced to acceptable limits. The structure size and surface distance was chosen as 0.5λx0.3λx0.1λ and 0.45λ respectively.

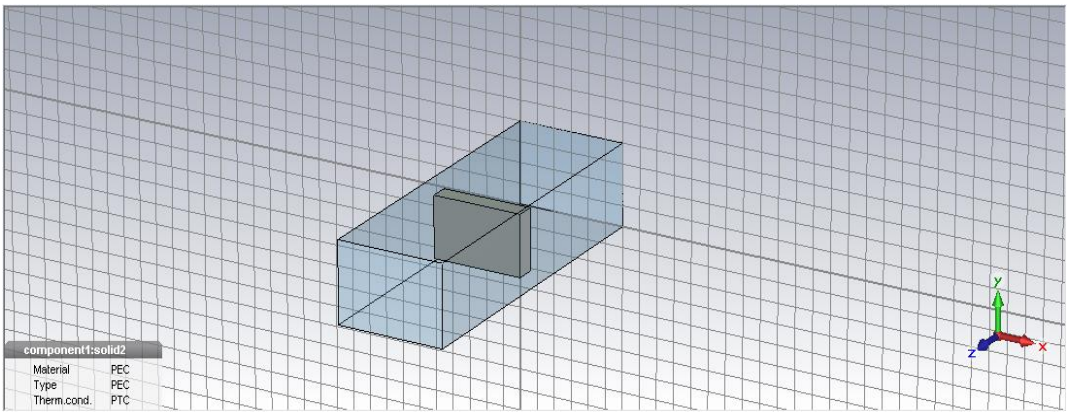

Figure 5.23: CST model of structure with sizes 0.5λx0.3λx0.1λ and short waveguide length

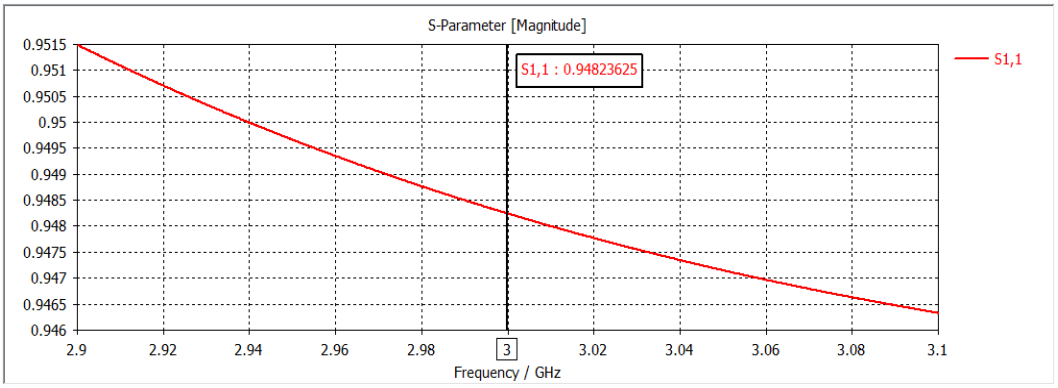

Figure 5.24: S_{11} of structure with sizes 0.5λx0.3λx0.1λ and short waveguide length in CST

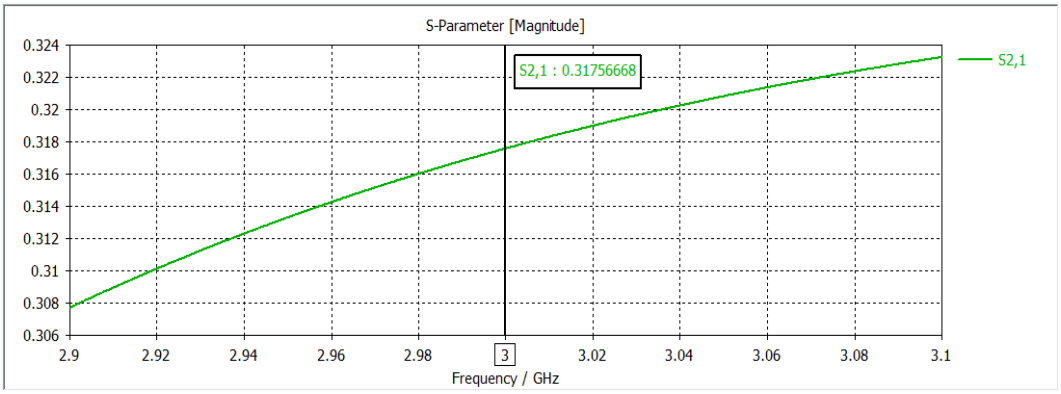

Figure 5.25: S_{21} of structure with sizes 0.5λx0.3λx0.1λ and short waveguide length in CST

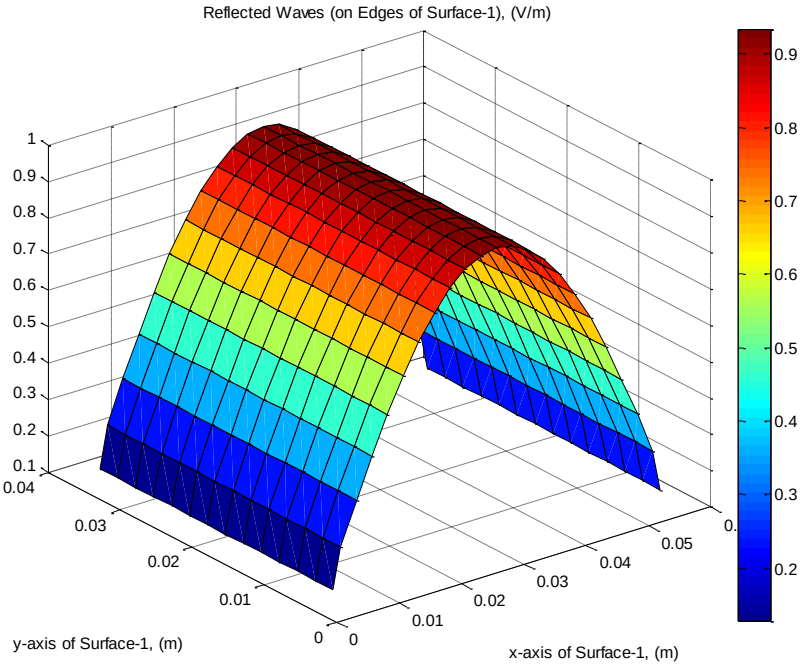

Figure 5.26: Reflected waves from structure with λ/40

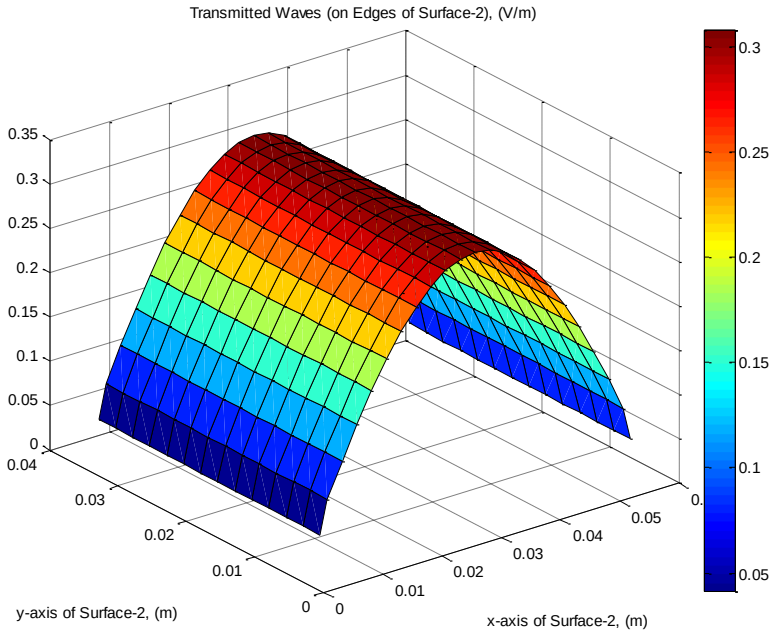

Figure 5.27: Transmitted waves from structure with λ/40

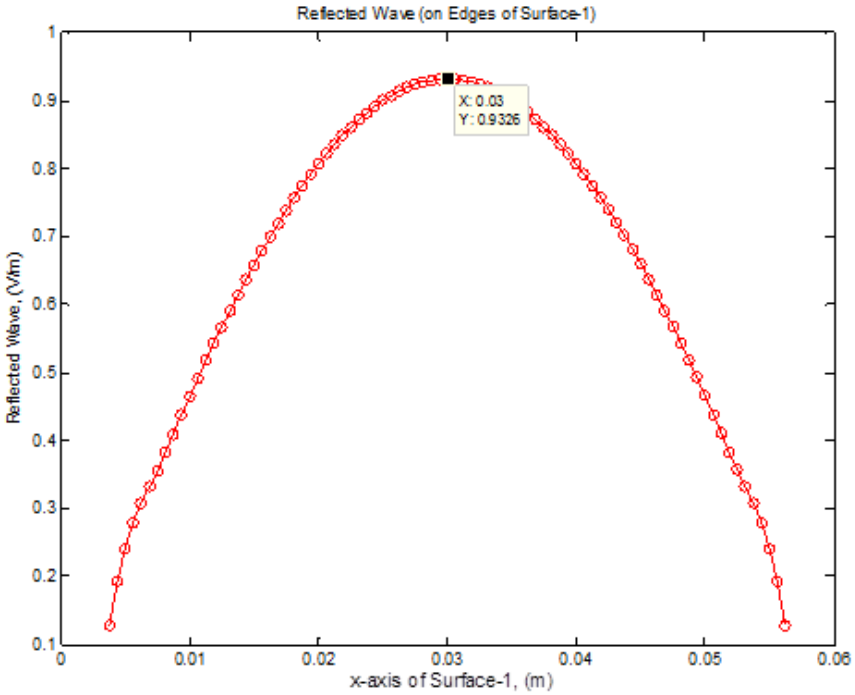

Figure 5.28: Reflected wave from structure with λ/40 (a single half sinusoid)

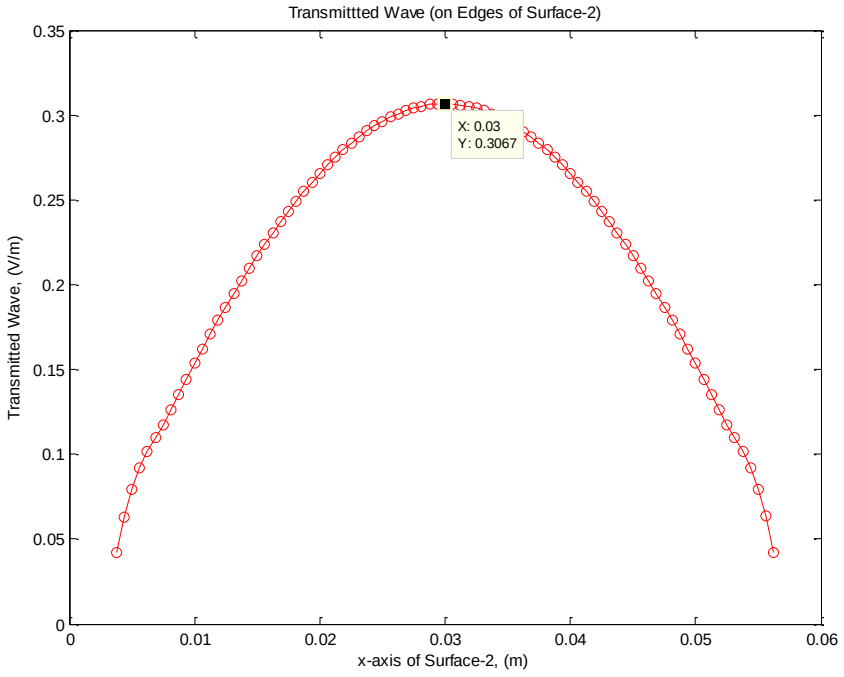

Figure 5.29: Transmitted wave from structure with λ/40 (a single half sinusoid)

Table 5.3: Change of scattering parameters with change of element size and comparison MATLAB code with CST (with size of 0.5λx0.3λx0.1λ)

	S_{11} (MATLAB)	S_{11} (CST)	S_{21} (MATLAB)	S_{21} (CST)
λ/20 element size	0.94	0.95	0.25	0.31
λ/40 element size	0.93	0.94	0.32	0.31

Furthermore, structure size was changed to 0.4λx0.2λx0.1λ to be sure that smaller element size allowed us to have more accurate results. Table 5.4 and figures 5.30-5.37 present the associated outputs.

Table 5.4: Change of scattering parameters with change of element size and comparison MATLAB code with CST (with size of 0.4λx0.2λx0.1λ)

	S_{11} (MATLAB)	S_{11} (CST)	S_{21} (MATLAB)	S_{21} (CST)
λ/20 element size	0.78	0.74	0.61	0.66
λ/40 element size	0.74	0.74	0.65	0.66

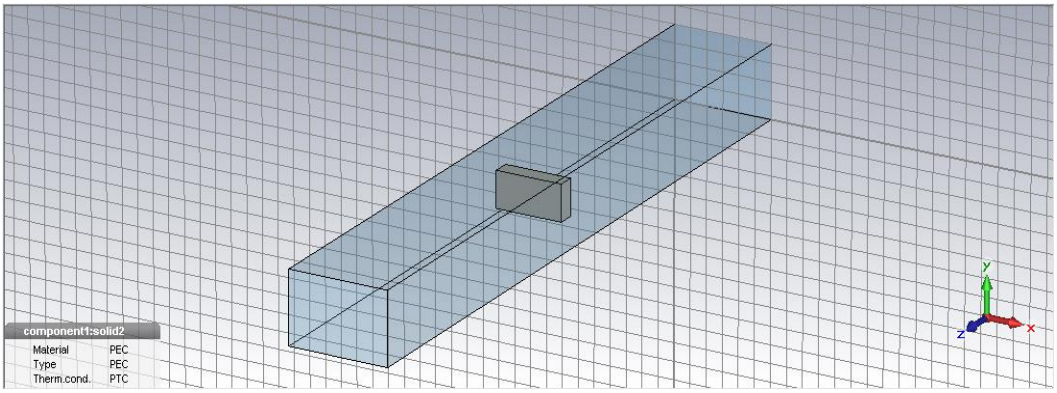

Figure 5.30: CST model of structure with sizes 0.4λx0.2λx0.1λ and long waveguide length

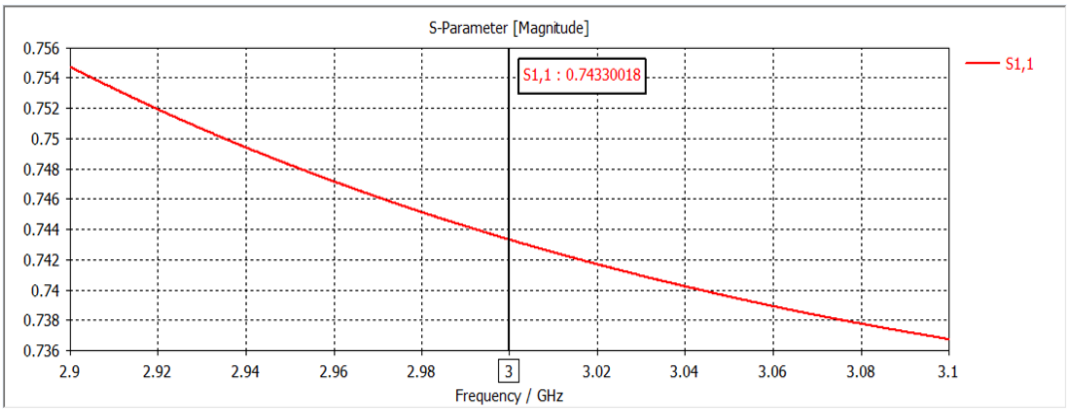

Figure 5.31: S_{11} of structure with sizes 0.4λx0.2λx0.1λ and long waveguide length in CST

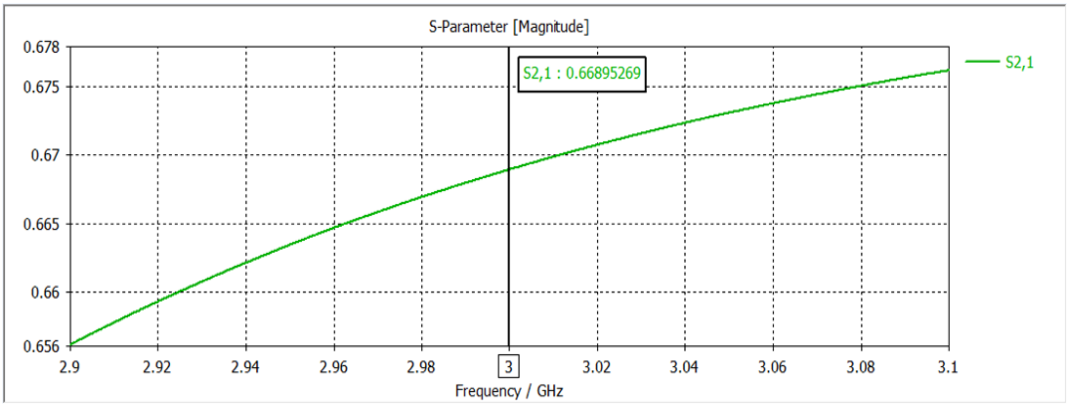

Figure 5.32: S_{21} of structure with sizes 0.4λx0.2λx0.1λ and long waveguide length in CST

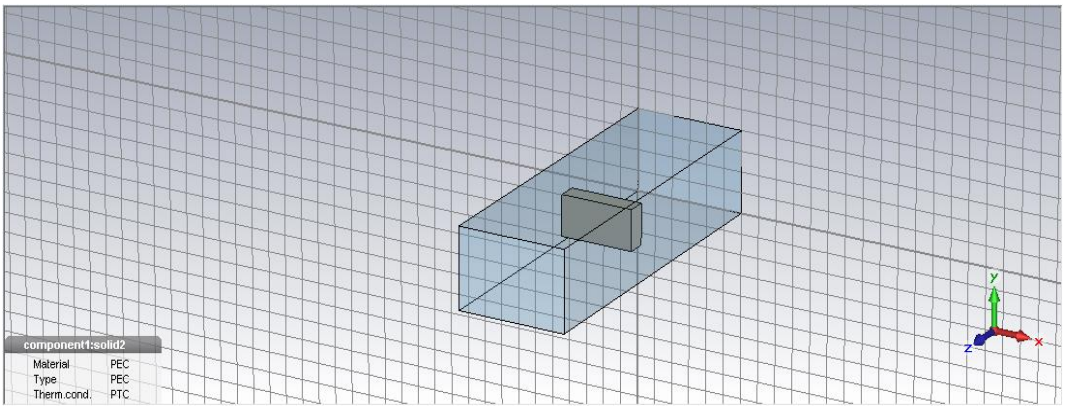

Figure 5.33: CST model of structure with sizes 0.4λx0.2λx0.1λ and short waveguide length

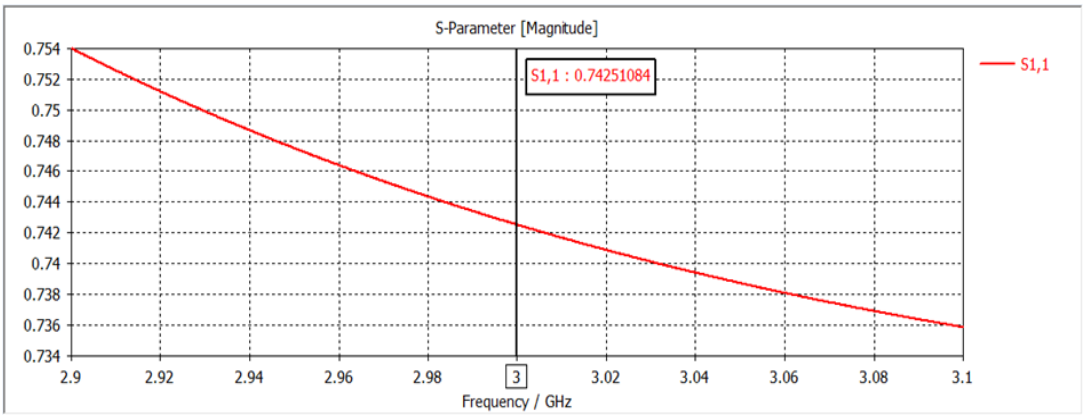

Figure 5.34: S_{11} of structure with sizes 0.4λx0.2λx0.1λ and short waveguide length in CST

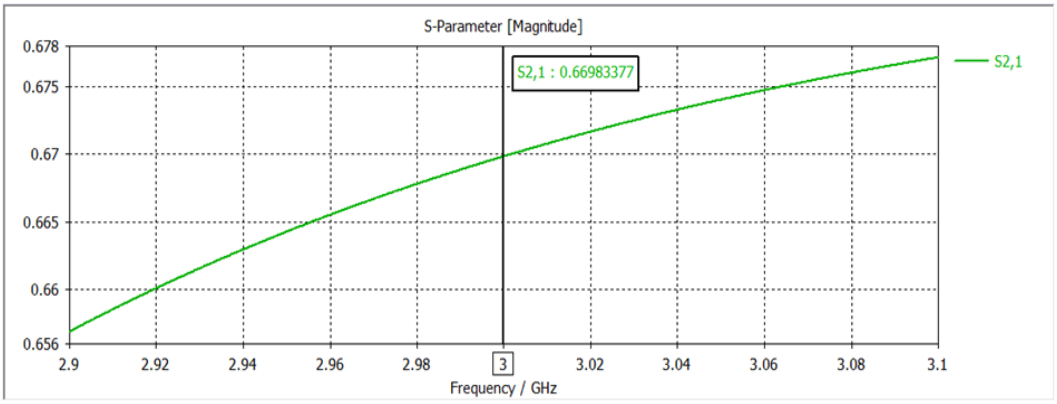

Figure 5.35: S_{21} of structure with sizes 0.4λx0.2λx0.1λ and short waveguide length in CST

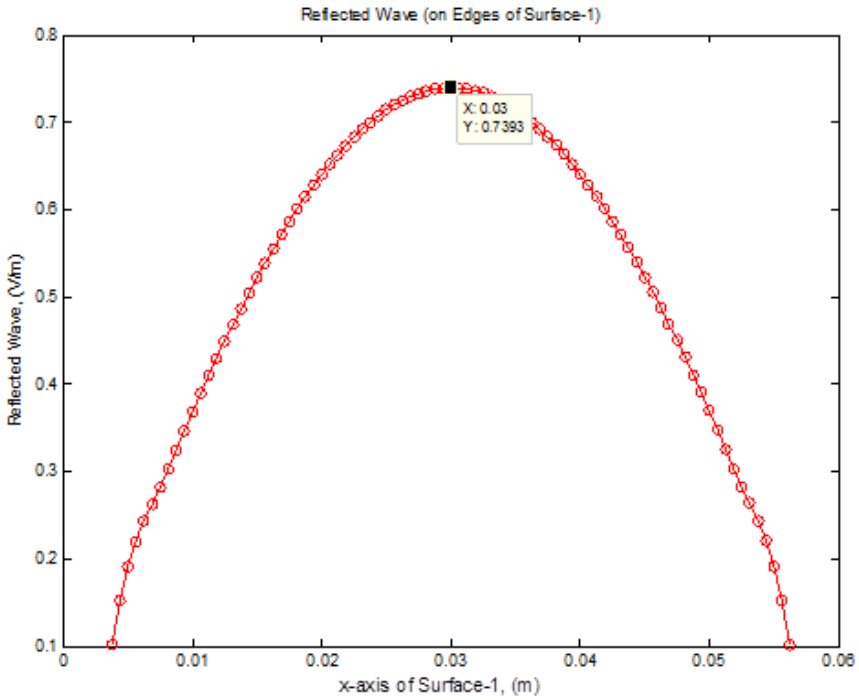

Figure 5.36: Reflected wave from structure with λ/40 (with size of 0.4λx0.2λx0.1λ)

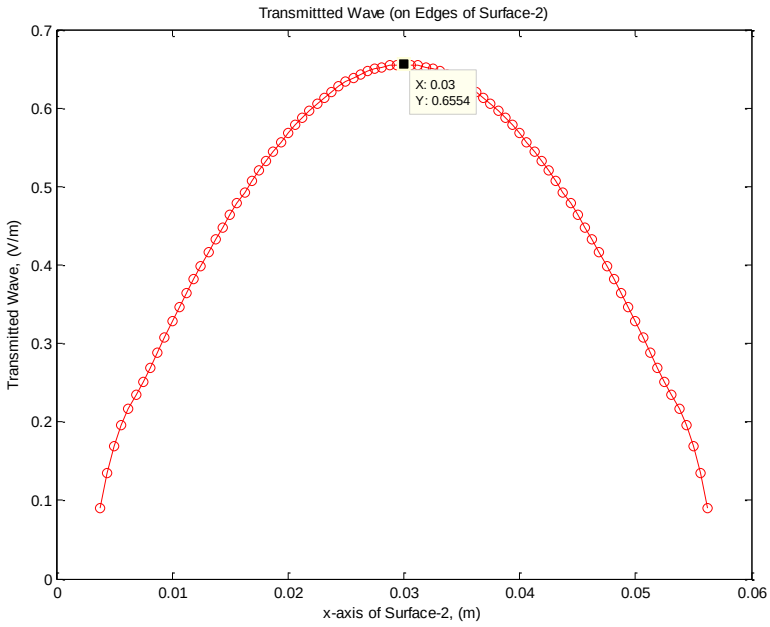

Figure 5.37: Transmitted wave from structure with λ/40

(with size of 0.4λx0.2λx0.1λ)

5.1. S-PARAMETERS OF SRRS VIA FEM

Before calculation of S-parameters of SRRs, the MATLAB code was tested by altering design parameters and CST results. After being sure that the program provided correct outputs, the simple structure was replaced with SRR structure. Since the surface of 3D structure was considered as PEC, the elements inside were excluded. Due to the shapes of SRRs, the excluded elements, except inside PEC ring, were taken into consideration again. Also, the regions where the PEC boundary conditions imposed changed. As a result of this, they were rearranged. Anew, in order to verify that the algorithm was developed in a correct way, initially, a rectangular piece of the structure was replaced with vacuum i.e. the rectangular prism was replaced with a rectangular ring and, the process mentioned was applied. The structure, whose shape was given in Figure 5.38, was designed with sizes as 0.4λx0.2λx0.025λ with sides' thicknesses of 0.05λ. The thickness was considered to contain only one element along z-axis, which was 0.025λ since in practice, the thicknesses of SRRs were very short compared with their widths and heights.

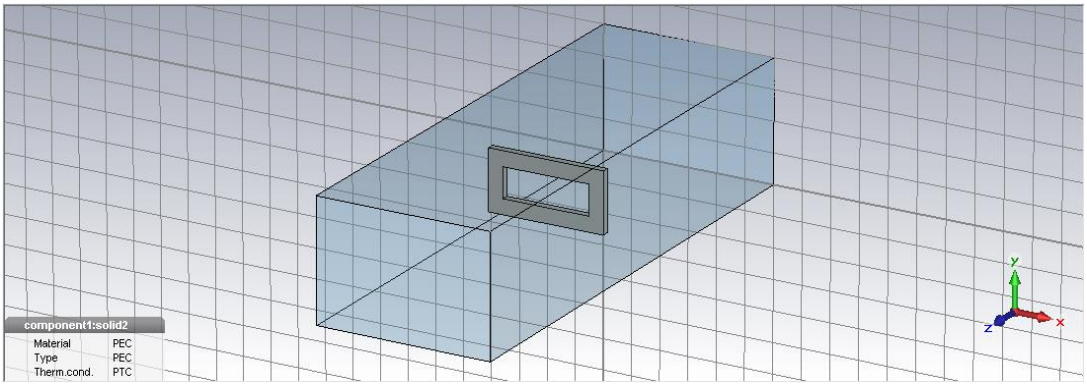

Figure 5.38: CST model of ring structure with sizes 0.4λx0.2λx0.025λ

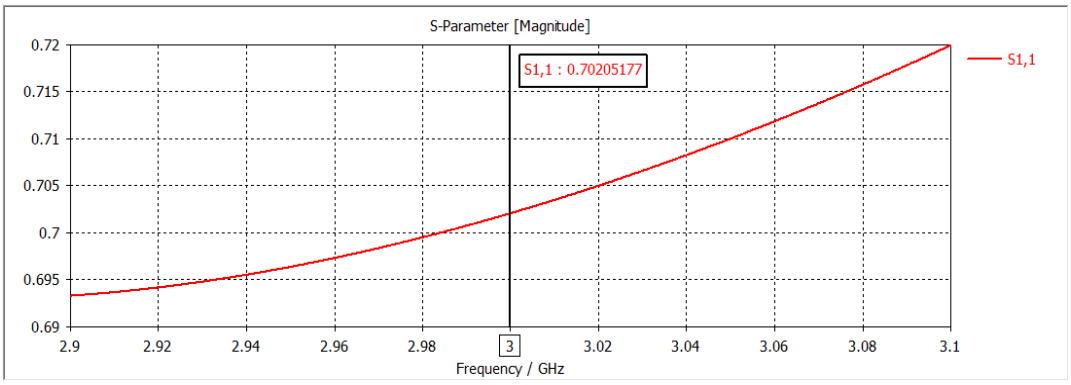

Figure 5.39: S_{11} of ring structure with sizes 0.4λx0.2λx0.025λ

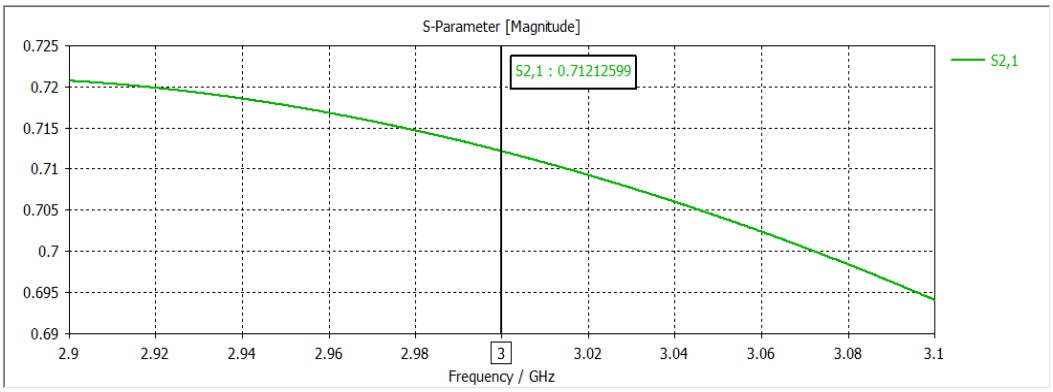

Figure 5.40: S_{21} of ring structure with sizes 0.4λx0.2λx0.025λ

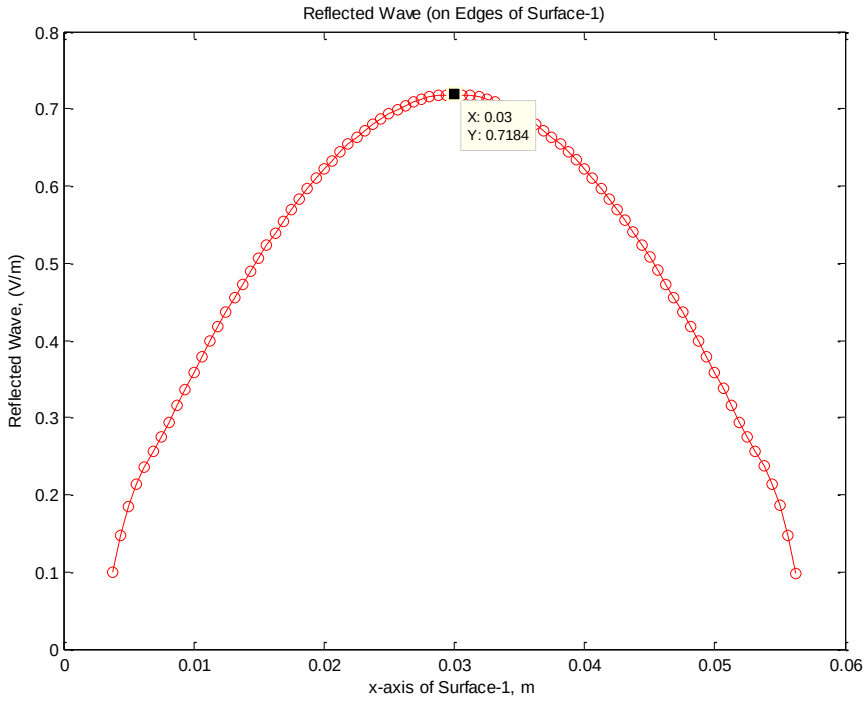

Figure 5.41: Reflected wave from ring structure (a half sinusoid)

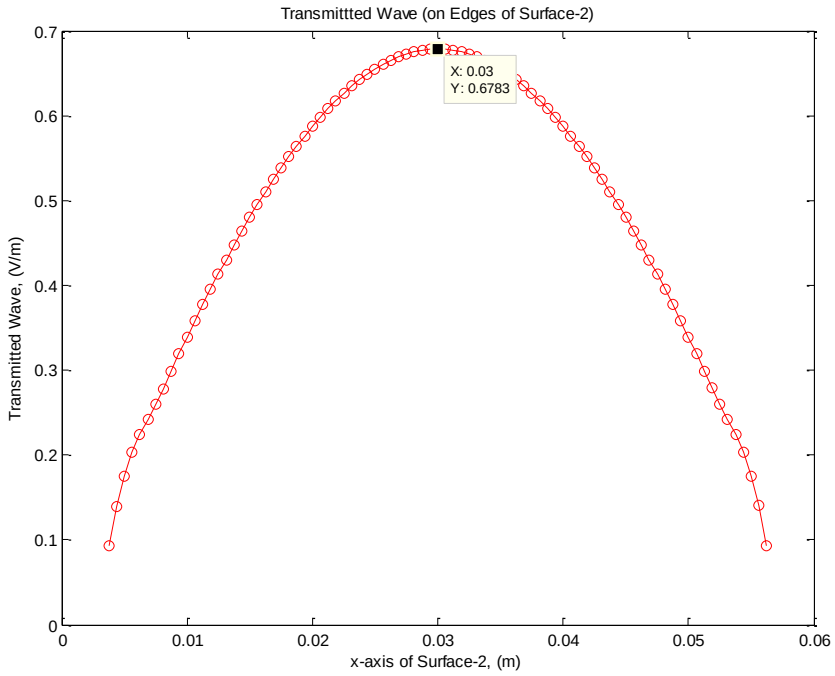

Figure 5.42: Transmitted wave from ring structure (a half sinusoid)

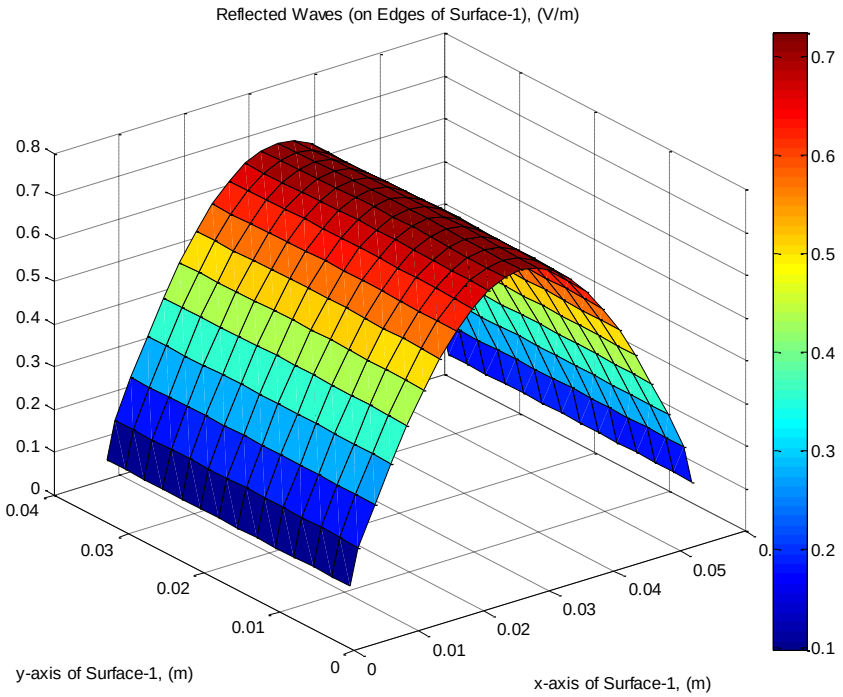

Figure 5.43: Reflected waves from ring structure

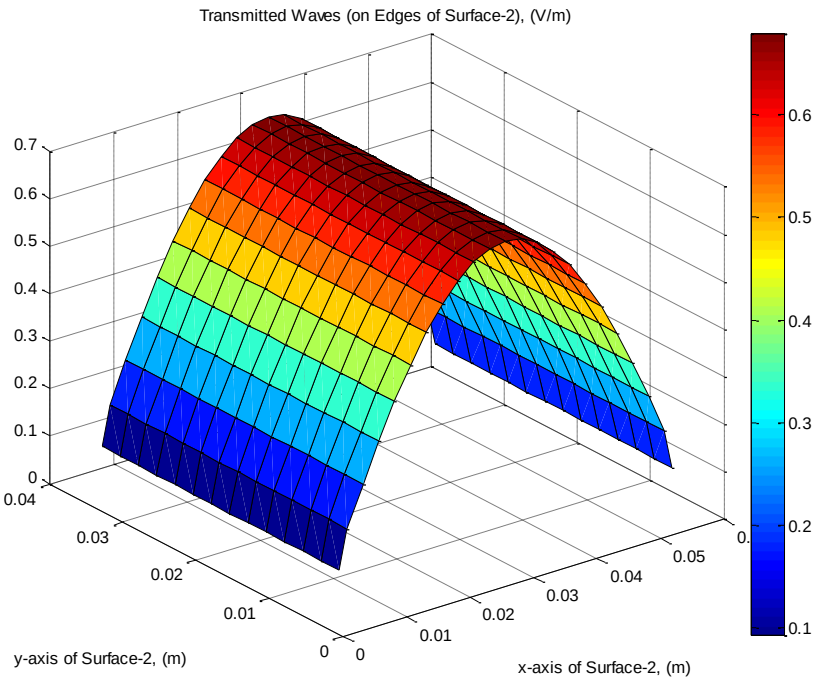

Figure 5.44: Transmitted waves from ring structure

SRRs composed of two rings and two slits on the rings as mentioned before. One step before testing the real design of SRRs, one more experiment was carried out and the width of slit was taken as 0.05λ by taking a slit into consider on top of ring.

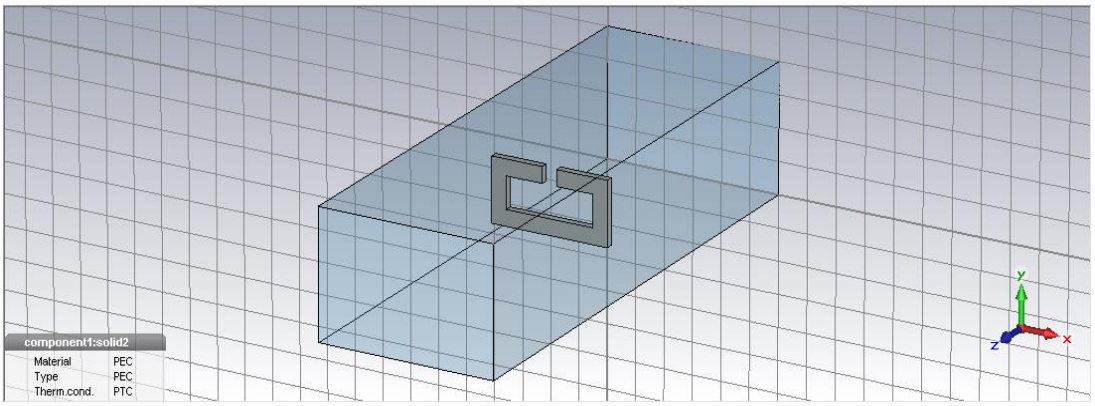

Figure 5.45: CST model of ring structure with slit

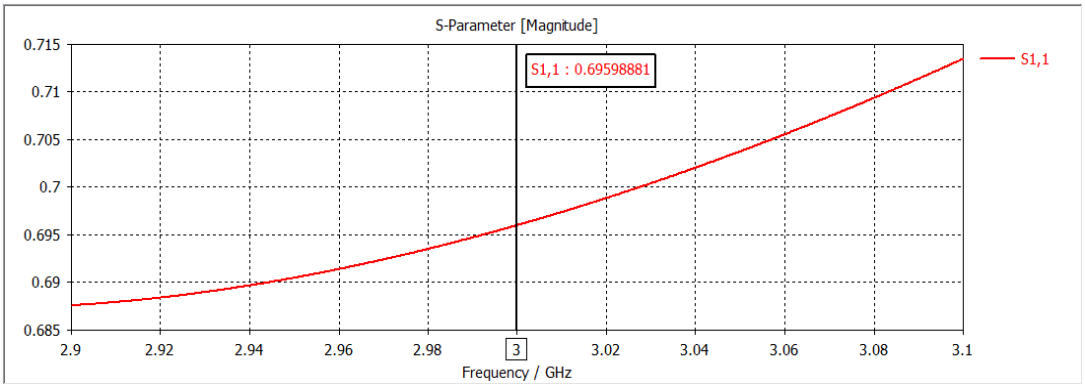

Figure 5.46: S_{11} of ring structure with slit

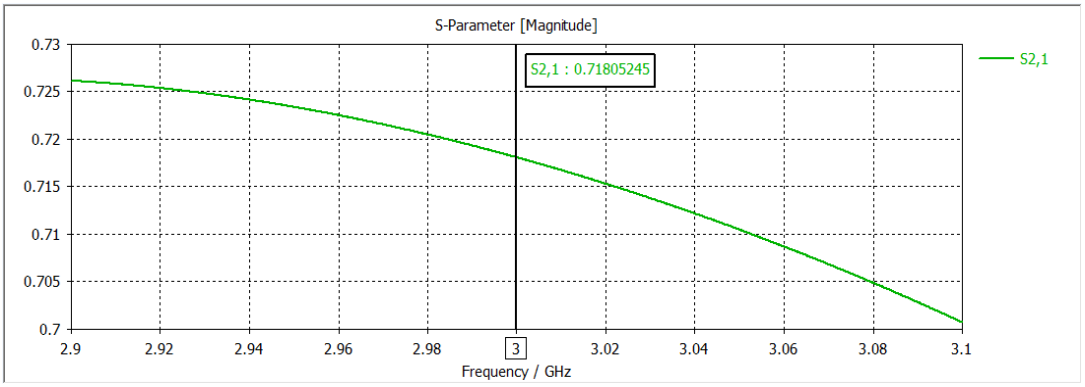

Figure 5.47: S_{21} of ring structure with slit

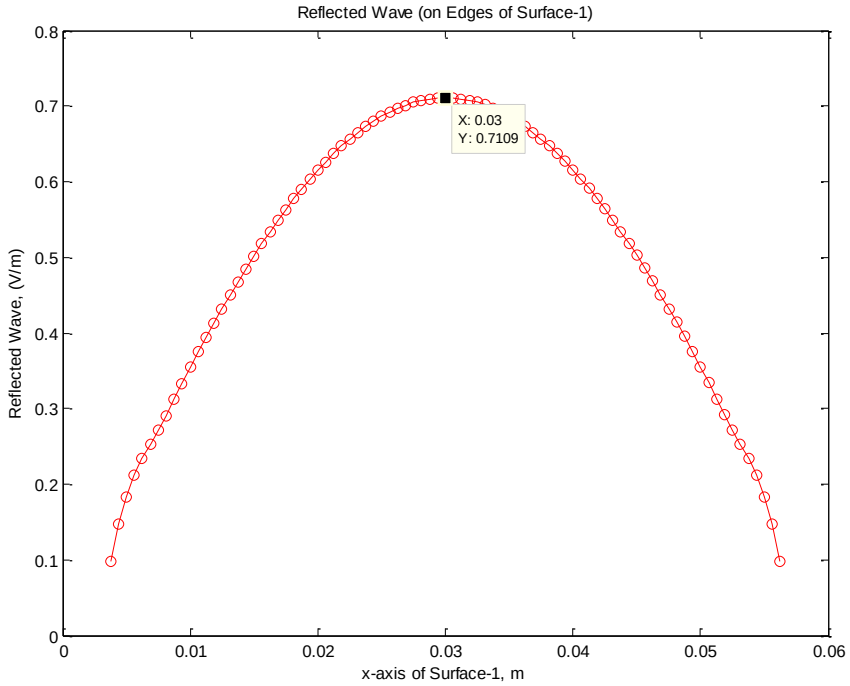

Figure 5.48: Reflected wave from ring structure with slit (a half sinusoid)

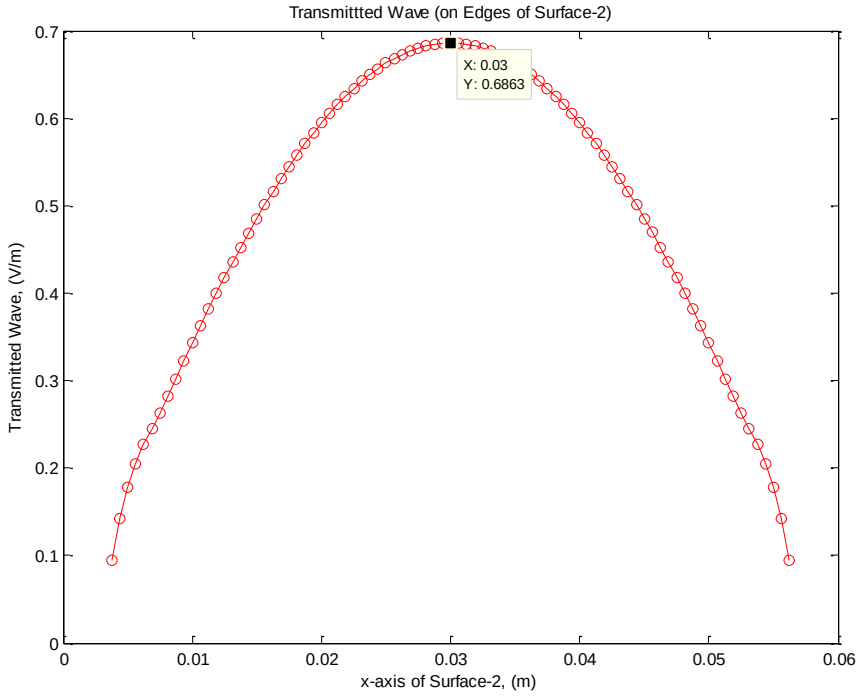

Figure 5.49: Transmitted wave from ring structure with slit (a half sinusoid)

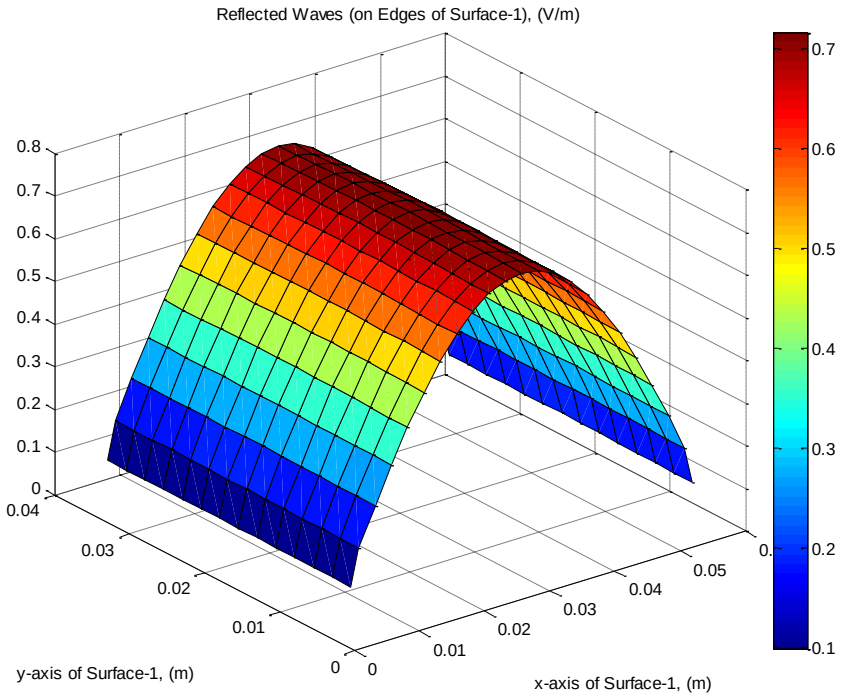

Figure 5.50: Reflected waves from ring structure with slit

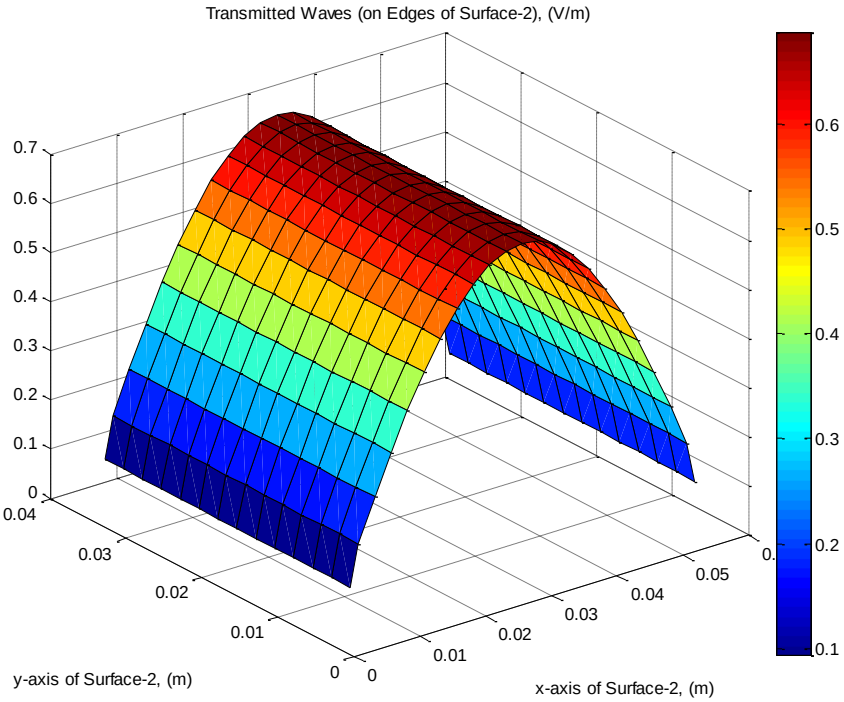

Figure 5.51: Transmitted waves from ring structure with slit

Table 5.5: S-parameters comparison of MATLAB code and CST results of ring structure and ring structure with slit

	S_{11} (MATLAB)	S_{11} (CST)	S_{21} (MATLAB)	S_{21} (CST)
Ring Structure	0.71	0.70	0.68	0.71
Ring Structure with Slit	0.70	0.71	0.69	0.71

As can be seen from figures 5.38-5.51 and also Table 5.5, MATLAB code's results matched up with CST's. As a result, the inference can be made that the post code was correct and calculations of s-parameters can be performed. The SRRs were designed as the height (on x-axis), width (on y-axis) and thickness (on z-axis) of the exterior slit ring to be 0.55λ, 0.35λ, and 0.025λ respectively while for the interior slit ring those lengths were 0.35λ, 0.15λ, and 0.025λ. The slit's widths were 0.05λ which equals to sides' thickness.

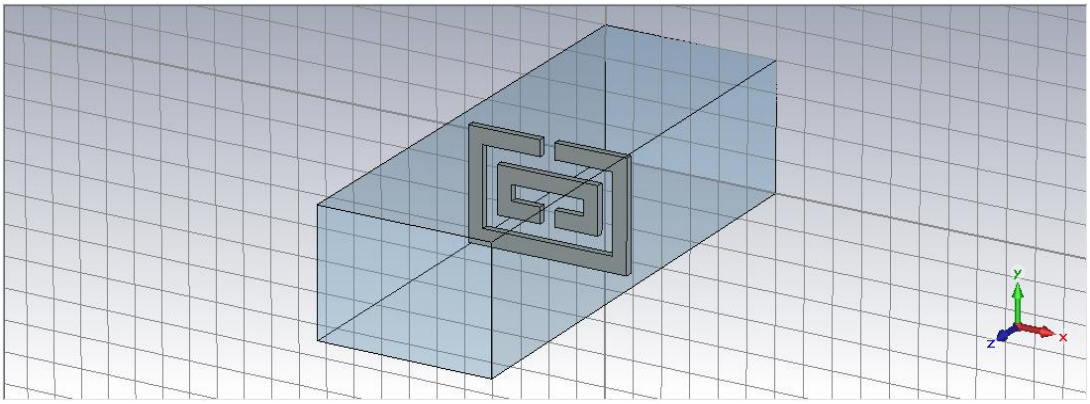

Figure 5.52: CST model of SRR

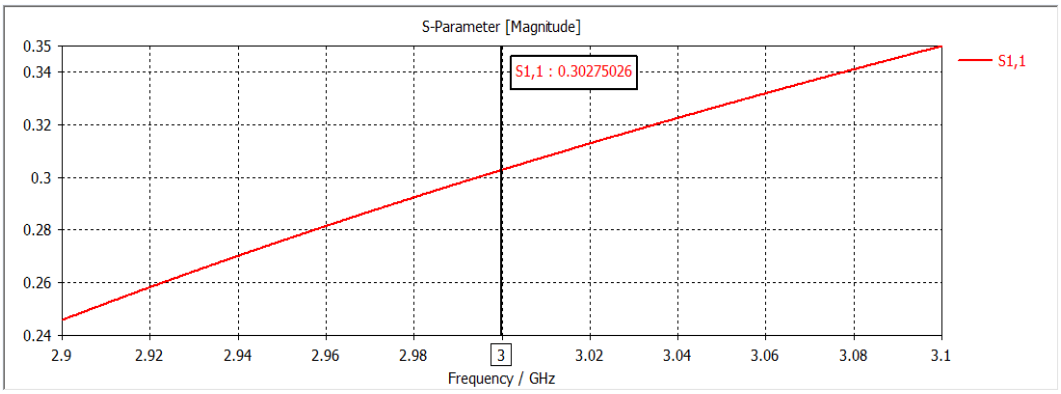

Figure 5.53: S_{11} of SRR

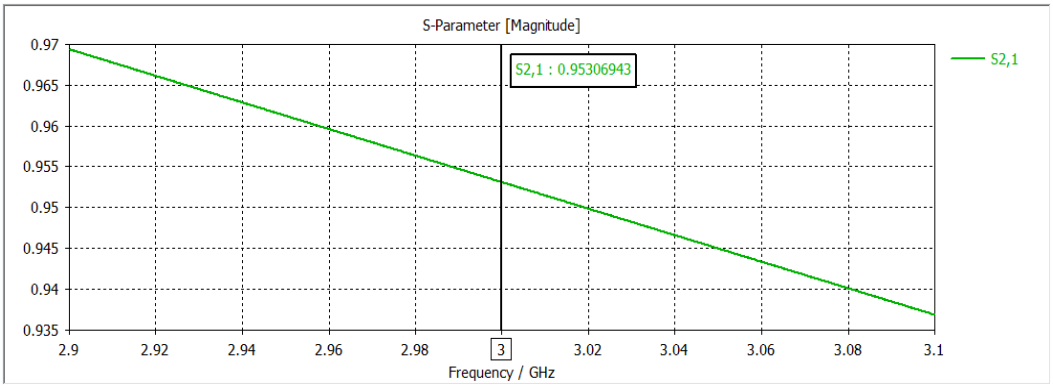

Figure 5.54: S_{21} of SRR

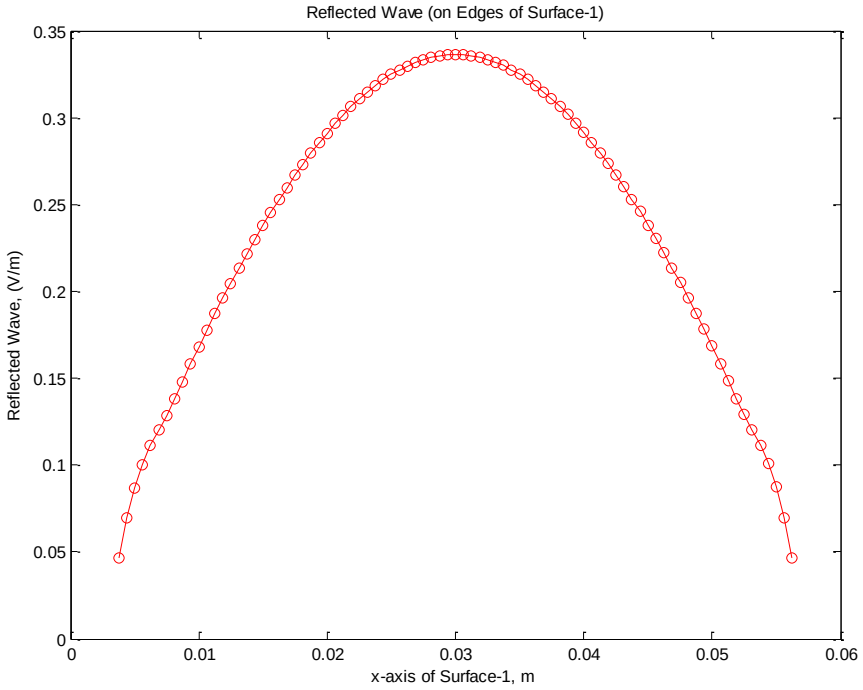

Figure 5.55: Reflected wave from SRR (a half sinusoid)

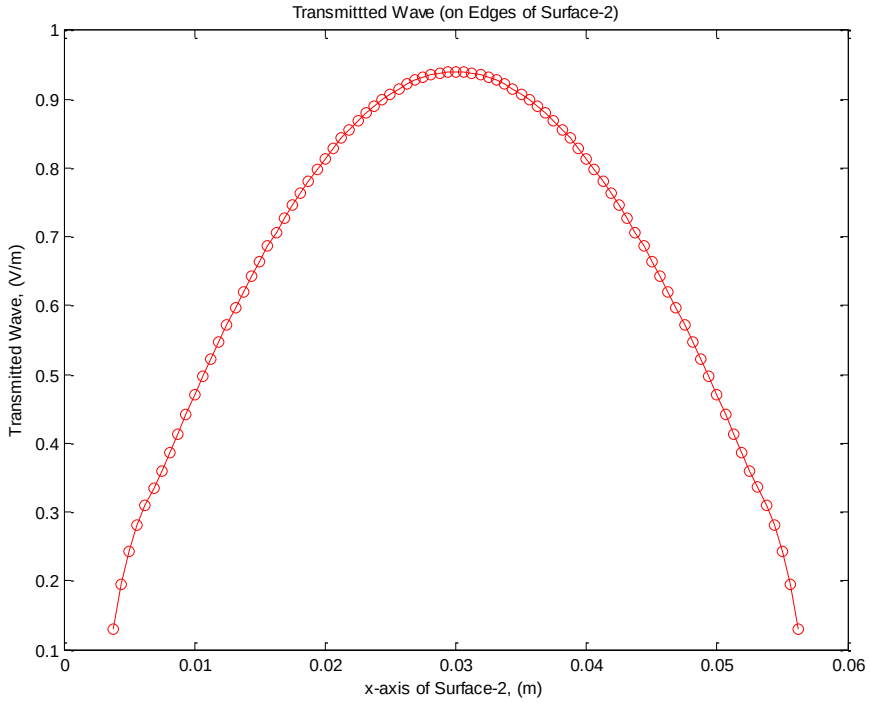

Figure 5.56: Transmitted wave from SRR (a half sinusoid)

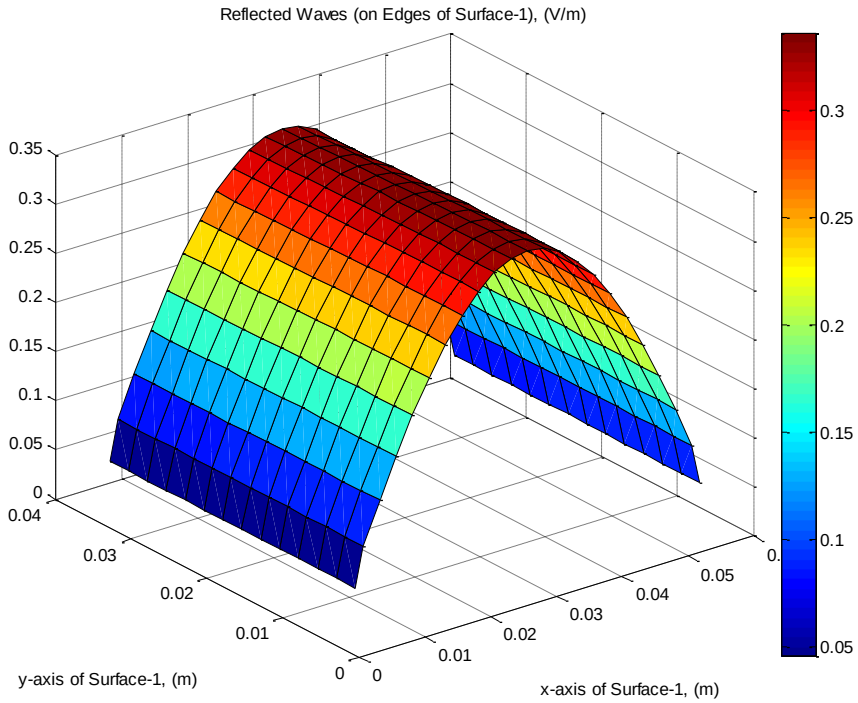

Figure 5.57: Reflected waves from SRR

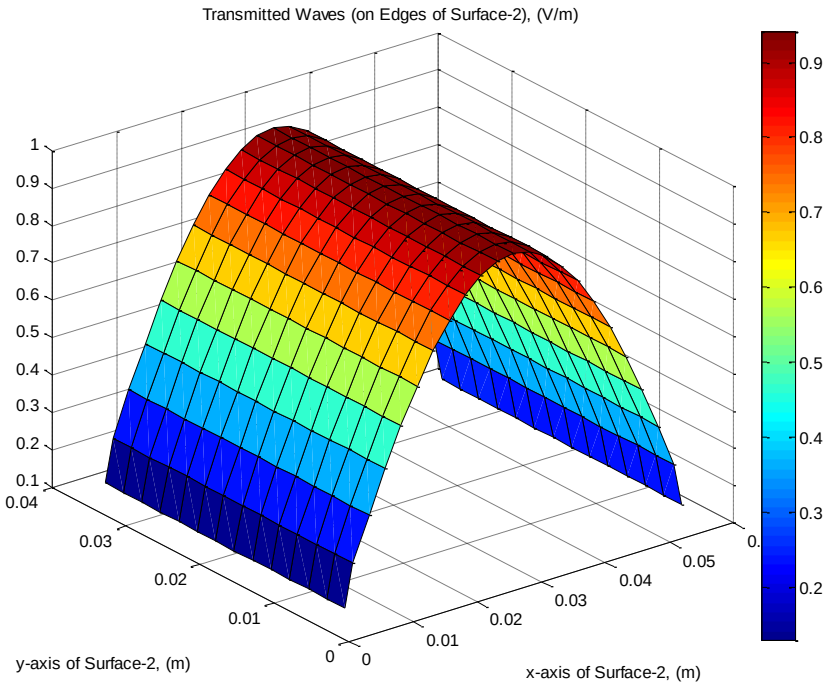

Figure 5.58: Transmitted waves from SRR

5.1.1. **Effects of change of slit width on s-parameters**

The designers were curious about how the resonant frequency affected by changing the slit widths and a good few of papers were published concerning this topic. In this thesis, under favor of CST, its influences on s-parameters were examined. For this purpose, the slit width was increased to 0.10λ and the outcomes were noted down. S_{11} was decreased but S_{21} was increased and these were expected results. Since the surface area of PEC region was decreased due to enlargement of slits.

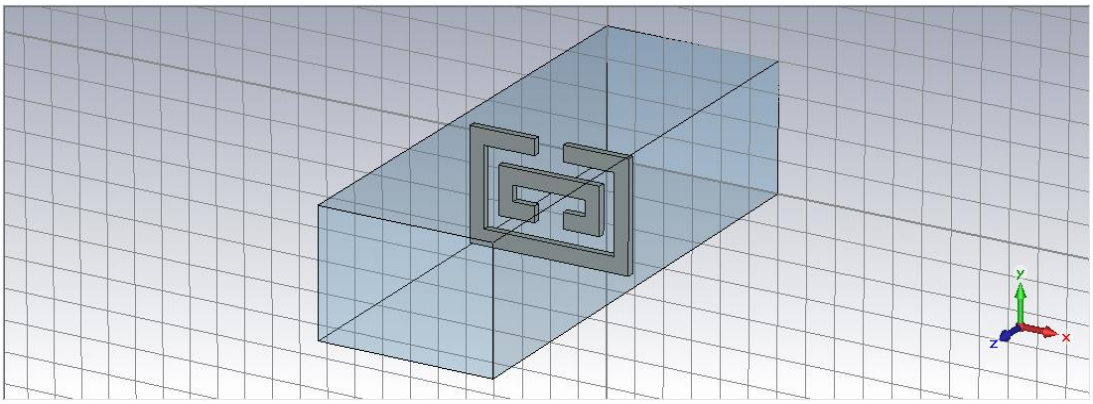

Figure 5.59: CST model of SRR with enlarged slit

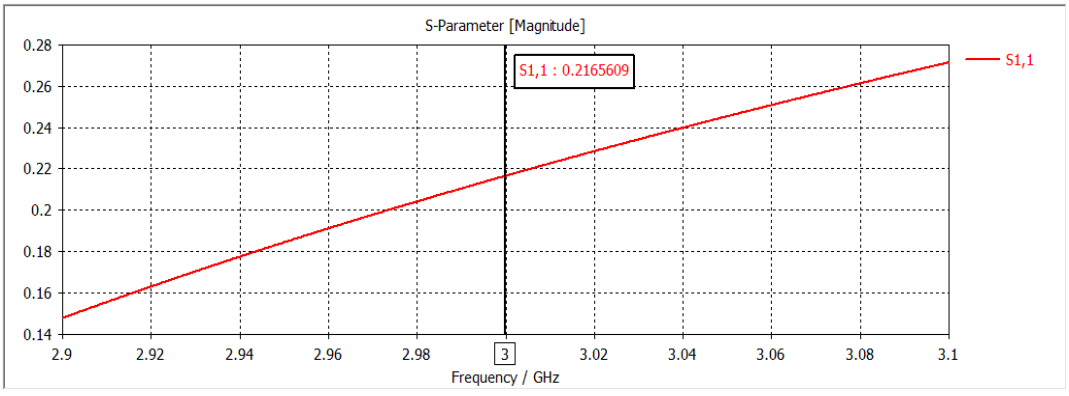

Figure 5.60: S_{11} of SRR with enlarged slit

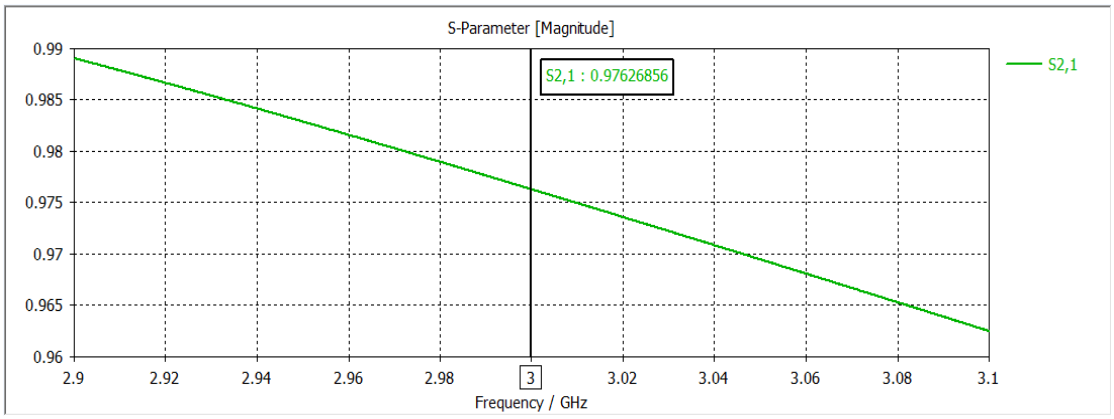

Figure 5.61: S_{21} of SRR with enlarged slit

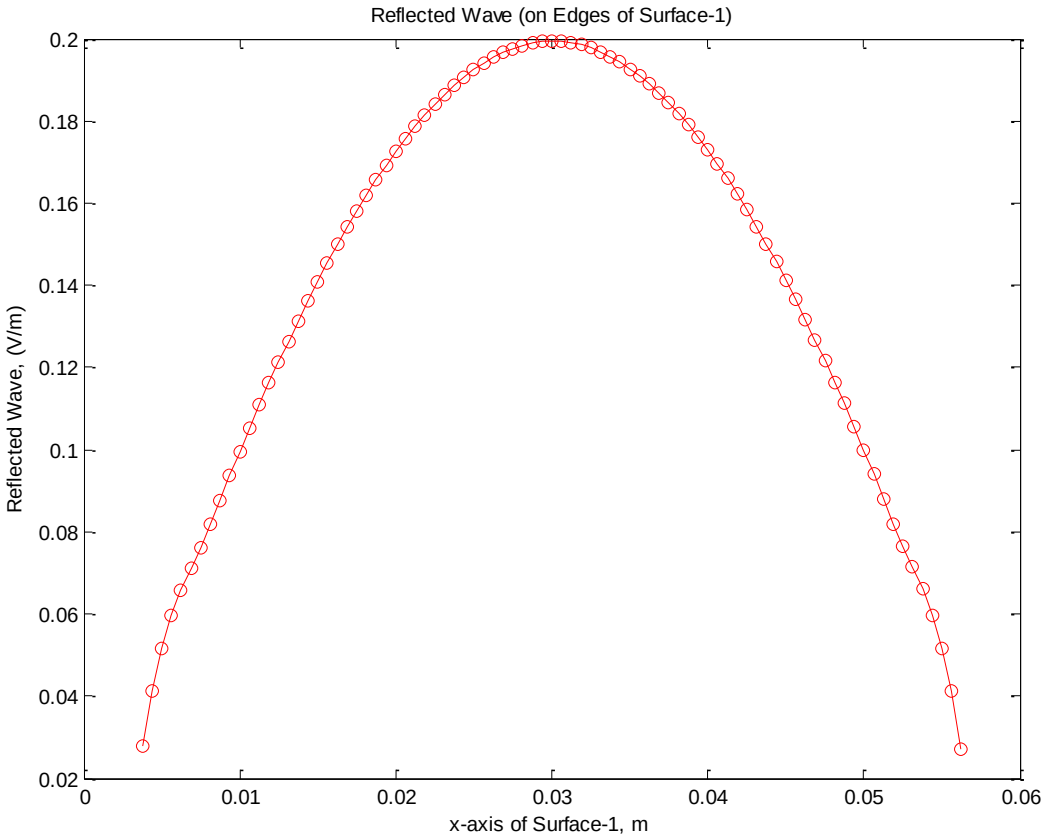

Figure 5.62: Reflected wave from SRR with enlarged slit (a half sinusoid)

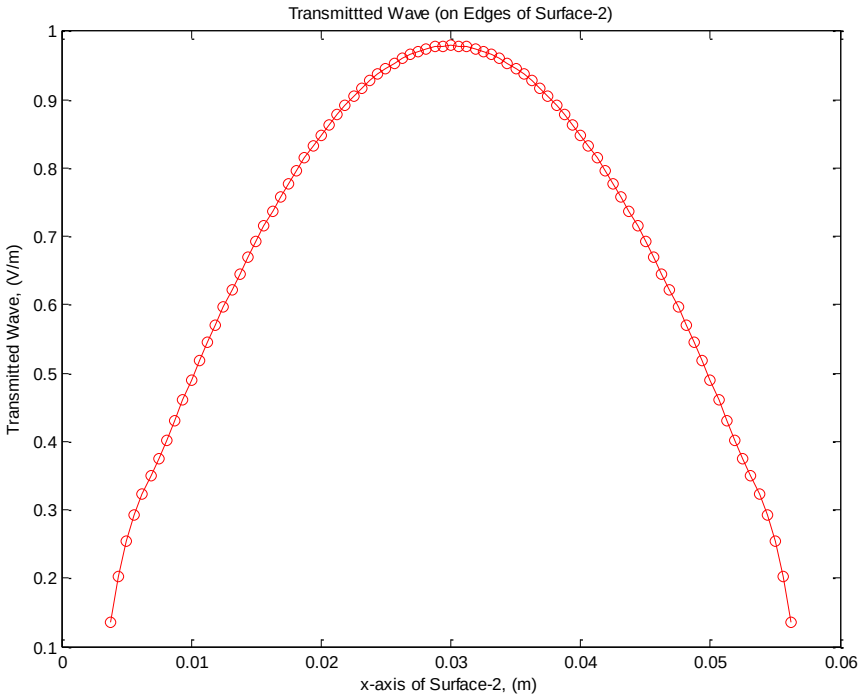

Figure 5.63: Transmitted wave from SRR with enlarged slit (a half sinusoid)

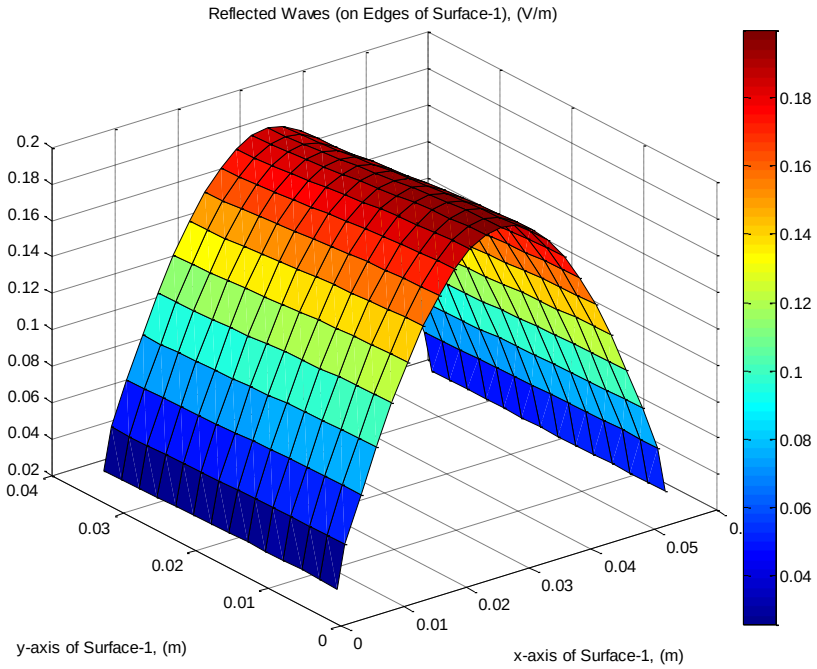

Figure 5.64: Reflected waves from SRR with enlarged slit

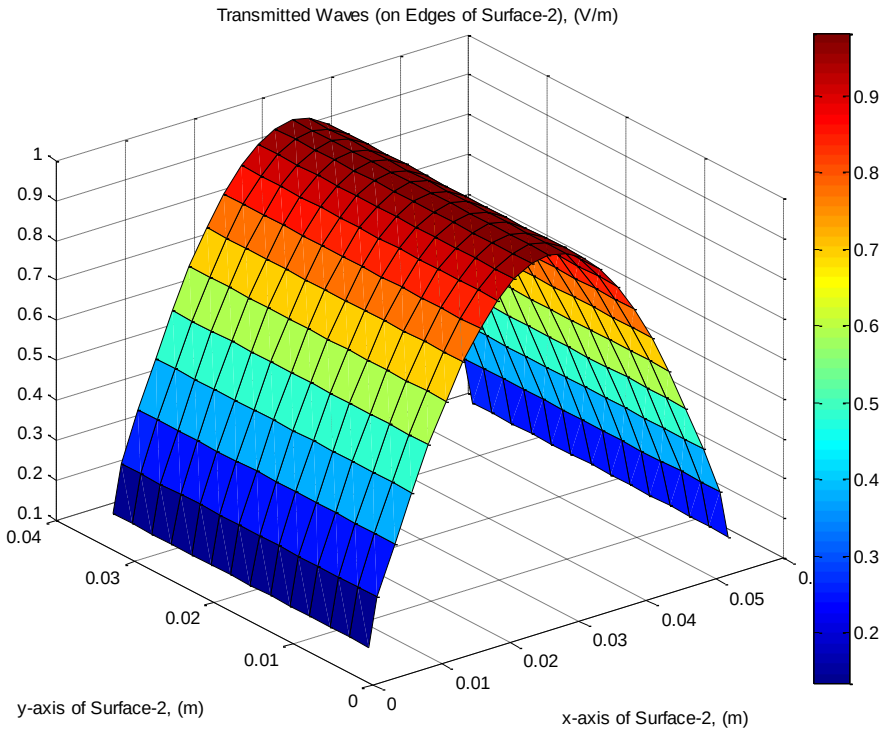

Figure 5.65: Transmitted waves from SRR with enlarged slit

5.1.2. Effects of change of side width on s-parameters

Like mentioned in section 5.1.1, another design concern for researchers was sides' width and they were interested in its effect on resonance frequency. On top of these studies, it was investigated how s-parameters affected when the sides' with was changed. The slit width was decreased to 0.025λ and the results were submitted in figures 5.66-5.72.

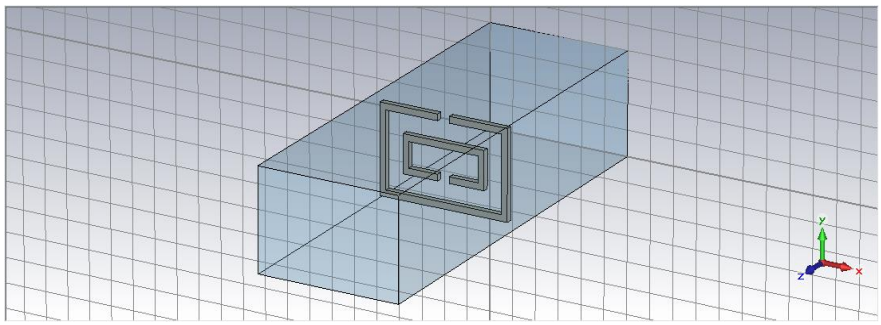

Figure 5.66: CST model of SRR with minified sides

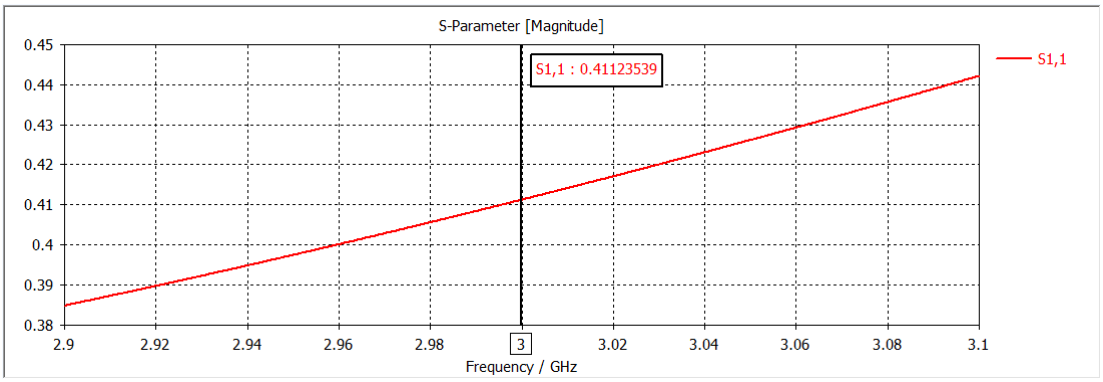

Figure 5.67: S_{11} of SRR with minified sides

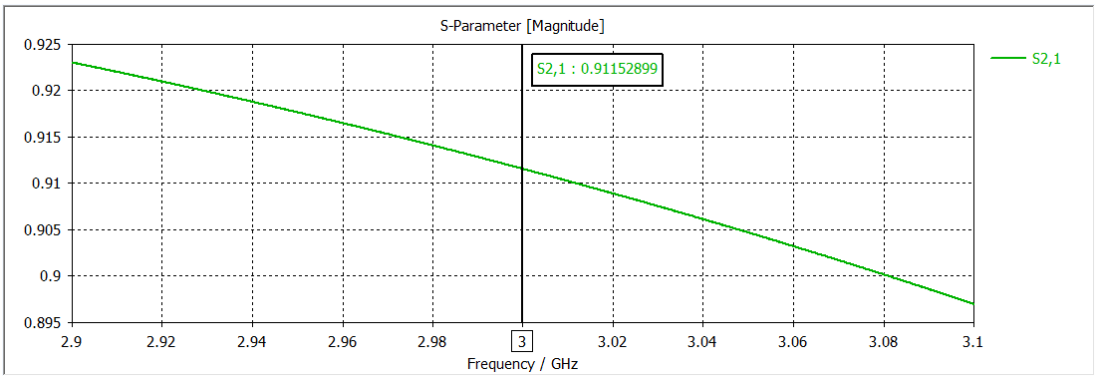

Figure 5.68: S_{21} of SRR with minified sides

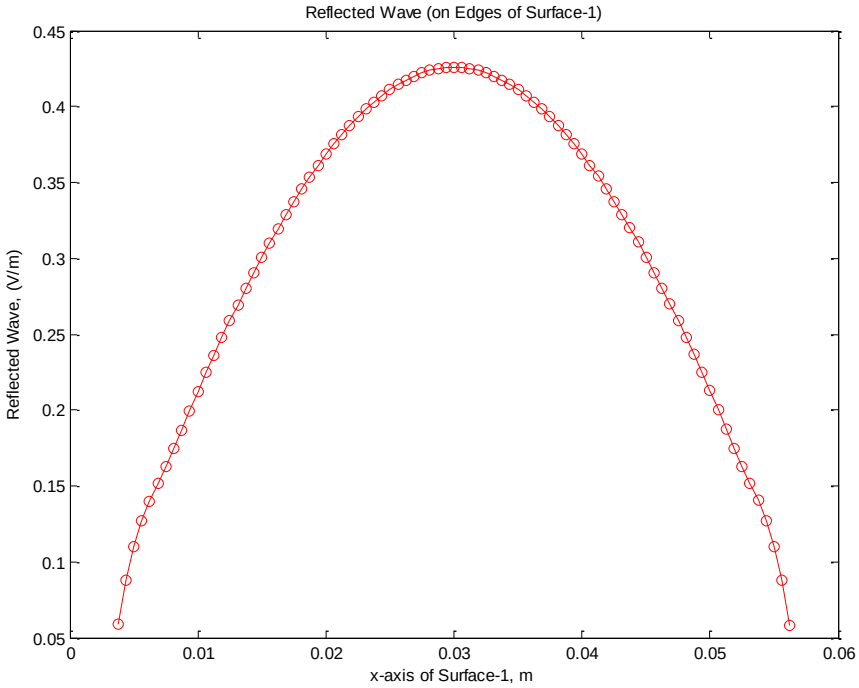

Figure 5.69: Reflected wave from SRR with minified sides (a half sinusoid)

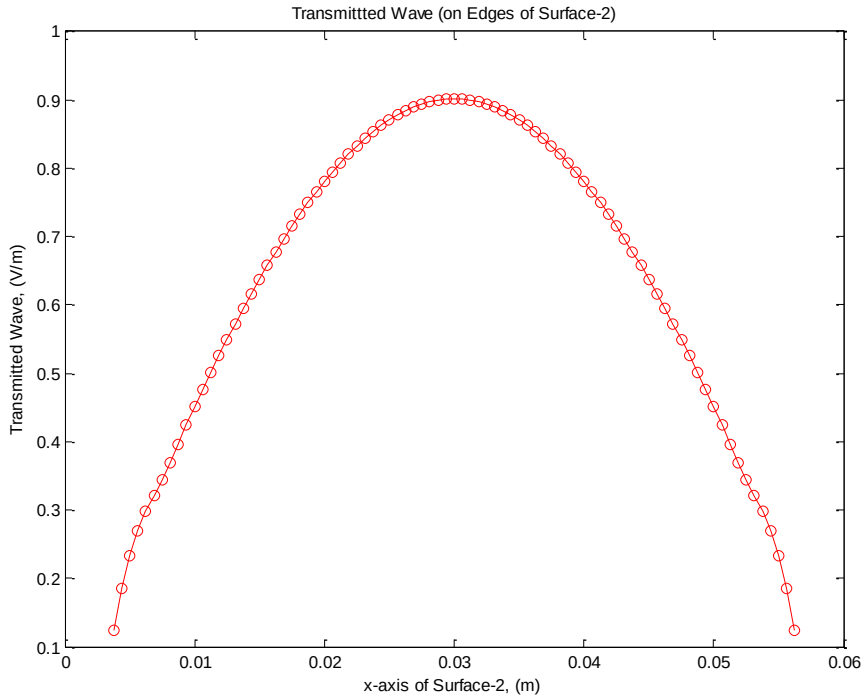

Figure 5.70: Transmitted wave from SRR with minified sides (a half sinusoid)

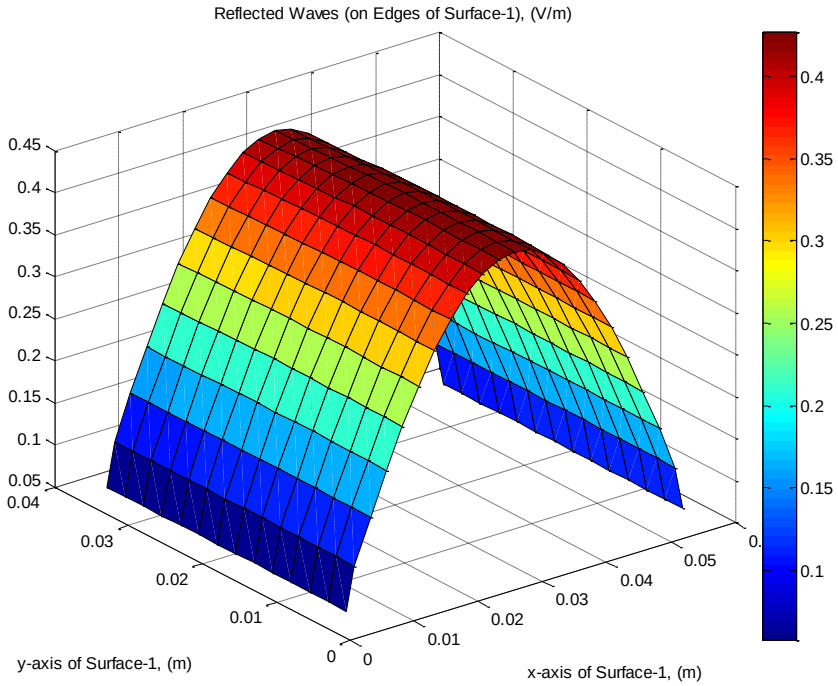

Figure 5.71: Reflected waves from SRR with minified sides

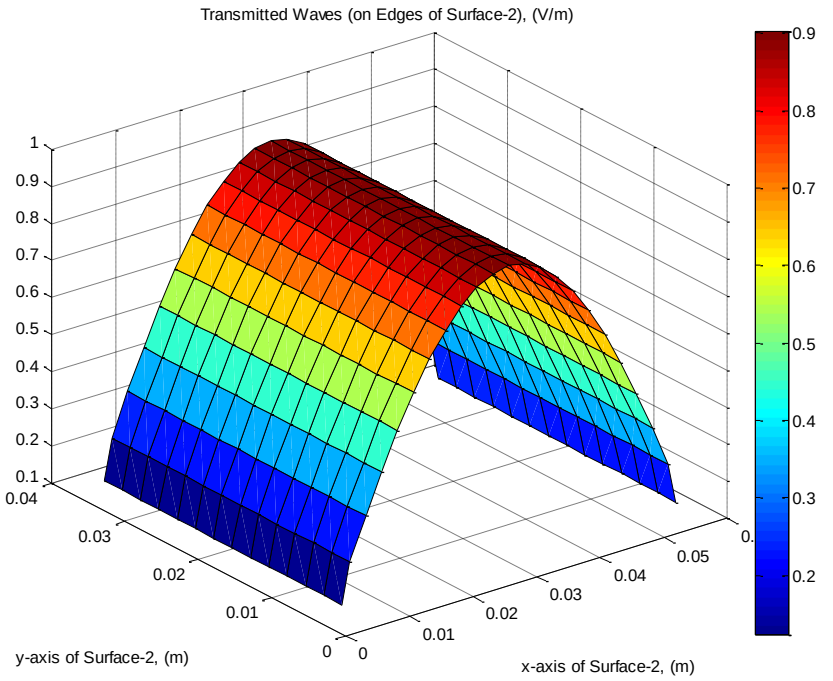

Figure 5.72: Transmitted waves from SRR with minified sides

When the widths of sides were shortened, the distance between the metals increased as a result of these two changes, the capacitance in the equivalent model is increased ([19] and [23]). Knowing that equivalent circuit model of SRRs with two coincident rings are parallel LC circuits; increase in equivalent capacitance makes the characteristic impedance decrease. Also by interpreting equations 3.20-3.21 and combining with this knowledge, the obtained results verified the theoretical information. In order to compare the changes of s-parameters with changes of slits' and sides' widths easily, the outputs were tabulated and presented below.

Table 5.6: Change of scattering parameters with change of slits' and sides' widths and comparison MATLAB code with CST

	S_{11} (MATLAB)	S_{11} (CST)	S_{21} (MATLAB)	S_{21} (CST)
SRR	0.32	0.31	0.94	0.95
SRR with enlarged slits	0.21	0.22	0.97	0.98
SRR with minified sides	0.42	0.41	0.90	0.91

5.1.3. Effects of change of operating frequency on s-parameters

So far the experiments were performed for 3 GHz frequency. By altering frequency from 2.9 GHz to 3.1 GHz and taking five samples, influences on s-parameters were observed. The design parameters were kept constant and only changes were done for frequency. For the model, the SRR, whose results were given in figures 5.52-5.58, without enlarged slits and minified sides was chosen.

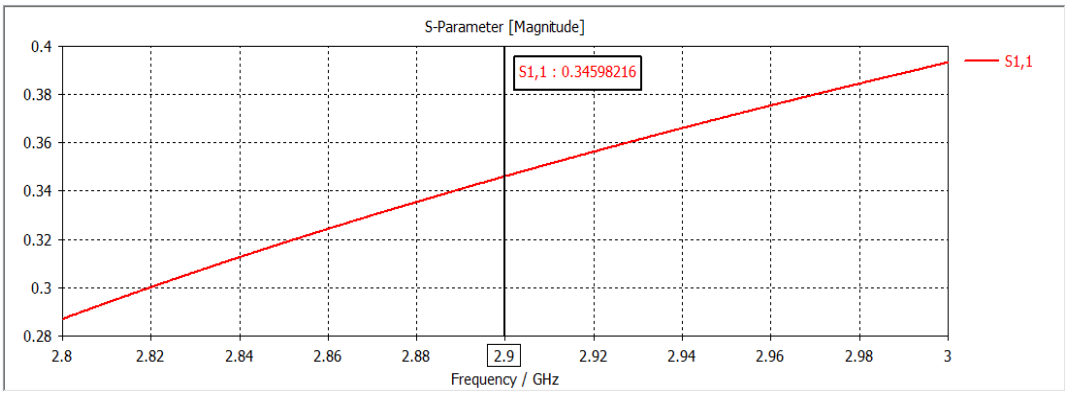

Figure 5.73: S_{11} of SRR when frequency is 2.9 GHz

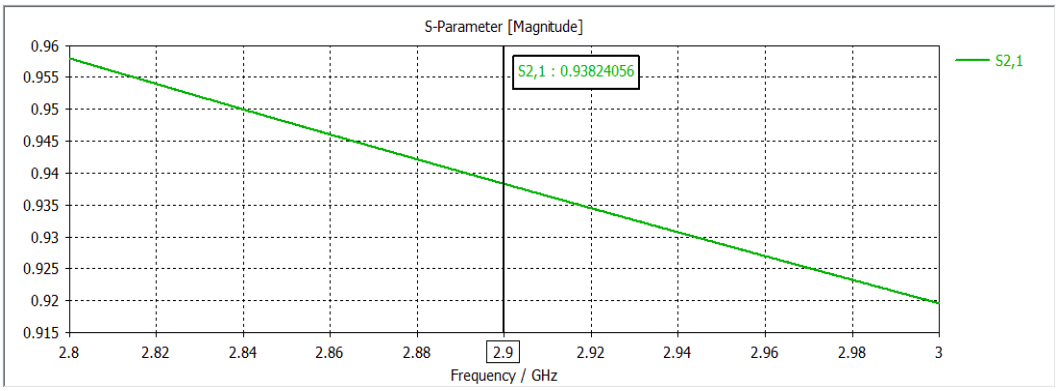

Figure 5.74: S_{21} of SRR when frequency is 2.9 GHz

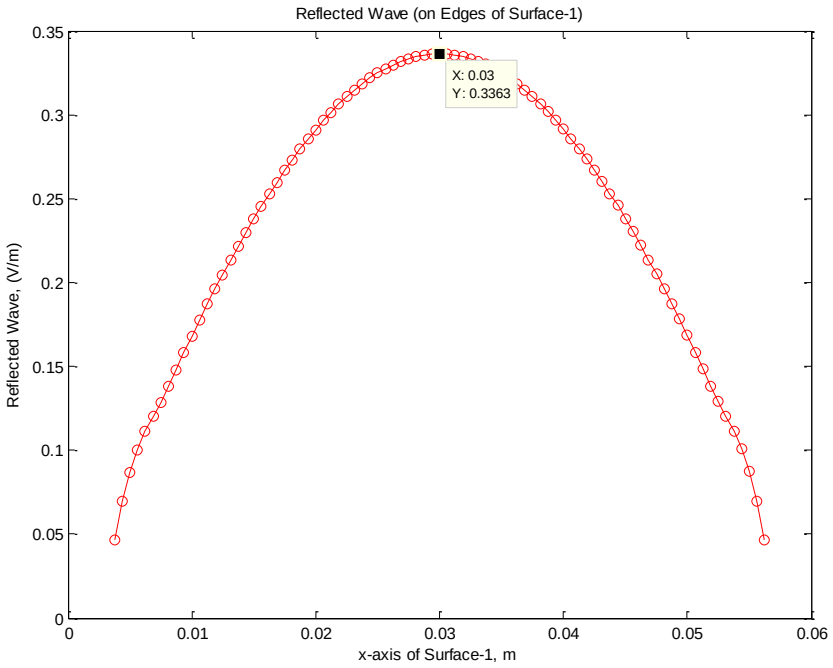

Figure 5.75: Reflected wave from SRR when frequency is 2.9 GHz (a half sinusoid)

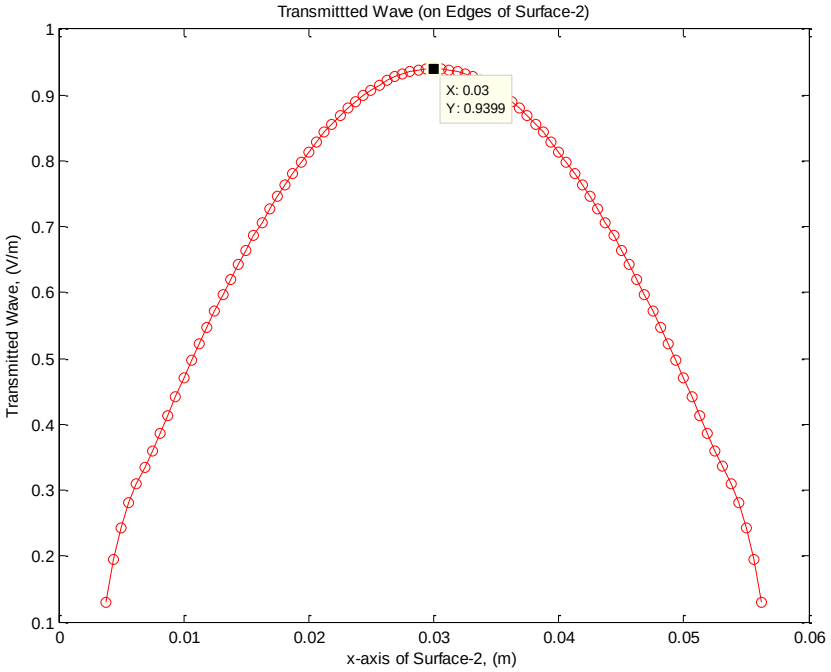

Figure 5.76: Transmitted wave from SRR when frequency is 2.9 GHz

(a half sinusoid)

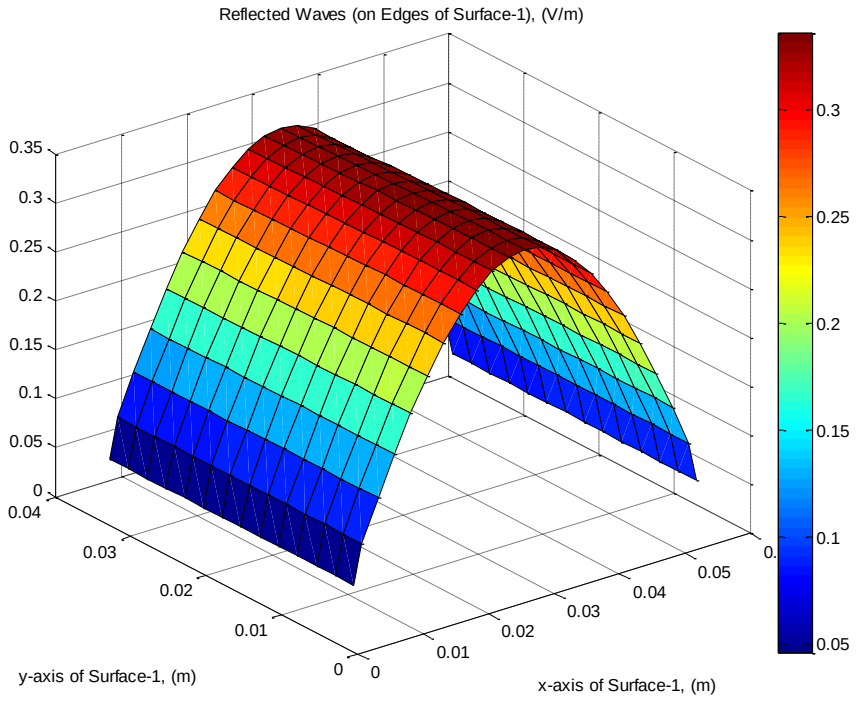

Figure 5.77: Reflected waves from SRR when frequency is 2.9 GHz

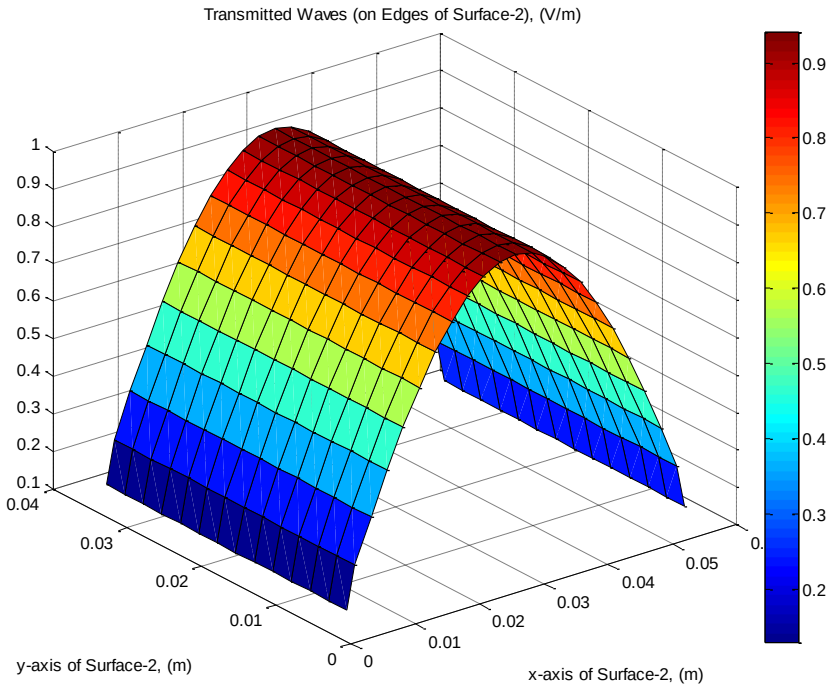

Figure 5.78: Transmitted waves from SRR when frequency is 2.9 GHz

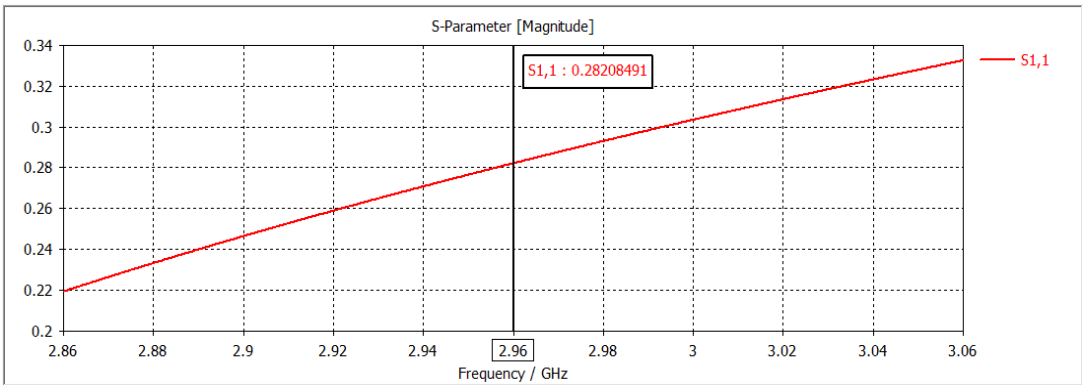

Figure 5.79: S_{11} of SRR when frequency is 2.96 GHz

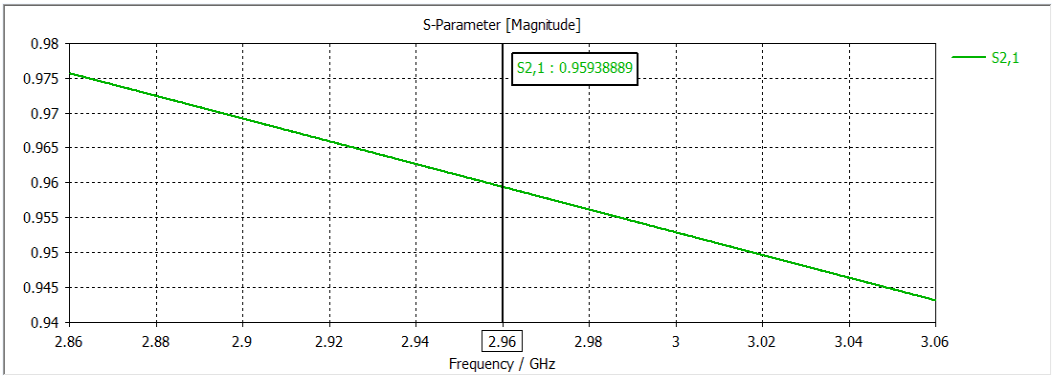

Figure 5.80: S_{21} of SRR when frequency is 2.96 GHz

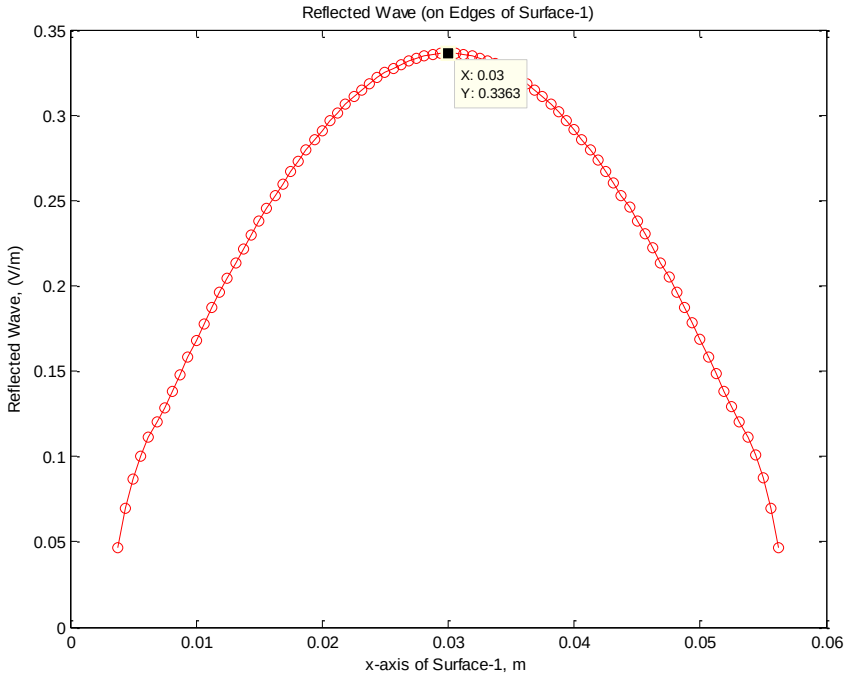

Figure 5.81: Reflected wave from SRR when frequency is 2.96 GHz (a half sinusoid)

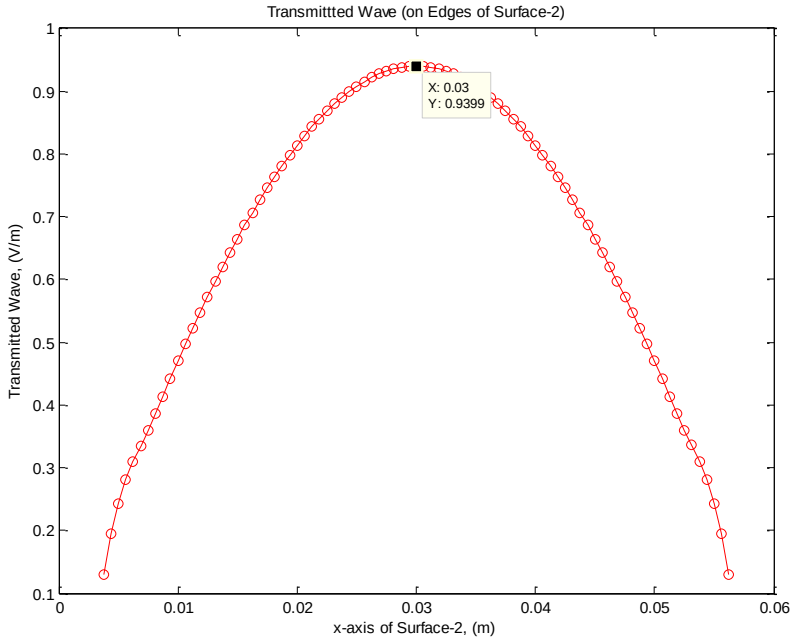

Figure 5.82: Transmitted wave from SRR when frequency is 2.96 GHz

(a half sinusoid)

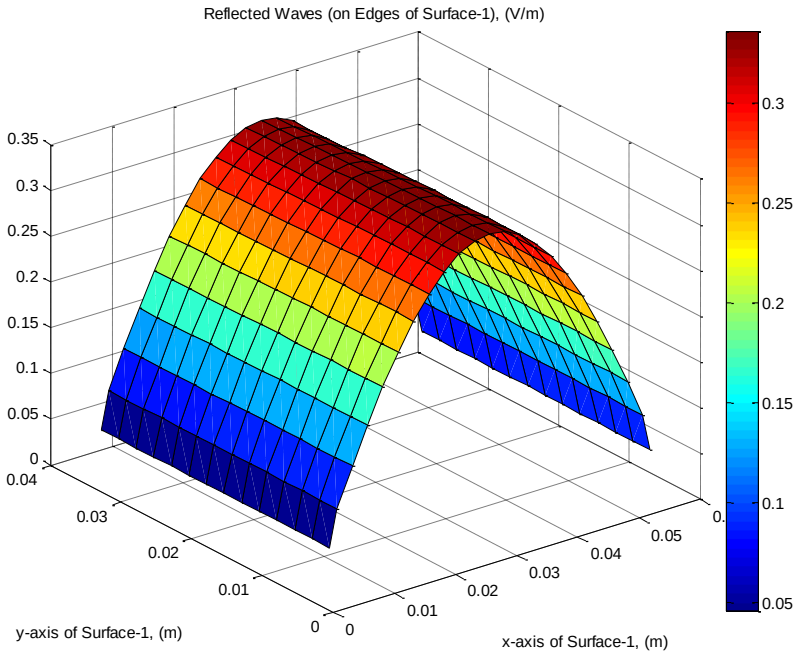

Figure 5.83: Reflected waves from SRR when frequency is 2.96 GHz

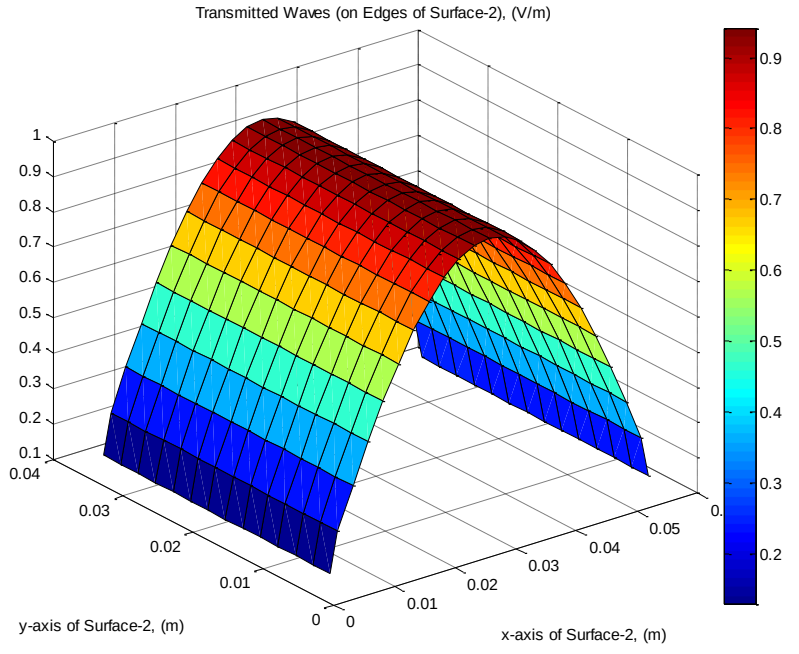

Figure 5.84: Transmitted waves from SRR when frequency is 2.96 GHz

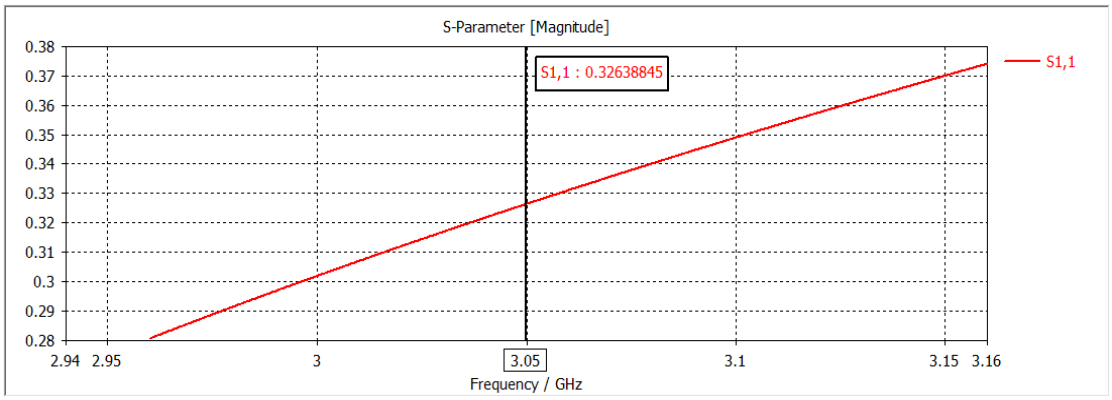

Figure 5.85: S_{11} of SRR when frequency is 3.06 GHz

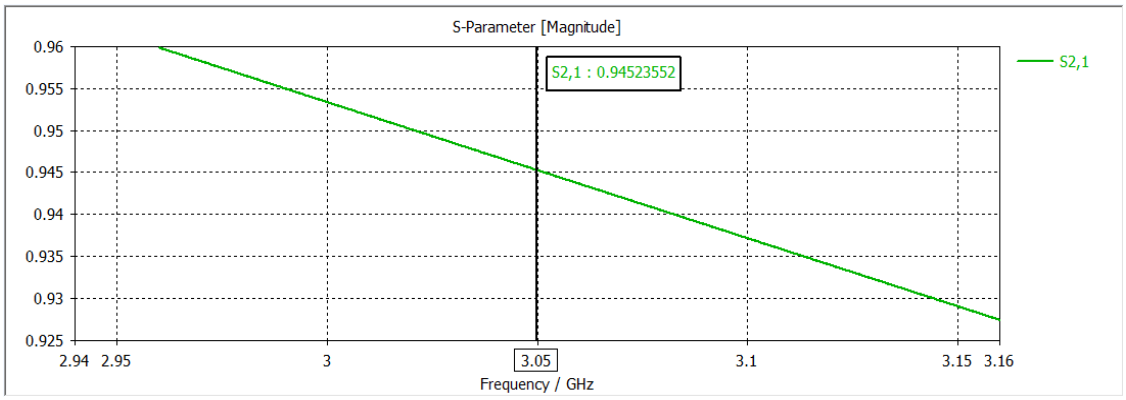

Figure 5.86: S_{21} of SRR when frequency is 3.06 GHz

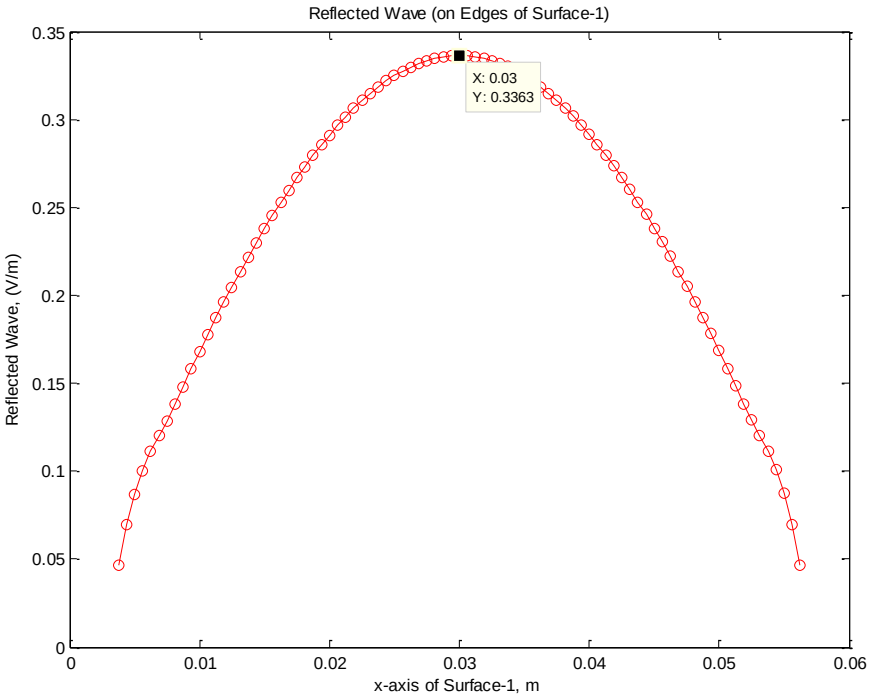

Figure 5.87: Reflected wave from SRR when frequency is 3.06 GHz (a half sinusoid)

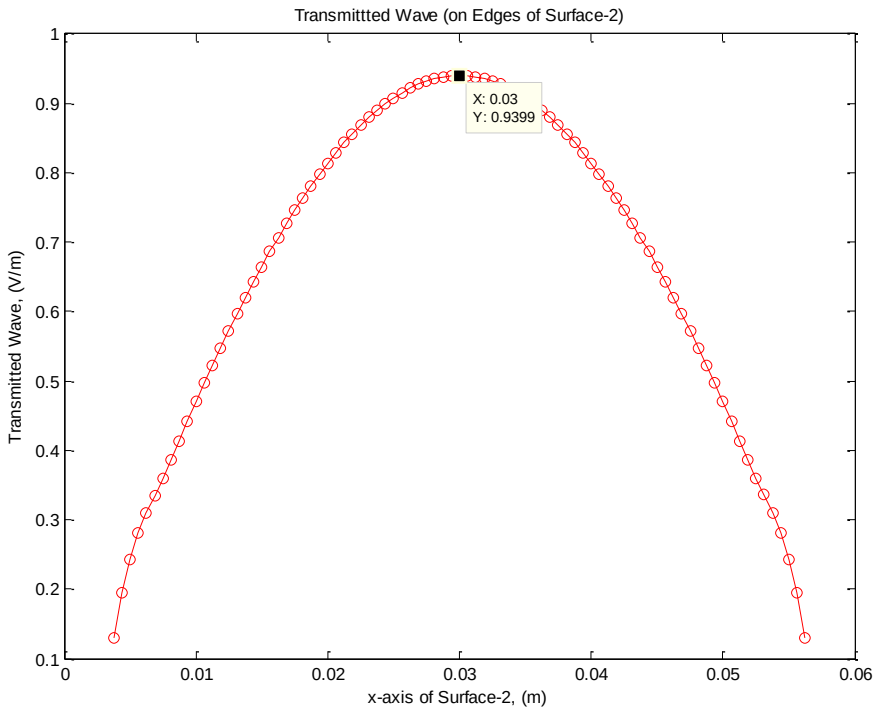

Figure 5.88: Reflected wave from SRR when frequency is 3.06 GHz (a half sinusoid)

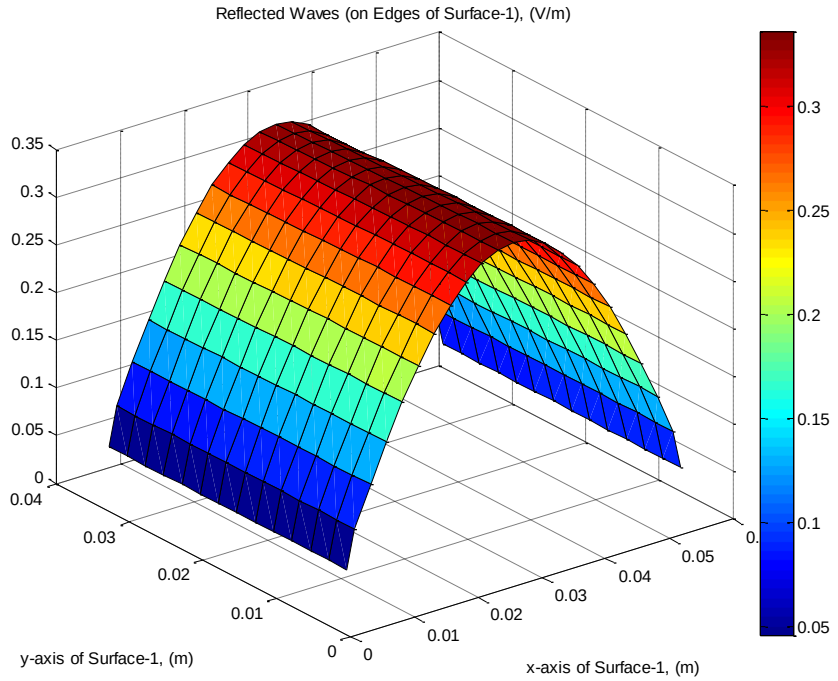

Figure 5.89: Reflected waves from SRR when frequency is 3.06 GHz

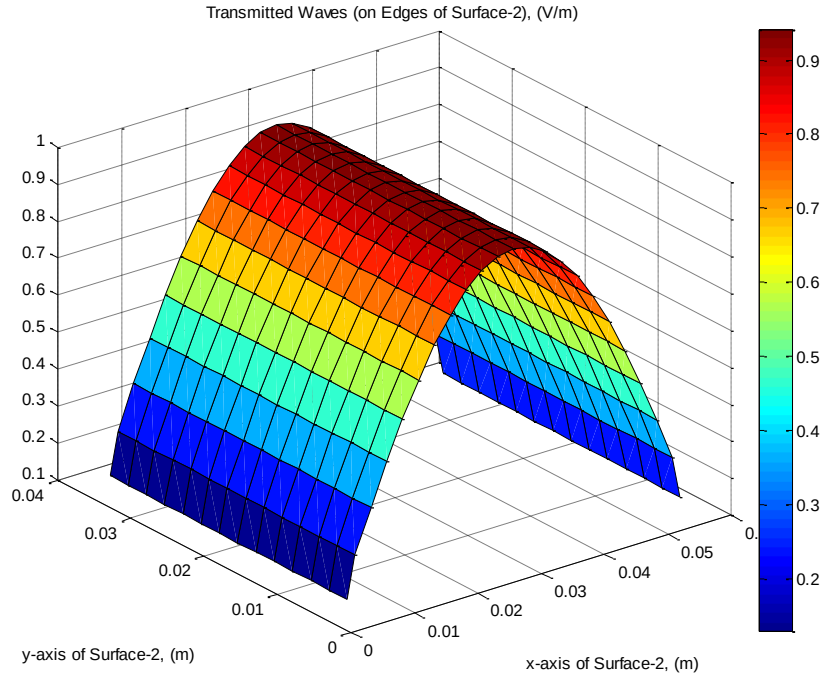

Figure 5.90: Transmitted waves from SRR when frequency is 3.06 GHz

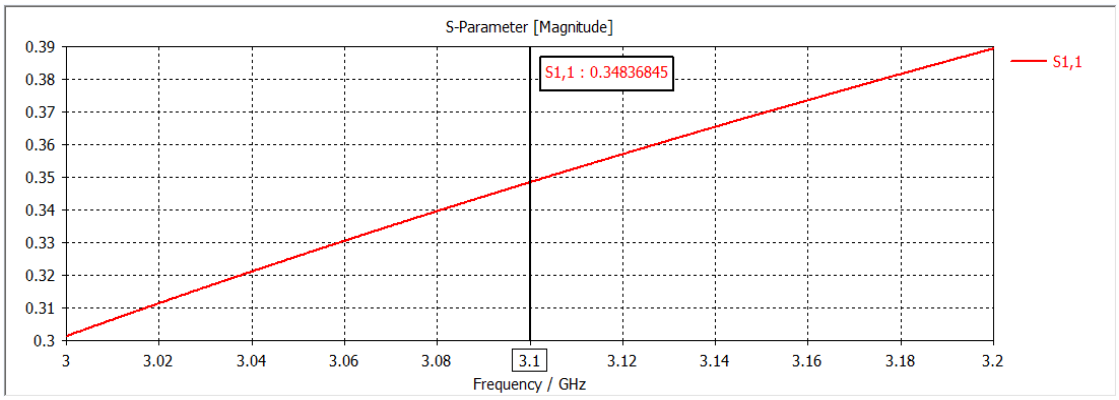

Figure 5.91: S_{11} of SRR when frequency is 3.1 GHz

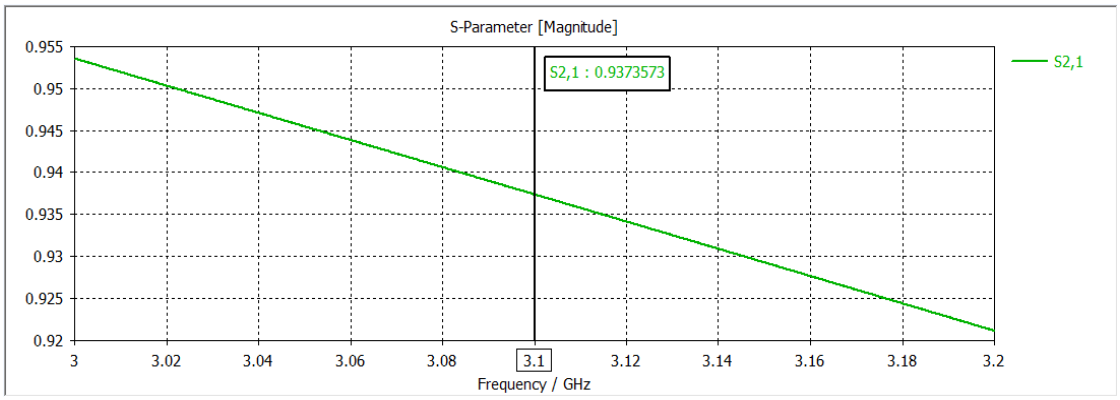

Figure 5.92: S_{21} of SRR when frequency is 3.1 GHz

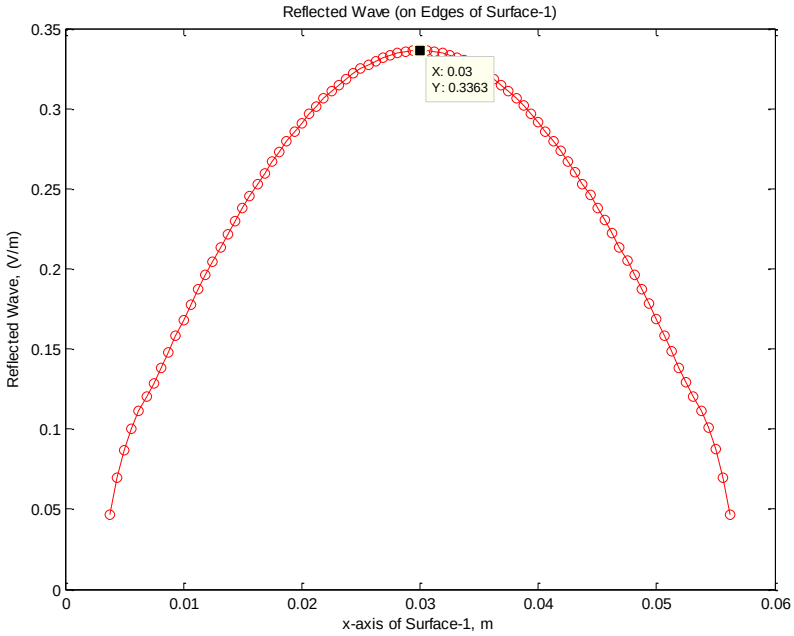

Figure 5.93: Reflected wave from SRR when frequency is 3.1 GHz (a half sinusoid)

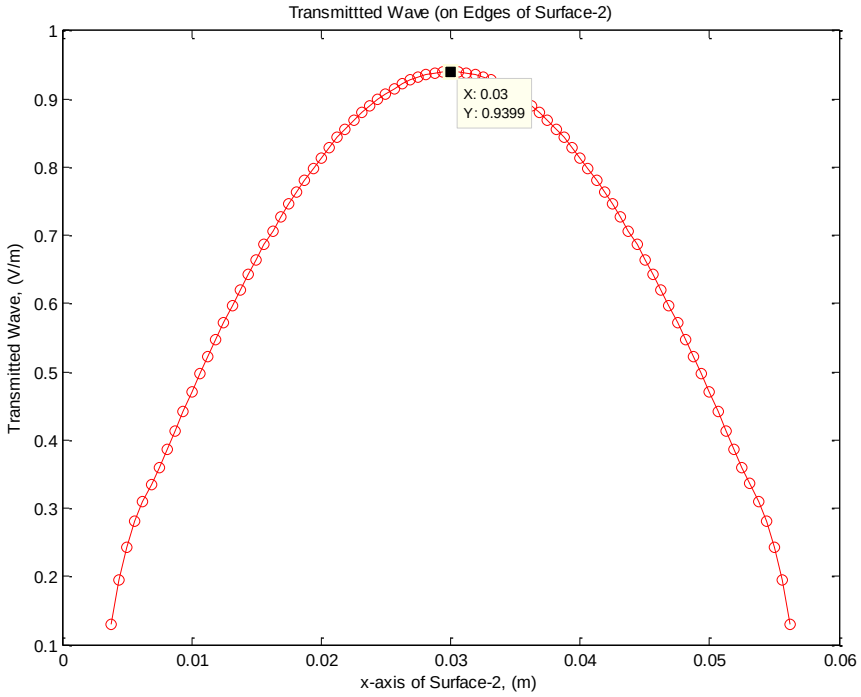

Figure 5.94: Transmitted wave from SRR when frequency is 3.1 GHz

(a half sinusoid)

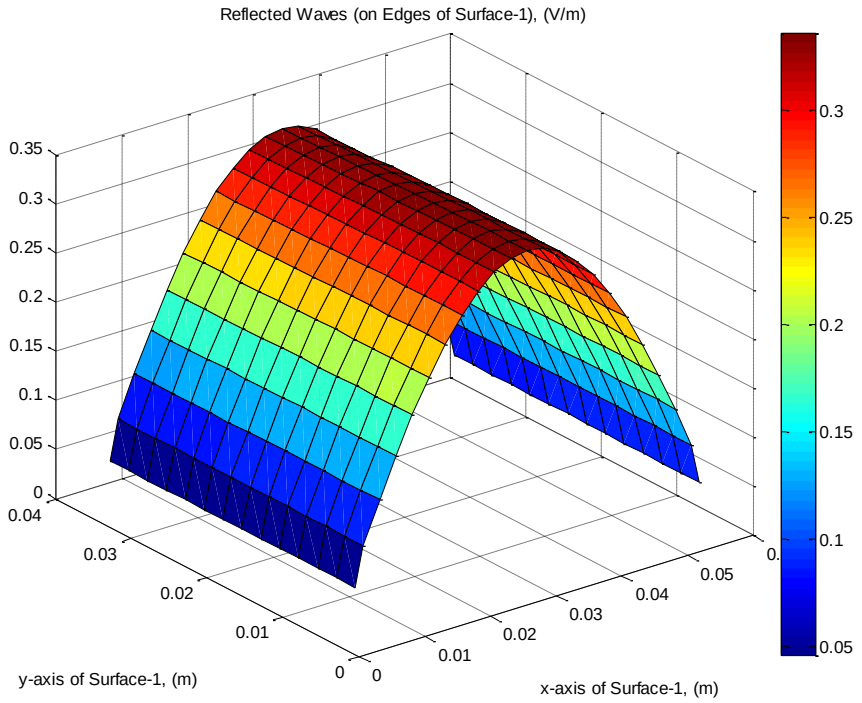

Figure 5.95: Reflected waves from SRR when frequency is 3.1 GHz

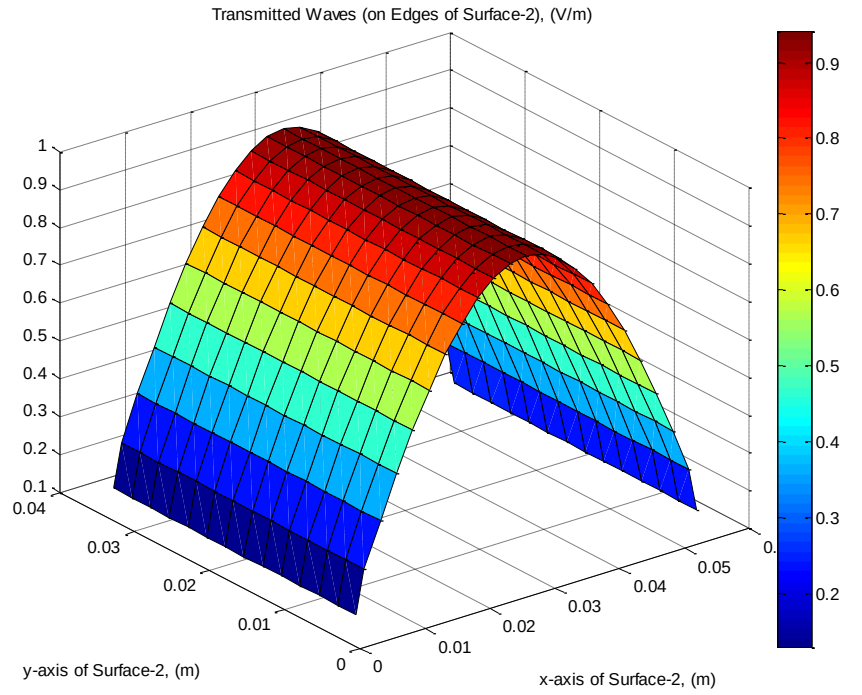

Figure 5.96: Transmitted waves from SRR when frequency is 3.1 GHz

Table 5.7: Change of scattering parameters with change frequency and comparison of MATLAB code with CST

	S_{11} (MATLAB)	S_{11} (CST)	S_{21} (MATLAB)	S_{21} (CST)
SRR with 2.9 GHz frequency	0.34	0.35	0.94	0.94
SRR with 2.96 GHz frequency	0.33	0.28	0.94	0.96
SRR with 3 GHz frequency	0.32	0.31	0.94	0.95
SRR with 3.06 GHz frequency	0.33	0.33	0.94	0.94
SRR with 3.1 GHz frequency	0.33	0.35	0.94	0.94

Approximately %3.3 frequency change did not affect s-parameters in an enormous amount since the wavelength did not change considerably. At first appearance, CST graphs made us think that this change would have a significant impact on s-parameters. Since CST's solver is a kind of time domain solver, s-parameters were shown by CST graphs as if they would be influenced by a small amount of change of frequency. In other words, s-parameters can be commented in terms of frequency change just by looking at a single graph in CST, but for every frequency change, the simulation has to be renewed by taking the new frequency as center frequency.

5.2. REFLECTION AND TRANSMISSION FROM DIELECTRIC STRUCTURE

All the results provided so far were belonged to reflected and transmitted properties of PEC structures. However, dielectric materials are also very widely used ones in electromagnetic applications due to their scattering properties. In order to determine which type of materials have stronger reflection and transmission properties and compare them for dielectric structures, a dielectric model was designed in MATLAB and CST. The structure size was 0.4λ, 0.2λ, and 0.1λ on x, y, and z axis respectively like in one of the PEC structures whose results were shared before. The element size was taken as λ/20 in MATLAB since the problem of a great number of increases in

element number was encountered. In order to avoid, increase in memory requirements and completion period of MATLAB code, this kind of a solution was preferred.

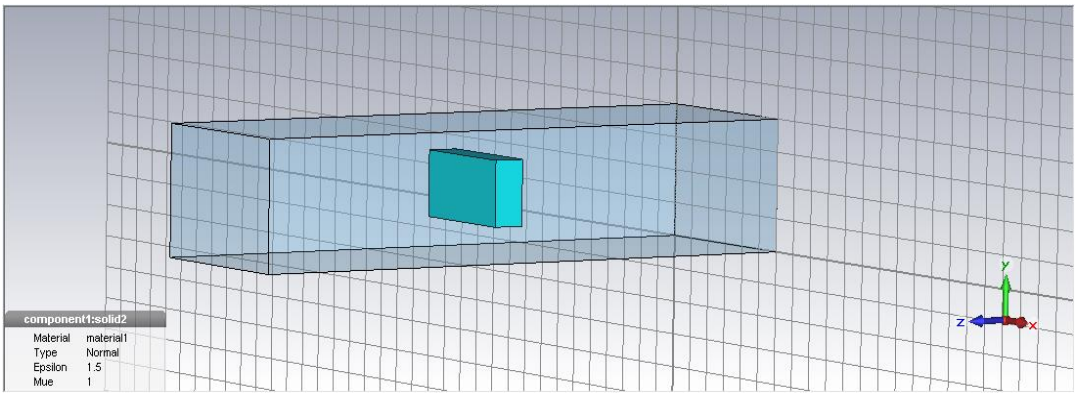

Figure 5.97: CST model of dielectric structure

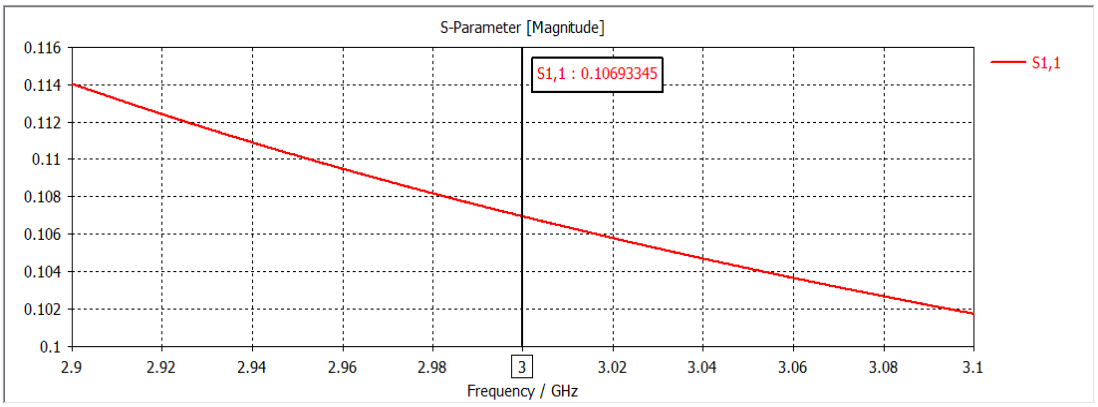

Figure 5.98: S_{11} of dielectric structure

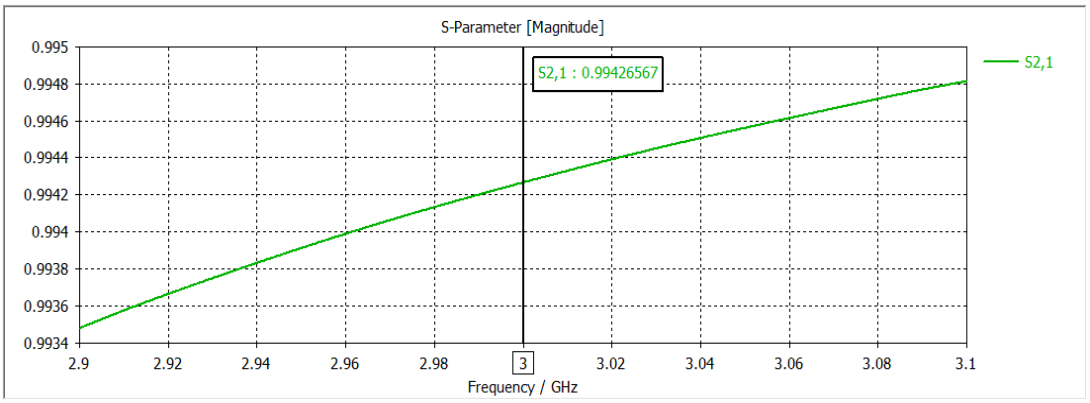

Figure 5.99: S_{21} of dielectric structure

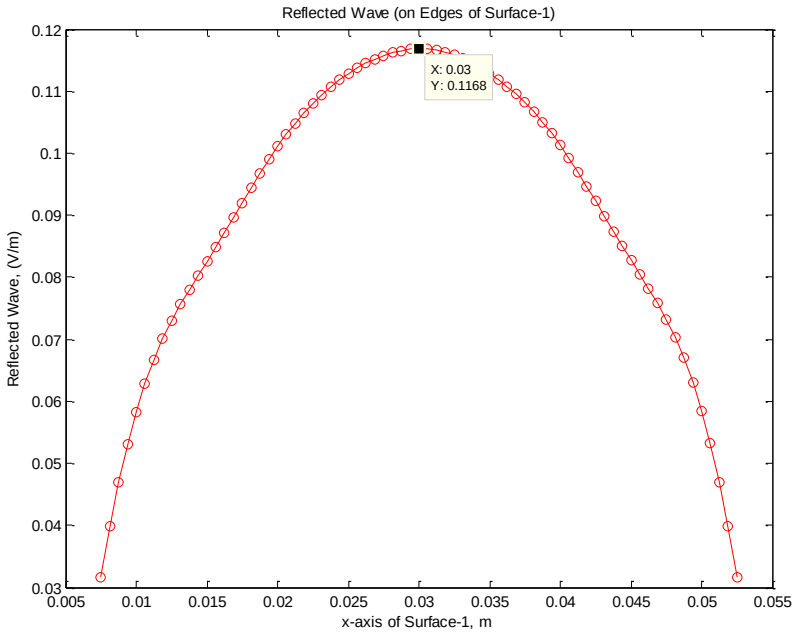

Figure 5.100: Reflected wave from dielectric structure (a half sinusoid)

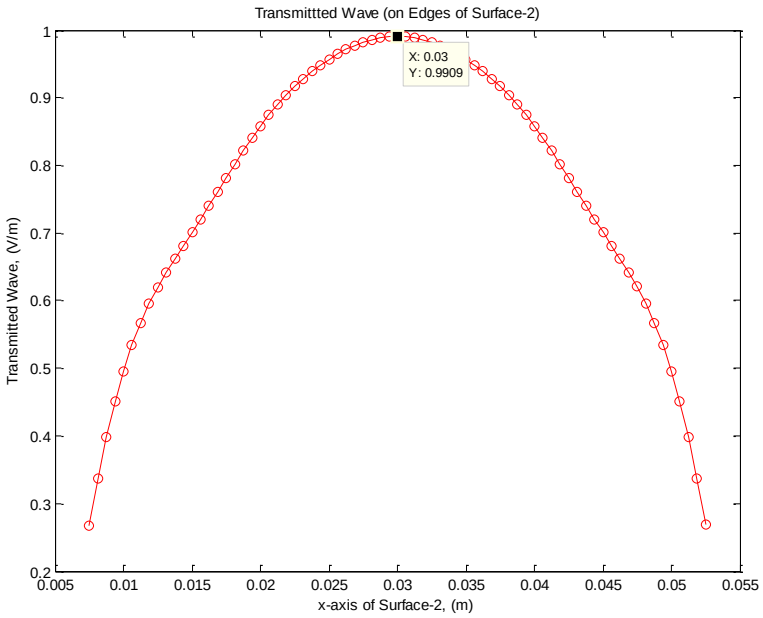

Figure 5.101: Transmitted wave from dielectric structure (a half sinusoid)

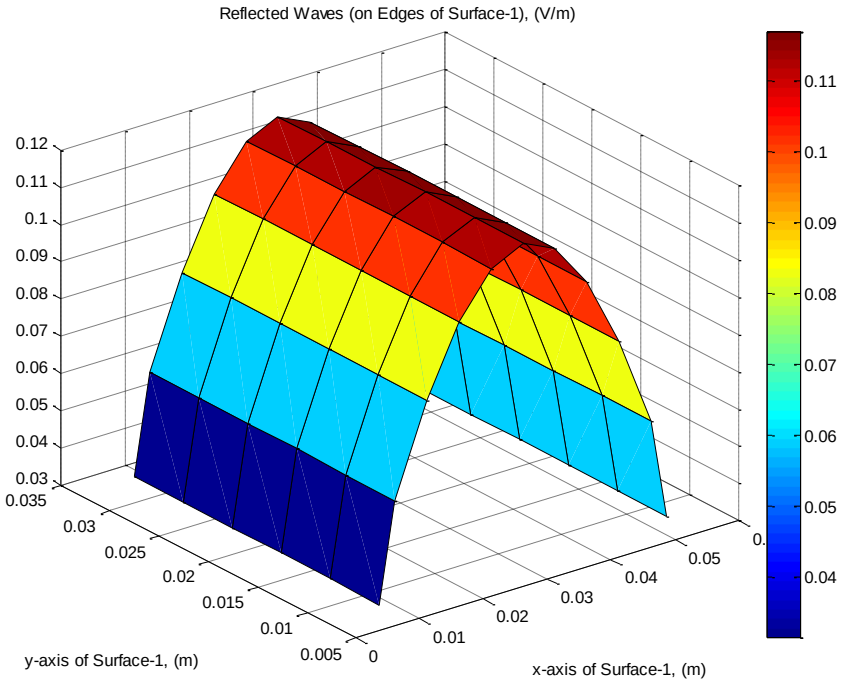

Figure 5.102: Reflected waves from dielectric structure

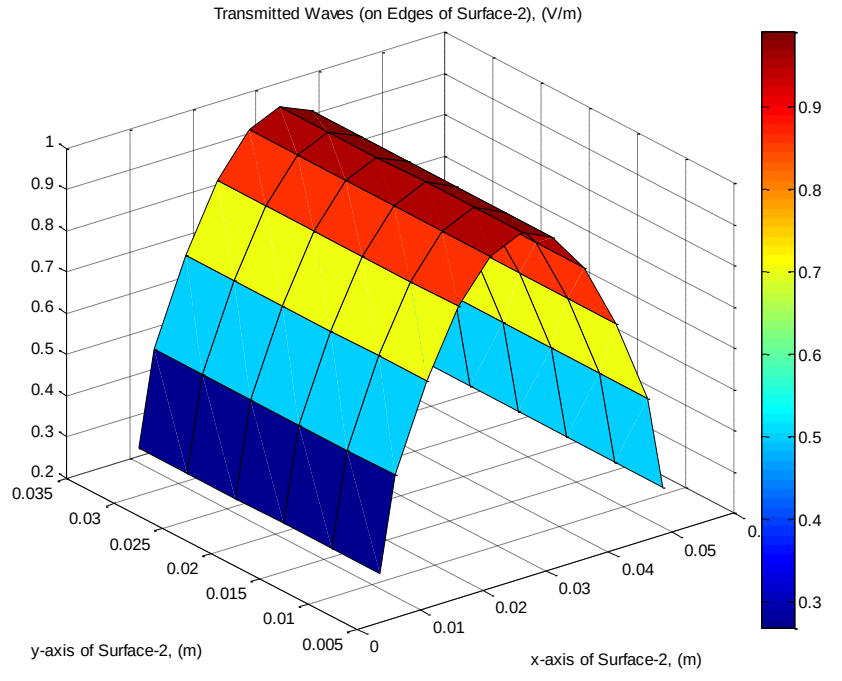

Figure 5.103: Transmitted waves from dielectric structure

Table 5.8: Change of scattering parameters with change of material type and comparison MATLAB code with CST

	S_{11} (MATLAB)	S_{11} (CST)	S_{21} (MATLAB)	S_{21} (CST)
PEC structure (λ/20 element size)	0.78	0.74	0.61	0.66
PEC structure (λ/40 element size)	0.74	0.74	0.65	0.66
Dielectric structure	0.11	0.11	0.99	0.99

For dielectric materials, transmission coefficients are greater than reflection coefficients. Also compared to the PEC structures, there are differences between the scattering properties that affect some application results like RCS ([26]-[28]). In this study, figures 5.30-5.37, figures 5.97-5.103 and Table 5.8 show that scattering properties of PEC structure differ from those of dielectric structures. Additionally, when dielectric structure was considered itself, it was confirmed that S_{11} had smaller values than S_{22}'s. Also, this was demonstrated with different software.

CHAPTER 6

CONCLUSION

Computation of scattering parameters of an object by FEM was proposed by Jin in his book. However given formulas were not so effective for precise calculations. For this reason instead of Jin's direct formula, conventional FEM procedures were preferred to calculate of scattered fields on the surfaces and to decide the optimum distances between the object and them. Also, regarding open boundaries in the system and including PMLs took the computation a step further.

Metamaterials and their applications are very popular research topics due to their remarkable properties. In microwaves, many systems are being designed by taking advantages of metamaterials and, SRRs are one of the most important system elements that have their properties. In literature, there are many researches about effects of split widths, metal widths, and gaps between the rings on resonance frequency. Scattering parameters are very important for microwave designs as well as the design parameters mentioned above. It is a deficiency that having no such studies combining these two important subjects.

This thesis, not only inform one of s-parameters of structures with different shapes and the SRRs but also of optimum waveguide size and surface distances. Thanks to these, memory and CPU requirements decrease significantly. Additionally, studies about how the changes in design parameters of SRRs affect the s-parameters were presented in detail. Furthermore, for better results, elements' sizes were changed and their effects were investigated. Moreover, the effect of incident field frequency was examined. Comparison of the scattering properties from dielectric and PEC surfaces takes part of the content. Also, all the outputs acquired from MATLAB code were checked against those of the CTS. Thereby, accuracy of the solution method and its outcomes demonstrated.

REFERENCES

[1] Sabah, C. "Multi-resonant metamaterial design based on concentric V-shaped magnetic resonators." Journal of Electromagnetic Waves and Applications 26.8-9 (2012): 1105-1115.

[2] Kaushal Gangwar, Paras, R.P.S. Gangwar, Metamaterials: Characteristics Process and Applications, vol. 4, no. 1, pp. 97-106, 2014, Research India Publications, ISSN 2231-1297.

[3] Pendry, John B., et al. "Magnetism from conductors and enhanced nonlinear phenomena." IEEE transactions on microwave theory and techniques 47.11 (1999): 2075-2084.

[4] Shelby, Richard A., David R. Smith, and Seldon Schultz. "Experimental verification of a negative index of refraction." science 292.5514 (2001): 77-79.

[5] Reddy, C. J., et al. "Finite element method for eigenvalue problems in electromagnetics." (1994).

[6] Ise, Kiyoshi, Kazuhiro Inoue, and Masanori Koshiba. "Three-dimensional finite-element solution of dielectric scattering obstacles in a rectangular waveguide." IEEE Transactions on Microwave Theory and Techniques 38.9 (1990): 1352-1359.

[7] Pontoppidan, Knud. "Numerical solution of waveguide problems using finite difference methods." 1st European Microwave Conference. 1969.

[8] Clarricoats, P. J. B., and K. R. Slinn. "Numerical solution of waveguide-discontinuity problems." Electrical Engineers, Proceedings of the Institution of 114.7 (1967): 878-886.

[9] Constantine A. Balanis, Advanced Engineering Electromagnetics, Second Edition, John Wiley & Sons, pages 13 and 106.

[10] Veselago V. G., The Electrodynamics of Substances With Simultaneously Negative Values of ε and μ, Soviet Physics Uspekhi, 10(4), s. 509-514, 1968.

[11] Ozbay, Ekmel, Kaan Guven, and Koray Aydin. "Metamaterials with negative permeability and negative refractive index: experiments and simulations." Journal of Optics A: Pure and Applied Optics 9.9 (2007): S301.

[12] Aydin, Koray, et al. "Investigation of magnetic resonances for different split-ring resonator parameters and designs." New journal of physics 7.1 (2005): 168.

[13] Jabita, Abdul-Nafiu Abiodun. "Design of singly split single ring resonator for measurement of dielectric constant of materials using resonant method." (2013).

[14] Fan, Jun-Wa, Chang-Hong Liang, and D. D. D. Li. "Design of cross-coupled dual-band filter with equal-length split-ring resonators." Progress In Electromagnetics Research 75 (2007): 285-293.

[15] Pendry, J. B., et al. "Low frequency plasmons in thin-wire structures." Journal of Physics: Condensed Matter 10.22 (1998): 4785.

[16] Pradeep, Anju, S. Mridula, and P. Mohanan. "Design of an Edge-Coupled Dual-Ring Split-Ring Resonator." IEEE Antennas and Propagation Magazine 53.4 (2011): 45-54.

[17] Castro, Pedro J., Joaquim J. Barroso, and Joaquim P. Leite Neto. "Experimental Study on Split-Ring Resonators with Different Slit Widths." Journal of Electromagnetic Analysis and Applications 5.9 (2013): 366.

[18] Institute for Microelectronics, http://www.iue.tuwien.ac.at/phd/orio/node48.html, last accessed date: 06 December 2016.

[19] Jin, Jian-Ming, The Finite Element Method in Electromagnetics, Second Edition, John Wiley & Sons, pages 308-311.

[20] Özgün, Ö., Finite Element Modeling of Electromagnetic Radiation/Scattering Problems by Domain Decomposition, PhD. Thesis, Middle East Technical University, 2007.

[21] Ozgun, Ozlem, and Mustafa Kuzuoglu. "Near-field performance analysis of locally-conformal perfectly matched absorbers via Monte Carlo simulations." Journal of computational Physics 227.2 (2007): 1225-1245.

[22] Ozgun, Ozlem, and Mustafa Kuzuoglu. "Non-Maxwellian locally-conformal PML absorbers for finite element mesh truncation." IEEE transactions on antennas and propagation 55.3 (2007): 931-937.

[23] Beriot, Hadrien, and Michel Tournour. "On the locally-conformal perfectly matched layer implementation for Helmholtz equation." NOVEM Noise and Vibration: Emerging Methods 20093 (2009).

[24] Collino, Francis, and Peter B. Monk. "Optimizing the perfectly matched layer." Computer methods in applied mechanics and engineering 164.1 (1998): 157-171.

[25] More, Shashikant T., and R. S. Bindu. "Effect of Mesh Size on Finite Element Analysis of Plate Structure."

[26] Faircloth, Daniel L., et al. "Investigation of reflection and transmission properties of dielectric slabs randomly doped with conducting objects." Microwave and optical technology letters 48.1 (2006): 83-86.

[27] Donepudi, Kalyan C., Jian-Ming Jin, and Weng Cho Chew. "A higher order multilevel fast multipole algorithm for scattering from mixed conducting/dielectric bodies." IEEE Transactions on Antennas and Propagation 51.10 (2003): 2814-2821.

[28] Chen, Yikai, and Chao-Fu Wang. "Scattering analysis for PEC and dielectric bodies using characteristic modes." 2015 IEEE International Symposium on Antennas and Propagation & USNC/URSI National Radio Science Meeting. IEEE, 2015.

Appendix A: MATLAB CODE SIMULATION PARAMETERS

As mentioned before, for the simulations MATLAB codes are developed. For each design in Chapter 5, different FEM parameters namely number of element (NoEl), number of node (NoN), number of edge (NoEd), and mesh generation time (MGT) result in. In this Appendix, numerical values of these parameters can be found.

Table A.1: Simulation parameters for structure with sizes 0.1λx0.1λx0.1λ

NoEl	NoN	NoEd	MGT (sec)
44880	9242	57456	55.20

Table A.2: Simulation parameters for structure with sizes 0.5λx0.3λx0.1λ

NoEl	NoN	NoEd	MGT (sec)
20116	4284	26114	27.09

Table A.3: Simulation parameters for structure with sizes 0.4λx0.2λx0.1λ (λ/40 element size)

NoEl	NoN	NoEd	MGT (sec)
20352	4685	27756	42.23

Table A.4: Simulation parameters for structure with sizes 0.4λx0.2λx0.1λ (λ/20 element size)

NoEl	NoN	NoEd	MGT (sec)
162816	30107	200500	259.77

Table A.5: Simulation parameters for ring structure

NoEl	NoN	NoEd	MGT (sec)
158496	29750	194773	160.57

Table A.6: Simulation parameters for ring structure with a slit

NoEl	NoN	NoEd	MGT (sec)
158520	29750	194778	161.81

Table A.7: Simulation parameters for SRR structure

NoEl	NoN	NoEd	MGT (sec)
157872	29750	194467	264.868

Table A.8: Simulation parameters for SRR structure with enlarged slits

NoEl	NoN	NoEd	MGT (sec)
157968	29750	194515	255.663

Table A.9: Simulation parameters for SRR structure with minified sides

NoEl	NoN	NoEd	MGT (sec)
158400	29750	194823	271.785

Table A.10: Simulation parameters for dielectric structure

NoEl	NoN	NoEd	MGT (sec)
21888	4563	28162	24.193